Diss. ETH No. 12928

Theoretical Investigations on the Structural, Electronic, and Optical Characteristics of Functionalized Tetraethynylethenes

A dissertation submitted to the
SWISS FEDERAL INSTITUTE OF TECHNOLOGY ZÜRICH

for the degree of
Doctor of Natural Sciences

Presented by
Anouk Hilger
Dipl. Chem. Ing. ETHZ

born 28.11.1970
citizen of the Grand-Duchy of Luxembourg

accepted on the recommendation of
PD Prof. Dr. Hans Peter Lüthi, examiner
Prof. Dr. François Diederich, co-examiner

Zürich 1998

fir meng Elteren

Acknowledgments

I would like to thank PD Prof. Dr. Hans Peter Lüthi for the support he gave to facilitate this project. I am grateful for the opportunity to work with him, which enabled me to enlarge my knowledge in the field of computational chemistry. I have greatly appreciated his advice and suggestions as well as the freedom I had in the execution of the work.

My thanks also go to Prof. Dr. François Diederich for the opportunity to work on a fascinating project, which allowed me to explore organic chemistry by means of quantum chemistry. I greatly appreciated his inspiring enthusiasm he put into this project.

I want to express my warmest gratitude to Prof. Dr. Rik Tykwinski for proof-reading this manuscript and for all the interesting discussions, helping to increase my knowledge in organic chemistry.

I must thank Prof. Maurice Gross, Dr. Corinne Boudon, and Dr. Jean-Paul Gisselbrecht for a fruitful collaboration and helpful discussions about electrochemistry.

I am very grateful to Prof. Jean-Luc Brédas who gave me the opportunity to visit his laboratory and to all the 'Brédateurs', who made my stays in Belgium enjoyable. Special thanks go to Dr. Jérôme Cornil and Dr. David Beljonne for their help to acquaint me with the techniques to calculate electronic absorption spectra and non linear optical properties.

I also thank Gabriele Petraglio for carrying out some of the calculations in the electron affinity study during his internship at CSCS in Manno.

I would like to thank all members of the Diederich group for their friendship and for the very pleasant time in the group. Furthermore, I thank all the people from SCSC for the good atmosphere in the group.

Last, I deeply thank my parents for their love and care, and for sharing with me all the joyful and difficult moments during my studies and dissertation time in Zurich.

Parts of this thesis were published.

- A. Hilger, J.-P. Gisselbrecht, R. R. Tykwinski, C. Boudon, M. Schreiber, R. E. Martin, H. P. Lüthi, M. Gross, F. Diederich, "Electronic Characteristics of Arylated Tetraethynylethenes: A Cooperative Computational and Electrochemical Investigation", *J. Am. Chem. Soc.* **1997**, *119*, 2069-2078.

- R. E. Martin, J. Bartek, F. Diederich, R. R. Tykwinski, E. Meister, A. Hilger, H. P. Lüthi, "Photochemical *trans-cis* Isomerisation of Donor/Acceptor-Substituted (*E*)-Hex-3-en-1,5-diynes (1,2-Diethynylethenes, DEEs) and 3,4-Diethynylhex-3-ene-1,5-diynes (Tetraethynylethenes, TEEs)", *J. Chem. Soc., Perkin Trans. 2* **1998**, 233-241.

Parts of this thesis were presented at international conferences.

- R. R. Tykwinski, M. Schreiber, F. Diederich, C. Bosshard, U. Gubler, P. Günter, A. Hilger, H. P. Lüthi, "Structure-Function Relationships in Donor-Acceptor Functionalized Tetraethynylethenes", poster presentation at the Third European Conference on Molecular Electronics (ECME), Leuven, Belgium, September 1-6, 1996.

- A. Hilger, H. P. Lüthi, R. R. Tykwinski, F. Diederich, "Modélisation *Ab Initio* des Priétes Electroniques de Tétraéthynyléthènes Substitués", oral presentation at the XXIII Congreso Internacional de Quimicos Teóricos de Expresión Latina, Cáceres, Spain, September 16-20, 1996.

- A. Hilger, H. P. Lüthi, R. R. Tykwinski, F. Diederich, "Electronic Structure and Optical Properties of Substituted Tetraethynylethenes", poster presentation at the 36th IUPAC Congress - "Frontiers in Chemistry, New Perspectives for the 2000s", Geneva, Switzerland, August 17-22, 1997.

Table of Contents

Table of Contents i
Abbreviations v
Summary vii
Zusammenfassung xi

1 Introduction 1
- 1.1 Designing Materials and Predicting Properties through Computational Approaches 1
  - 1.1.1 Computational Chemistry Tools 1
  - 1.1.2 How to Establish Structure-Property Relationships and Predict Molecular Properties 3
- 1.2 An Overview on Structure-Property Relationships of Conjugated Organic Molecules and Polymers 4
  - 1.2.1 The Nature of the Conjugated Bridge 6
  - 1.2.2 Influence of the Variation of the Donor or Acceptor Strength and Effect of Derivatization of the Conjugated Bridge 14
  - 1.2.3 Chain Length Dependence 16
  - 1.2.4 Bond Length Alternation as Structural Parameter for Trend Predictions 19
- 1.3 Acetylenic Carbon-Rich Compounds 21
- 1.4 Objectives of the Present Work 25
- 1.5 References 26

2 Molecular Characteristics of Functionalized Diethynylethenes and Tetraethynylethenes 41

2.1 Introduction 41
2.2 Computational Details and Validation Studies 43
  2.2.1 Validation Studies on Tetraethynylethene 45
  2.2.2 Validation Studies on Nitrobenzene 47
2.3 Molecular Structures of Neutral and Reduced Forms of *p*-Nitrophenyl Tetraethynylethene Derivatives 49
2.4 A Look at π-Conjugation in Functionalized Diethynylethenes and Tetraethynylethenes 54
  2.4.1 Impact of the Extent of π-Conjugation: Comparison between Diethynylethene and Tetraethynylethene Architecture 61
  2.4.2 Impact of the Mode of Conjugation: Comparison between Linear and Cross Conjugation 64
2.5 Conclusions 65
2.6 References 67

3 Electrochemical and Electronic Properties of Substituted Tetraethynylethenes 71

3.1 Introduction 71
3.2 Electrochemical Studies of Poly(*p*-nitrophenyl) Diethynylethenes and Tetraethynylethenes: The Experimental Findings 73
3.3 Computational Methodology and Validation Studies 77
3.4 Electronic Structures and Energetics of Tetraethynylethene Derivatives ... 81
  3.4.1 Electronic Characteristics and Electron Affinities of Mono- and *trans*-Bis(*p*-nitrophenyl) Tetraethynylethenes 81
  3.4.2 Modulation of Electron Affinities Through Extension of the π-Conjugation and Through Donor and/or Acceptor Substitution..... 86
3.5 Formation of Charge States in Nitrophenyl Diethynylethene and Tetraethynylethene Oligomers 89
  3.5.1 Polaron-like Radical Anions and Bipolaron-like Dianions as Charge Carriers in Bis(*p*-nitrophenyl) Substituted Tetraethynylethenes........ 89

3.5.2 Experimental Evidence of Bipolaron Formation Through Spectroelectrochemical Studies of Mono- and Bis(*p*-nitrophenyl) Substituted Tetraethynylethenes 93

3.6 Concluding Remarks 95

3.7 References 97

4 *Cis-Trans* Isomerization of Functionalized Diethynylethenes and Tetraethynylethenes 103

4.1 Introduction 103

4.2 Computational Details 106

4.3 Study of the Barriers to Rotation in Bis(*p*-nitrophenyl) Substituted Tetraethynylethene 107

4.4 Electrochemical Isomerization: The Experimental Evidence 111

4.5 Photochemical Isomerization of (*p*-Dimethylaminophenyl) and/or (*p*-Nitrophenyl) Substituted Tetraethynylethenes 113

4.6 Concluding Remarks 117

4.7 References 119

5 Design of Nitrosubstituted Conjugated Systems with High Electron Affinities 125

5.1 Introduction 125

5.2 Computational Details 126

5.3 Results and Discussion 127

5.3.1 Donor- or Acceptor-Substituted TEEs 128

5.3.2 Chain Elongation 128

5.3.3 Nature of the π-Conjugated Backbone 129

5.3.4 One- vs. Two-Dimensional Architectures 137

5.4 Concluding Remarks 139

5.5 References 141

Appendix A 144

Appendix B 152

6 Electronic Spectra of Nitrophenyl and Nitrothienyl Donor-Acceptor Tetraethynylethenes 155

6.1 Introduction 155
6.2 Methodology and Validation of the Computational Procedure 157
6.3 Absorption Spectra and Electronic Transitions 159
  6.3.1 Absorption Spectra of Arylated and Heteroaromatic Tetraethynylethenes 160
  6.3.2 Electronic Transition Analysis 164
  6.3.3 Charge Difference Density Distribution 170
  6.3.4 Exchange of Aromatic Ring: Comparison Between Arylated and Heteroaromatic Tetraethynylethenes 172
6.4 Conclusions 174
6.5 References 176

Abbreviations

α	polarizability
AM1	Austin Model 1
β	first hyperpolarizability
B3LYP	Becke3 exchange functional with Lee-Yang-Parr correlation functional
BLA	bond length alternation
BOA	bond order alternation
CC	Coupled Cluster
CI	Configuration Interaction
CV	cyclic voltammetry
Δl	bond length difference
$\Delta\mu_{ge}$	change in dipole moment between the ground and excited state
DEE	1,2-diethynylethene, hex-3-ene-1,5-diyne
DFT	Density Functional Theory
ε	molar extinction coefficient
EA	electron affinity
E_g	band gap
E_{ge}	optical transition energy between the ground and excited state
E_{max}	lowest energy absorption maximum
γ	second hyperpolarizability
Fc	ferrocene
FF	finite field
$\Phi_{c \to t}$	partial quantum yield of isomerization from *cis* to *trans*
$\Phi_{t \to c}$	partial quantum yield of isomerization from *trans* to *cis*
HF	Hartree Fock

HOMO	highest occupied molecular orbital
INDO	Intermediate Neglect of Differential Overlap
IP	ionization potential
λ_{max}	longest wavelength absorption maximum
LED	light-emitting diode
LUMO	lowest unoccupied molecular orbital
$\mu = \lVert\vec{\mu}\rVert$	ground state dipole moment
μ_{ge}	transition dipole moment between the ground and excited state
$M = \lVert\vec{M}\rVert$	transition dipole moment
MCSCF	Multi Configuration Self Consistent Field
MNDO	Medium Neglect of Differential Overlap
MPn	Møller-Plesset perturbation theory, where n is the order of correction
NBZ	nitrobenzene
NLO	nonlinear optics
PA	polyacetylene
p-NA	*p*-nitroaniline
PPP	poly(*para*-phenylene)
PPV	poly(*para*-phenylenevinylene)
PPy	polypyrrole
PT	polythiophene
PVDZ	polarized valence double-zeta (correlation consistent basis set of Dunning)
QSAR	Quantitative Structure-Activity Relationship
QSPR	Quantitative Structure-Property Relationship
RDE	rotating disc electrode
RHF	restricted Hartree Fock theory
ROHF	restricted open-shell Hartree Fock theory
S_0	ground state
S_1, S_2	excited singlet state
SCF	self consistent field
SOS	sum-over-state
SSV	steady state voltammetry
θ	rotation angle
TEE	tetraethynylethene, 3,4-diethynylhex-3-ene-1,5-diyne
ZINDO	Zerners' INDO

Summary

The theoretical studies described in the present thesis outline the application of computational chemistry techniques to the field of molecular carbon-rich organic materials. The principal topic of this thesis embodies the investigations of the molecular, electronic, and optical characteristics of a series of organic molecules with a delocalized π-electron system that are organized around the unique all-carbon framework of tetraethynylethene (TEE). By analyzing these properties, the project aims to advance the fundamental knowledge of π-electron delocalization in extended acetylenic systems.

Chapter 1 briefly describes computational chemistry and the various approaches applied to the present work. Furthermore, the established significance of computational chemistry techniques as a reliable tool for the design of new compounds and for predicting properties in materials is related. In order to illustrate general design guidelines for the optimization of material properties on the basis of computational investigations, a survey of established structure-property relationships of π-conjugated organic molecules and polymers is then presented. Chapter 1 concludes with an overview of a series of known TEE derivatives which have been used as building blocks for carbon-rich nanometer-sized compounds.

The present study starts with the examination of the molecular structures of the neutral and reduced species of *p*-nitrophenyl substituted tetraethynylethenes (TEEs) and their 1,2-diethynylethenes (DEEs) homologues as described in Chapter 2. One of the most revealing observations from the calculations on *trans*-bis(*p*-nitrophenyl) substituted TEE is that upon reduction the system experiences considerable structural rearrangement, leading to a cumulenic/quinoid form of TEE core and phenyl rings. Most importantly, the cen-

tral bond gains significant single bond character. Further investigations on the extent of π-conjugation upon reduction reveal that, compared to their DEE homologues, the bis(*p*-nitrophenyl) TEE derivatives experience less structural changes on the acetylenic carbon moieties of the core linking the two substituents, but a stronger lengthening of the central bond. This behavior has been explained by the extended π-conjugated framework of the two-dimensional TEE architecture. Finally, the stronger tendency towards bond length alternation observed upon reduction in the *trans*- and *cis*-TEE derivatives compared to the *gem*-TEEs is ascribed to the dominance of the linear conjugation over the cross conjugation pathway.

The electrochemical and electronic properties of a series of (*p*-nitrophenyl) TEE systems are presented in Chapter 3. The experimental observation that the nitrophenyl groups behave essentially as independent redox centers conflicts with the results from the calculations, which clearly predict that the incurred charges are effectively distributed throughout the π-conjugated system. A possible bipolaron formation mechanism rationalizes the two opposing observations.

The dramatic structural change in *trans*-bis(*p*-nitrophenyl) substituted TEE upon reduction suggests that the torsion about the central olefinic bond, which acquires significant single bond character in the dianion, should adopt a very low value. In Chapter 4, this prediction is confirmed by the calculated low barriers to rotation. The resulting facile isomerization in the dianion has been subsequently validated experimentally by the electrochemical *cis-trans* isomerization of a model DEE derivative. Chapter 4 also includes the attempts to explain the experimentally observed *trans-cis* photochemical isomerization of TEEs substituted with electron-donating [*p*-(dimethylamino)phenyl] and/or electron-accepting (*p*-nitrophenyl) groups. Unfortunately, the expected explanation with regard to different isomerization behaviors could not be obtained from the calculated potential energy surfaces.

In Chapter 5, studies concentrate on the calculated electron affinities of a comprehensive series of modeled nitrosubstituted π-conjugated carbon-rich systems, formed of double bonds, triple bonds, and aromatic rings. The following guidelines for the design of novel materials with high electron affinities have crystallized out: the electron accepting nitro group, triple bonds, and a two-dimensionally conjugated framework enhance the electron affinities, whereas, interestingly, the insertion of a phenyl ring between the acceptor substituent and the π-conjugated carbon chain reduces the electron affinities of the modeled compounds if the carbon chain contains at least one triple bond. However, replacement of the phenyl ring by a heteroaromatic group (thiophene and pyridine) seems to result in an increase of the electron affinities.

Finally, in Chapter 6, the calculations of the optical properties of a series of nitrophenyl and nitrothienyl donor-acceptor TEEs are described. The computed electronic absorption spectra excellently reproduce the experimentally observed spectra. The optical characteristics are further analyzed as a function of substitution pattern (*trans*-, *cis*-, or *gem*-orientation of the substituents) and nature of the acceptor substituent (*p*-nitrophenyl or 2-nitrothienyl). As expected, the absorption spectra reveal a bathochromic shift of the lowest energy absorption band upon changing from a geminal cross conjugated substitution pattern to the *trans* and *cis* linearly conjugated paths, demonstrating that cross conjugation is less effective than linear conjugation. The nitrothienyl substituted TEEs absorb at lower energy compared to the nitrophenyl homologues, showing the ability of the thiophene moiety to better participate in the charge delocalization. Most importantly, the calculations can explain the observed intensities of the absorption bands. Of great interest is the second lowest lying energy absorption band of the *trans*-derivatives, which is very weak compared to the *cis*- and *gem*-systems. Analysis of the computed data reveals that the transition moments of the two singly excited configurations describing this band are oriented parallel to each other, but in opposite directions, thus cancelling each other and resulting in a negligibly small oscillator strength.

Leer - Vide - Empty

Zusammenfassung

Die vorliegende Arbeit beschreibt die Untersuchung kohlenstoffreicher Materialen mit Hilfe quantenchemischer Methoden. Im Mittelpunkt stehen dabei die molekularen, elektronischen und optischen Eigenschaften einer Reihe organischer Verbindungen der Klasse der Tetraethinylethene (TEE), die sich durch ein delokalisiertes π-System auszeichnen. Die Analyse dieser Charakteristika soll zu neuen Erkenntnissen über die Delokalisierung von π-Elektronen in erweiterten, acetylenischen Systemen führen.

Kapitel 1 beschreibt zunächst kurz das Gebiet der computergestützten Chemie und die verschiedenen Methoden, welche in dieser Arbeit angewendet wurden. Ferner wird auf die steigende Bedeutung dieser Berechnungstechniken als Werkzeug zum Design neuer Verbindungen und zur Vorhersage deren Materialeigenschaften hingewiesen. Anhand einer Zusammenstellung von Struktur-Eigenschafts-Beziehungen in π-konjugierten Molekülen und Polymeren werden anschliessend einige Strategien zum Design von Materialen mit optimalen Eigenschaften erläutert. Kapitel 1 schliesst mit einer Übersicht bekannter TEE-Derivate, welche als Bausteine in kohlenstoffreichen Nanomaterialen eingesetzt werden.

In Kapitel 2 werden die molekularen Strukturen der neutralen und reduzierten *p*-Nitrophenyl-Tetraethinylethene (TEEs) und *p*-Nitrophenyl-1,2-Diethinylethene (DEEs) untersucht. Von grossem Interesse ist die beobachtete, beträchtliche Strukturänderung im reduzierten *trans*-Bis(*p*-nitrophenyl) substituierten TEE. Die TEE-Brücke nimmt eine kumulenische und die Phenylringe nehmen eine quinoide Form an, während die mittlere Doppelbindung beträchtlichen Einfachbindungscharakter gewinnt. Weitere Untersuchungen über das Ausmass der π-Konjugation in den reduzierten Verbindungen ergaben, dass

die Bis(*p*-nitrophenyl)-TEE-Derivate, im Vergleich zu den entsprechenden DEEs, geringere Strukturänderungen in den acetylenischen Armen und eine längere zentrale Doppelbindung aufweisen. Dieses Verhalten wird durch die erweiterte π-Konjugation des zweidimensionalen TEE Chromophors erklärt. Ausserdem zeigen die reduzierten *trans*- und *cis*-TEEs grössere Strukturänderungen als die geminalen (*gem*) TEE-Derivate, was auf den höheren Wirkungsgrad der linearen Konjugation gegenüber der Kreuzkonjugation zurückzuführen ist.

In Kapitel 3 werden die elektrochemischen und elektronischen Eigenschaften einiger (*p*-Nitrophenyl)-TEE-Systeme vorgestellt. Die Reduktionspotentiale des ersten und zweiten Reduktionsschrittes sind identisch, was auf eine fehlende Kommunikation zwischen Nitrophenylgruppen hindeutet. Die Berechnungen hingegen zeigen deutlich, dass die Ladungen in der reduzierten Verbindung gleichmässig über das ganze π-System verteilt sind. Diese zwei gegenüberstehenden Betrachtungen werden durch einen Bipolaronmechanismus in Einklang gebracht.

Die erheblichen Strukturänderungen im reduzierten, *trans*-Bis(*p*-nitrophenyl)-substituierten TEE deuten auf eine leichte Rotation um die sich bildende zentrale Einfachbindung im Dianion hin. Diese Vorhersage wird in Kapitel 4 durch die berechneten niedrigen Rotationsbarrieren bestätigt. Die freie Drehbarkeit um die zentrale Bindung in der reduzierten Form wurde anschliessend elektrochemisch in der *cis-trans*-Isomerisierung einer DEE-Modellverbindung demonstriert. Versuche zur Erklärung des experimentell beobachteten photochemischen *trans-cis*-Isomerisierungsverhaltens von TEEs, die mit elektronenschiebenden [*p*-(Dimethylamino)phenyl]- und/oder elektronenziehenden (*p*-Nitrophenyl)-Gruppen substituiert sind, werden auch in Kapitel 4 vorgestellt. Die berechneten Energiepotentialkurven konnten leider die unterschiedlichen Isomerisierungsver-halten nicht erklären.

Kapitel 5 konzentriert sich auf die Studie der Elektronenaffinitäten einer represäntativen Serie von nitrosubstituierten π-konjugierten kohlenstoffreichen Systemen, welche aus Doppelbindungen, Dreifachbindungen und aromatischen Ringen gebildet wurden. Folgende Richtlinien für den Entwurf von neuartigen Materialen mit hoher Elektronenaffinität sind aus den Berechnungen hervorgegangen: die elektronenziehende Nitrogruppe, Dreifachbindungen und ein zweidimensional konjugiertes Baugerüst erhöhen die Elektronenaffinität, wogegen die Einführung von Phenylringen zwischen dem Akzeptor und der konjugierter Kohlenstoffkette, die Elektronenaffinität der entworfenenen Verbindungen verringert, falls die Kohlenstoffkette mindestens eine Dreifachbindung enthält. Werden die Phenylringe durch heterozyklische Segmente (Thiophen und Pyridin) ersetzt, scheint eine Zunahme der Elektronaffinität zu erfolgen.

Im abschliessenden Kapitel 6 werden die optischen Eigenschaften einer Serie von Nitrophenyl- und Nitrothienyl-TEE-Derivaten mit Donor-Akzeptor-Eigenschaften beschrieben. Die berechneten Absorptionsspektren stimmen hervorragend mit den experimentell beobachteten überein. Die optischen Eigenschaften werden als Funktion des Substitutionsmusters (*trans*-, *cis*-, oder geminale Orientierung der Substituenten) und des Akzeptor-Typs (*p*-Nitrophenyl- oder 2-Nitrothienylgruppe) untersucht. Wie erwartet, zeigen die *trans*- und *cis*-linear-konjugierten Verbindungen gegenüber den geminal kreuzkonjugierten eine bathochrome Verschiebung der energetisch tiefstliegenden Absorptionsbanden. Diese Beobachtung zeigt deutlich die geringere π-Elektronendelokalisierung durch Kreuzkonjugation. Die Nitrothienyl-TEE-Derivate absorbieren bei tiefer er Energie als die nitrophenylierten Systeme. Dies deutet darauf hin, dass der Thiophenring eine bessere Ladungsverteilung ermöglicht. Die Berechnungen konnten auch die beobachteten Intensitäten der Absorptionbanden erklären. Bei den *trans*-Derivaten weist die energetisch zweittiefstliegende Bande gegenüber den *cis*- und *gem*-Verbindungen eine sehr geringe Intensität auf. Die Analyse der berechneten Daten ergab, dass die Übergangsmomente der zwei Konfigurationen, welche diese Bande bilden, parallel, aber in entgegengesetzter Richtung liegen. Sie heben sich daher auf und formen eine Bande mit äusserst kleiner Oszillatorstärke.

1 Introduction

1.1 Designing Materials and Predicting Properties through Computational Approaches

1.1.1 Computational Chemistry Tools

Over the past few years, the steadily growing number of publications dedicated to the field of computational chemistry,[1] as well as the increasing integration of computational chemistry in chemical education programs,[2-4] evidences the remarkable advances in this discipline. Computational chemistry has become an indispensable, one can even say, a “must-have” tool in almost every area of modern chemical research.[5] The meaning of computational chemistry being somewhat arbitrary and subjective, this first part of the introduction intends to describe the way in which computational chemistry is used in the present work.

Computational chemistry comprises all the areas of chemistry where the computer serves essentially as instrument to solve research problems.[4] It can roughly be divided in the following subfields:

- chemical information processing, and
- “number generating” computational chemistry.

The latter forms the classical area of computational chemistry and consists of molecular modeling applications and molecular graphics.

The modeling applications themselves encompass a wide variety of different theoretical methods, of which three are most commonly employed:

- *Ab initio* quantum chemistry uses quantum mechanics rigorously, *i.e.* these approaches are independent of any experiment. Among first principle methods[6-9] are the Hartree-Fock method, Møller-Plesset perturbation theory (MPn, where n is the order of correction),[10] Multi Configuration Self Consistent Field (MCSCF),[11] Configuration Interaction (CI),[12] and Coupled Cluster theory (CC).[13] An alternative method is Density Functional Theory (DFT).[14-16]
- Semiempirical molecular orbital theories incorporate empirical parameters to determine the two-electron integrals involved in solving the Schrödinger equation.[17-19]
- Molecular mechanics are based on classical concepts and rely on parameters obtained from experiment or other theoretical methods.

Computational chemistry is applied to molecular systems in order to examine structures, energies, and other chemical and physical properties. With the multitude of methods available in numerical quantum chemistry (all the semiempirical methods and *ab initio* approaches), it is important to select the best technique to solve a particular problem. The size of the molecule, the information needed, and the desired quality weighed against the cost of the calculation are some of the criteria that have to be considered in the choice of the method. The advantage of *ab initio* methods is that, in general, they give very good qualitative results and can provide very accurate quantitative results for small molecules. However, these methods often take enormous amounts of computer time, memory, and disk space, and are therefore expensive. Semiempirical methods are usually many orders of magnitude faster than *ab initio* methods, and for some classes of compounds yield results as good or better. Their disadvantage is that they can produce extremely inaccurate results when applied to classes of molecules not included in the parameterization set.

The present work uses mainly with the *ab initio* quantum chemical approach Hartree-Fock (HF), the density functional theory (DFT) method employing Becke's three-parameter hybrid method[20] in conjunction with the Lee-Yang-Parr correlation functional[21] (B3LYP), and the semiempirical methods Austin Model 1 (AM1)[22] and Intermediate Neglect of Differential Overlap (INDO).[23-25] Moreover, visualization techniques are employed in order to represent and analyze graphically chemical systems and properties obtained from the computations.

1.1.2 How to Establish Structure-Property Relationships and Predict Molecular Properties

Driven by a fundamental principle of chemistry, that all the information that determines the chemical, biological, and physical properties of a compound is coded within its structural formula, structure-property relationship methods can be established.[26,27] Structure-property relationships are qualitative or quantitative defined relationships between molecular structure and observed properties. The basic concept of quantitative structure-property relationship methods is to relate the structure of a compound expressed in terms of descriptive parameters (descriptors) that characterize one particular molecular feature (*e.g.*, the number of carbon atoms) to the property of interest (*e.g.*, electron affinity, ionization potential). These mathematical relationships are most often derived by fitting techniques to find the linear or nonlinear correlations between the molecular properties and one or several structural factors of the molecule.[28] When the property being described is a physical property, this is referred to as a Quantitative Structure-Property Relationship (QSPR). When the property being described is a type of biological activity, such as drug activity, this is referred to as a Quantitative Structure-Activity Relationship (QSAR).

Until recently, most QSPR correlations have been derived from experimentally based data, but QSPR models employing *ab initio* and semiempirical calculations are becoming more and more frequent. Quantum chemical calculations can give geometric data, but most importantly, they can also provide information about the electronic properties of molecules which is not available by other means. Among quantum chemical descriptors are charge densities, dipole moments, polarizabilities, highest occupied molecular orbital (HOMO) and lowest unoccupied molecular orbital (LUMO) energies, ionization potentials, electron affinities, and σ- or π-bond order.[26]

The ultimate goal in material research is to create materials with optimal properties for a given application. To design such a novel material, a fundamental understanding of the properties and functions of the existing materials is first developed, and then the ability to predict properties of future materials, *i.e.* a structure-property relationship, has to be established. This begins by studying well-known systems, characterizing their molecular structure, evaluating their molecular properties, and gaining a better insight into the observed phenomena at an electronic level. The molecular properties can be obtained from molecular modeling computations or experimental measurements. The interplay between measurements and calculations leads to a semi-quantitative understanding of properties.

Experimentally determined data are used for comparison and verification of the theoretical methods. Theoretical models, validated by experiment, can be used to examine a wider range of systems. Correlation schemes between physical properties and structures can be derived and extended to the prediction of the properties for hypothetical compounds. The advantage of the quantum chemical approach to material design is that less experiments need to be carried out, thus reducing time and cost of development of new materials. Hence, accurate quantum chemistry studies provide efficient tools to understand the physical bases beyond the phenomena and to derive structure-property relationships, in addition to offer a reliable comparison with experimental data. With the help of the QSPR methodology, the behavior of a material can rapidly be predicted and promising systems, that best fulfill the requested properties for a specific application can be selected and subsequently investigated experimentally. Thus, computational chemistry can give useful guidelines to plan synthetic strategies for designing novel compounds in a more efficient and effective way.[29]

Katritzky et al. stated that, in the 21st century, the QSPR approach will become the tool of choice for many academic and industrial chemists. The enormous benefit of QSPR is that it combines the ability to predict chemical and physical properties of yet unknown compounds with the ability to understand the influence of the structure on a practical chemical or physical property.[27] With materials research being time-consuming and expensive, and computing becoming faster and less costly, computational modeling will undoubtedly gain importance as a design approach for the creation of novel materials.[30]

1.2 An Overview on Structure-Property Relationships of Conjugated Organic Molecules and Polymers

Conjugated organic molecules and polymers are emerging as key materials for practical applications in molecular electronics and photonics, due to their appealing electronic and optical properties. The combination of the semiconducting properties and high luminescence efficiency has made them promising candidates in the development of polymeric light-emitting diodes (LEDs).[31-36] The high optical nonlinearities of π-conjugated organic systems have opened the way to the field of nonlinear optics with its wide application in the photonics-based information and telecommunication technologies of optical signal processing, optical switching, optical sensing, *etc.*[36-42] The advantages of conjugated oligomers and polymers lie in their synthetic flexibility and diversity, and their processability, allowing them to tune the material properties needed for a specific task. Another asset is their thermal and chemical stability. Improvements in processing technologies allow them to become plastics and can ultimately provide light-weight and flexible compounds with excellent mechanical properties.[43] Moreover, they are relatively inexpensive, which is an important criteria for making their way into applications.

Attracted by the manifold of practical applications feasible with organic polymeric systems, numerous groups have concentrated their research efforts on the optimization of the electronic properties and molecular hyperpolarizabilities in organic chromophores, and on understanding the factors that affect conductivity and optical nonlinearities.[44-46] The typical molecular chromophore used in nonlinear optics (NLO) applications comprises an electron donor (D) linked to an electron acceptor (A) by means of a π-conjugated electron system (bridge) such as a benzene ring or polyene, the simplest of which is *p*-nitroaniline. In such a system, there is an asymmetry in the polarization of electrons, leading to a dipole. The π-conjugated bridge provides the pathway for the electronic charge distribution by creating a very narrow energy gap between the valence band and the conduction band, whereas the donor and acceptor substituents provide the required ground state charge asymmetry.

On one hand, the NLO properties are intimately linked to the electronic properties of the conjugated molecules, which can be illustrated using the two-state model expression for the first hyperpolarizability β (eq. 1). This formula is frequently used to describe the trends in β.[47]

$$\beta_{two-level} \propto \Delta\mu_{ge} \frac{\mu_{ge}^{2}}{E_{ge}^{2}} \qquad (1)$$

According to this simple model (eq. 1), the value of β depends on (i) the change in dipole moment between the ground and excited state ($\Delta\mu_{ge}$), (ii) the square of the transition dipole moment ($\mu^{2}{}_{ge}$), and (iii) the inverse of the square of the optical transition energy between the two states ($E^{2}{}_{ge}$). On the other hand, the architecture and length of the conjugated compounds play a significant, even decisive role in the determination of the electronic properties of these π-conjugated systems. Therefore, in order to understand and optimize the NLO behavior of an organic chromophore, a thorough investigation of its molecular and electronic characteristics is of primary importance.[48,49]

In the past few years, numerous experimental research activity as well as theoretical efforts at various levels of computational treatment have concentrated on optimizing the molecular characteristics (electrochemical redox potentials, optical transitions, nonlinear optical responses, *etc.*) in organic chromophores by probing their molecular structure-property relationships.[44,47,50-52] In the following survey, selective examples from the exponentially growing literature on π-conjugated oligomers and polymers have been chosen to illustrate the hitherto established structure-property relationships.

One commonly used approach to design π-electron conjugated chromophores exhibiting optimal properties with substantial interest for further applications is a systematic variation of the molecular construction units. A number of topological criteria which have crystallized out to be useful in designing new generations of chromophores with enhanced electronic and optical properties are reviewed in Sections 1.2.1, 1.2.2, and 1.2.3. The three most commonly used variables which can be classified as topological descriptors in π-bridged donor-acceptor chromophores are

- the nature of the conjugated bridge (aromatic structures such as benzene, thiophene, pyrrole, and nonaromatics like polyenes, polyynes, or some combinations of these) (Section 1.2.1),
- the strength, number, and position of the substituents (Section 1.2.2), and
- the chain length of the π-conjugated bridge (Section 1.2.3).

Another strategy, proposed by *Marder* and coworkers[52-58] is to optimize the electronic and optical properties of a given molecular chromophore by distorting the nature of the conjugation itself. This approach is outlined in Section 1.2.4.

1.2.1 The Nature of the Conjugated Bridge

The type of monomer unit used as the basic building block in the conjugated bridge is an essential structural parameter which modulates the electronic and optical properties of a chromophore by regulating the π-electron delocalization. The strong structural influence of the conjugated bridging fragment on the overall properties of a material controls its suitability for a specific application.

In the field of conducting polymers, major research efforts have been directed towards the investigation of the electrical conductivity and doping characteristics of π-conjugated organic polymers. An important observation was that the band gap E_g *decreased* linearly as a function of *increasing* quinoid character of the backbone. *Brédas* demonstrated by valence effective Hamiltonian (VEH)[59] calculations that in conjugated polymers based on aromatic rings, such as poly(*para*-phenylene) (PPP), polypyrrole (PPy), polythiophene (PT) (Figure 1.1), an upwards-shift in the highest occupied molecular orbital (HOMO) energy and a downwards-shift in the lowest unoccupied molecular orbital (LUMO) energy was noted with increasing quinoid character, thus resulting in a smaller band gap E_g, a lower ionization potential (IP), and a larger electron affinity (EA) than in the aromatic structure.[60] This observation explains that upon n-type or p-type doping, the polymer chain geometry will tend to relax locally around the charges that appear on the chain in order to adopt the quinoid geometry that has a larger EA than the benzoid alternative.

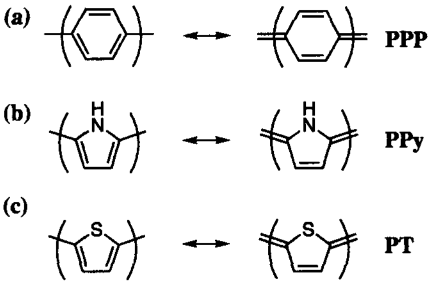

Figure 1.1. Resonance structures (aromatic ground-state structures on the left side and quinoid structures of higher energy on the right side) for (a) poly(*para*-phenylene) (PPP), (b) polypyrrole (PPy), and (c) polythiophene (PT). The quinoid structures give smaller band gaps.

Along the structural modifications imposed to the systems, the band gap E_g of PT was in both configurations (benzoid as well as quinoid) more than 1 eV lower than the one of PPP or PPy. Furthermore, the band gap E_g for PT was reduced to almost zero in the quinoid structure. However, the band gaps of aromatic polymers can never close, since the HOMO and the LUMO belong to the same irreducible representation and therefore, as the two frontier orbitals approach each other, they start to mix, resulting in an increase of the band gap again.

In summary, these results showed that in conjugated polymers based on aromatic rings the band gap E_g does not decrease as a function of *decreasing* bond length alternation as known in polyacetylene-like compounds, but rather as a function of *increasing* quinoid character of the polymer backbone. Furthermore, of the aromatic ring systems considered as possible bridging fragments, PT was best for the design of new organic polymers with small gaps.[60]

Although most of the organic chromophores used in NLO applications contain an aromatic moiety such as a benzene or heterocyclic ring as bridge, a number of theoretical and experimental investigations have suggested that nonaromatic bridges such as polyenes, cumulenes, and polyynes exhibit much larger NLO response properties than comparable aromatic analogues.[53,61-68]

For example, analyzing the optical nonlinearities of 1-(dimethylamino)-4-nitro-*cis*-buta-1,3-diene (**1**), which mimics best the conjugation path of the benzenoid bridging moiety of *p*-nitroaniline (*p*-NA, **3**), the first hyperpolarizability β of **1** has been predicted by the sum-over-states (SOS) approach to be about twice that of the aromatic counterpart *p*-NA.[69] The β-value of 1-(dimethylamino)-6-nitro-*trans*-hexa-1,3,5-triene (**2**), having the same number of π-electron centers as *p*-NA (**3**), has been found to be about five times larger than the one of *p*-NA.[67,69] The smaller response of *p*-NA could be explained by the difficulty of polarizing an aromatic bridge. Restricted Hartree-Fock (RHF) self consistent field (SCF) calculations on oligomers of poly(*p*-phenylene), polypyrrole, and polythiophene have indicated that going from fully aromatic to a fully quinoid structure costs about 15-20 kcal/mol per ring.[70] The electronic redistribution in the benzoid ring, coupled with the bond length rearrangement, is thus hindered, resulting in a reduced NLO response.[71]

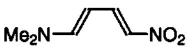

1

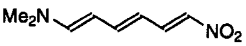

2

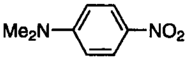

3

Polyenes are often used as π-conjugating units in NLO active materials, as they provide the most effective pathway for an efficient charge transfer between the donor and acceptor groups.[53,72] *Albert*, *Morley*, and *Pugh* have computed the nonlinear optical coefficients β and γ of a series of donor-acceptor functionalized oligomeric chains using the correction vector approach on the basis of a modified Complete Neglect of Differential Overlap (CNDO) method including singly and doubly excited configurations (SDCI). They predicted the donor-acceptor polyenes **4** to be significantly more efficient NLO systems than the corresponding polyynes **5**, which in turn have been superior to the corresponding polyphenyls **6**.[73,74] In donor-acceptor polyynes **5** and polyphenyls **6**, respectively, the charge localized at the end groups to preserve the energetically favored acetylenic form or the aromatic stabilization in the center of the π systems, respectively. *In polyene derivatives **4**, on the other hand, the neutral and charge separated forms* consisted of similar π system with alternating single and double bonds that are isoenergetic and thus, allow more effective charge delocalization. These energetic consideration may account for the enhanced NLO properties of polyenes **4**.

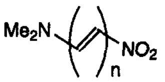

4

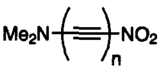

5

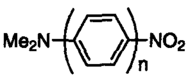

6

The first hyperpolarizabilities β of donor-acceptor disubstituted α,ω-diphenylpolyenes **7** and the corresponding disubstituted α,ω-diphenylpolyynes **8** (D=donor, A=acceptor) have been calculated by a finite-field (FF) approach with the PM3-parametrization of the semiempirical Medium Neglect of Differential Overlap (MNDO) Hamiltonian. The results confirmed that polyynes (**8**) are less efficient than the homologous polyenes (**7**).[44,64,65]

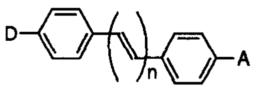

7

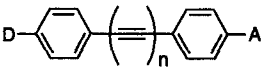

8

An explanation of the higher efficiency of *polyenes* can be found in the consideration of the electronic transition states. Whereas only one major charge transfer state, namely the HOMO-LUMO transition, contributes to the polarization of the donor-acceptor *polyenes*, there are several states with large oscillator strength that determine the hyperpolarizabilities values in the *polyynes*. These additional states are mainly derived from transitions involving p_y orbitals in the perpendicular π-system. The transition moment vectors of these π-electron contributions oppose the usual direction of charge transfer along the chain from donor to acceptor and, thus, negatively influence the overall value. These extra components of opposite sign are the consequence of having two π-electron planes in the acetylenic bridge. [61,75-77]

From the previous discussions, it becomes clear that incorporation of benzene rings into the donor-acceptor polyenes has been observed to limit the hyperpolarizabilities. The barrier due to the aromatic delocalization energy of the benzene ring is believed to be responsible for the reduced values. To overcome the problem of limitation of molecular nonlinearities, recently several groups have shown that utilizing easily delocalizable five-membered heteroaromatic rings instead of homocyclic rings as chromophore bridge leads to enhanced NLO responses.[63,71,78-82] The benefit of heteroaromatic rings *vs.* benzene moieties is that it costs less energy to break the aromatic stabilization, while substantial thermodynamic stabilization is retained.

Rao et al. studied several classes of donor-acceptor compounds, where benzene was replaced by a wide variety of heterocycles containing one heteroatom, such as thiophene, furan, and pyrrole (X or Y=S, O, or NH, respectively, **9–12**) or two heteroatoms, such as thiazole, oxazole, and imidazole (X=S, O, or NH, respectively, **13** and **14**) as a conjugating bridge.[83]

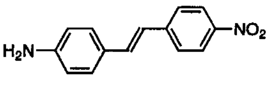

9

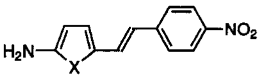

10

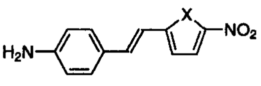

11

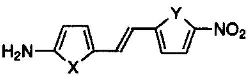

12

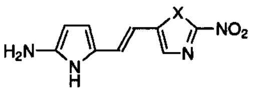

13

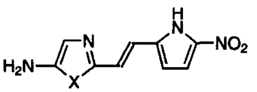

14

The computations in that study used the Hartree-Fock (HF) and semiempirical AM1 method for the geometry optimizations. Properties associated with the lowest excitation process were determined at the AM1/SCI level, whereas the first hyperpolarizabilities were studied by the finite field (FF) method, the coupled perturbed Hartree-Fock (CPHF) procedure, and the sum-over-states (SOS) approach. The computed values for the transition wavelength λ_{max}, the change in dipole moment between ground state and first excited singlet state $\Delta\mu$, and the first hyperpolarizability β indicated that the replacement of benzene rings in the substituted stilbene **9** with heteroaromatic rings significantly altered the molecular properties. In accord with the relation described by the simplified two-state model for β (eq. 1), the systems with longer transition wavelength λ_{max}, *i.e.* lower optical transition energy E_{ge}, and larger dipole moment change $\Delta\mu_{ge}$ were computed to have a higher β. Smaller energy differences E_{ge} between the ground and charge-transfer excited states generally result from a more extended conjugation, thus, leading to a more efficient charge polarization. The resulting higher dipole moment change $\Delta\mu_{ge}$ makes a compound a better candidate for enhanced second-order nonlinear responses.

It was observed that the effects were more pronounced with rings containing two heteroatoms (**13**, **14**). The magnitude of variation of λ_{max}, $\Delta\mu$, and β with respect to the model stilbene **9** depended on both the nature of the heteroaromatic ring and its position in the molecular framework. The replacement of the phenyl ring on the *donor* end of **9** caused the properties enhancement effect to decrease in the order pyrrole > furan > thiophene for monoheterorings (**10**), and imidazole > oxazole > thiazole for diheterorings (**14**). On the other hand, in molecular systems where the same heteroaromatic rings (**11** and **13**) were present on the *acceptor* end, the opposite trends were noted. The larger β values were thus obtained when pyrrole was placed on the *donor* end in system **10**, and the thiophene and thiazole ring were positioned at the *acceptor* end of systems **11** and **13**. Similar trends were obtained from the calculation for doubly heteroaromatic compounds **12**. System **12**, with pyrrole on the *donor* and thiophene on the *acceptor* end, was predicted to be the most active one. Within the series of molecules, two thiophene units present in the system led to enhanced second-order NLO activity compared to just one thiophene. Experimental β values obtained for the thiophene compounds support the conclusions drawn from the calculated data.[78]

The observed trends in the molecular characteristics were rationalized by analyzing the delocalization energy and the electronic nature of the ring systems. First, the energy barrier imposed by the conjugating bridge significantly affects the coupling between the donor and acceptor substituents. The lower the aromatic delocalization energy barrier of the bridge, the higher the first hyperpolarizabilities should be. The five-membered heteroaromatics thiophene (29 kcal/mol), pyrrole (21 kcal/mol), and furan (16 kcal/mol) possess lower delocalization energy relative to benzene (36 kcal/mol)[84] and are expected to be more effective than benzene in promoting charge transfer, thus increasing β. However, since the position of the heterocyclic ring determines the nonlinear properties of molecules as well, the computed β values did not follow a simple increasing pattern along the series benzene, thiophene, pyrrole, and furan, expected from the decreasing order of aromaticity of the rings.

Indeed, the Hückel derived as well as the semiempirical INDO computed carbon atom electron densities showed that the electron richness or deficiency of the π-conjugating bridge, *i.e.* the heterocycle in this case, can alter the electron-donating and -accepting ability of the substituents, and thereby change the effective charge transfer and molecular nonlinearity.[83] The electron richness of the five-membered rings varies in the order pyrrole > furan > thiophene > benzene, the last of which is neither electron rich nor deficient. The electron deficiency of the rings with two heteroatoms follows the order thiazole > oxazole > imidazole.[84] The actual effect is that, as the electron richness of the heterocyclic systems decreases, the donor ability of the amino substituent decreases since electron withdrawal of the heterocycle from the amino group through inductive effects increases. Similarly, with a decrease in electron richness of the heterocycles, the acceptor ability of the nitro group increases because of the electron donation from the heterocycle to the nitro group decreases.

Pyrrole, being the most *electron-rich* five-membered heteroaromatic ring considered, augmented the donor ability of the amino group in **10** resulting in a more pronounced charge transfer and an increase in $\Delta\mu$ and β. In **11**, on the other hand, pyrrole counteracts the electron-withdrawing effect of the nitro group resulting in a decrease in $\Delta\mu$ and β. In contrast to the monoheterocycles, rings with two heteroatoms (such as thiazole, oxazole, and imidazole) are *electron-deficient* in nature, due to the –C=N– linkage. Thiazole being the most electron-deficient ring assists the nitro group resulting in a more pronounced electron-accepting effect in **13** and counteracts the electron-donating effect of the amino group in **14**.

In conclusion, this study by *Rao* et al. speculated that the *electron density* criterion governed the electronic and second order NLO properties, as the heterocycle acted as an additional donor in the bridge.[83]

Ratner and coworkers investigated the origin of the variation in the NLO response with the nature of the bridge by examining similar donor-acceptor substituted chromophores composed of one five-membered and one six-membered heterocycle (**15**,**16**) where X = CH=CH, S, or O and Y, Z = CH, or N.[69] The NLO properties were calculated with the correction vector approach, using the INDO method. They demonstrated that the second order NLO coefficients were influenced more by the bridge *electron density* than by the reduced *aromaticity* of the heterocycle compared to the benzene ring.

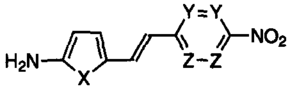

15

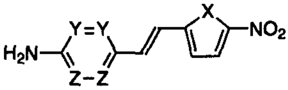

16

In the series of molecules **15**, the longest absorption wavelength λ_{max} and the nonlinearity β increased with the increase in electron richness on the *donor* end and electron deficiency on the *acceptor* end (electron deficiency of the six-membered rings follows the order tetrazine ≈ triazine > diazine > pyridine > benzene). The opposite trend was observed for series **16**. Additionally, it was observed that the effect of the electron-rich ring was far stronger than that of the electron-poor ring. Thus, of the three electron-rich five-membered heterocycles examined, pyrrole, being most electron-rich, clearly had the strongest effect on the NLO properties.

In summary, appending a strong donor to an electron-rich system such as pyrrole, furan, or thiophene and a strong electron acceptor to an electron-deficient system such as pyridazine or tetrazine yields chromophores with substantially larger NLO responses. Clearly, the electron density criterion has proved to be significant and useful for optimizing new chromophores with enhanced second order NLO properties.

1.2.2 Influence of the Variation of the Donor or Acceptor Strength and Effect of Derivatization of the Conjugated Bridge

The strength and the position of donor and acceptor substituents on a conjugated backbone are essential parameters that influence the molecular, electronic, and optical properties of organic materials.

Brédas and coworkers studied the molecular and electronic characteristics of butadienes **17**-**19** end capped with different electron donor (D = $-NH_2$, $-NMe_2$, $-OH$) and electron acceptor substituents (A = $-CHO$, $-CN$, $-NO_2$).[85] The geometry optimizations were carried out with the semiempirical AM1 method, and based on these geometries, the Intermediate Neglect of Differential Overlap/Multi-Reference Determinant-Configuration Interaction (INDO/MRD-CI) method was used to describe the lowest singlet excited states of the investigated systems. By comparison with unsubstituted butadiene, the largest geometric modifications and charge transfers occurred in the D/A derivatives **17**. The largest bathochromic shift of the first transition energy was also found in the D/A substituted compounds **17** followed by the D/D (**18**), and finally the A/A (**19**) derivatives.

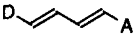

17

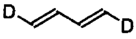

18

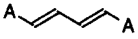

19

Furthermore, the transition energy in D/A derivatives **17**, which depends on the strength of the coupling between the end groups, decreased with increasing π-donating or π-accepting strength. This behavior demonstrated a more effective π-charge redistribution in the bis(dimethylamino) and bisnitro functionalized systems.

The highest polarizabilities α and second hyperpolarizabilities γ were calculated for the D/A derivatives **17** based on the SOS approach. The maximal enhancement of α and γ was achieved with the strongest π-accepting respectively π-donating group, *i.e.* the NMe_2/NO_2 combination. For the symmetric chains, higher α and γ values were obtained by attaching electron-accepting end groups (in **19**) rather than donor substituents (in **18**). Whereas in the D/D-substituted **18**, the α and γ values depended on the nature of the substituent, less variations between different substituents were observed for the A/A compounds **19**. In summary, the expected enhancement of the first optical transition and the nonlinearities β and γ with unsymmetric substitution and increasing donor and acceptor strength was confirmed.

PPV and its derivatives have been exploited as active layer in light-emitting diodes (LEDs), due to their high yield of electroluminescence and their ease of processability.[32,33] *Brédas* and coworkers also investigated the influence of derivatization by donor (methoxy) and/or acceptor (cyano) groups on the geometries and electronic structures (band gap E_g, HOMO, and LUMO energies) of poly(*para*-phenylenevinylene) (PPV) **20**-**25**.[86-88] The geometries were optimized by means of the AM1 technique, whereas the transition energies were determined using the INDO/SCI approach.

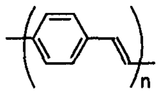

20

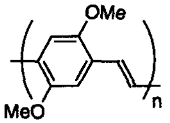

21

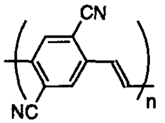

22

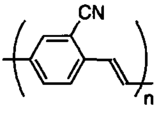

23

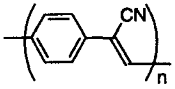

24

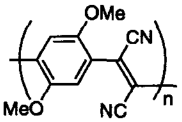

25

Through inductive effects within the σ-framework, the side groups exclusively increased the length of the two adjacent C–C bonds in the ring or the vinylene units to which they were connected. Analysis of the electronic structure showed that substitution by methoxy donor groups (**21**) led, with respect to unsubstituted PPV **20**, to an asymmetric *destabilization* of the frontier orbitals, whereas substitution by cyano acceptor groups (**22**) provided an overall asymmetric *stabilization* of the frontier levels. The methoxy donors had a larger impact on the valence band (HOMO), while the cyano acceptors affected more strongly the conduction band (LUMO). Considering monocyano derivatives, the stabilization effect was calculated to be more significant when the cyano group was located on the vinylene moiety (**24**) than on the phenyl ring (**23**), thus forming a smaller band gap in compound **24**. The use of combined methoxy and cyano substituents (**25**) allowed a significant stabilization of the LUMO band and a less pronounced stabilization of the HOMO band, resulting in a strong red shift of the optical band gap versus **20**. Upon derivatization, the changes of the lowest lying transition energy E_{ge} followed the trends calculated for the HOMO-LUMO gap. The variation in the red shifts of E_{ge} with different substitution patterns rationalized the color modulation observed in LED devices when going from PPV to a derivatized polymer chain as active layer.[32-34]

1.2.3 Chain Length Dependence

In conjugated compounds, an important consideration in predicting physical properties and tailoring organic compounds for a specific task is the extent to which polymer properties can be deduced from extrapolating oligomer data, *i.e.* the dependence of the molecular characteristics on chain length. A simple method is to plot the physical properties *vs.* the reciprocal chain length (1/n), with n being the number of monomer units.

The valence effective Hamiltonian (VEH) calculations by *Brédas* and coworkers showed that for polyacetylene (PA), poly(*para*-phenylene) (PPP, **26**), polythiophene (PT, **27**), polypyrrole (PPy, **28**), and poly(*para*-phenylenevinylene) (PPV, **20**) a linear relationship exists between the inverse conjugation length 1/n and the band gap E_g. In the analyzed series, the E_g value decreases in the order PPP > PPy > PPV > PT > PA.[60,90]

They also investigated the dependence of the first vertical transition energies on the chain length with the Intermediate Neglect of Differential Overlap/Multi-Reference Determinant-Configuration Interaction (INDO/MRD-CI) method. The calculated first transition energies of PPP **26**, PT **27**, PPy **28**, and PPV **20** decreased with increasing chain length as a result of the extension of the π-conjugated path.[91,92] Assuming a linear evolution of the first transition energies with respect to 1/n, extrapolation to an infinite chain length of the calculated transition energies led to a bandgap value of 2 eV for PT **27**,[93] of 2.3 eV for PPy **28**,[94] and of 2.85 eV for PPV **20**.[95] As stated above, the band gap decreased with increasing quinoid character in the backbone geometry. As quinoid resonance structures contribute more to the electronic configuration of polythiophenes than of polypyrrole and poly(*para*-phenylene),[84] the sequence, PT < PPy < PPV, of the vertical transition energies was in accord with this observation.

PPP

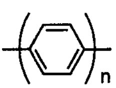

26

PT

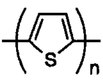

27

PPy

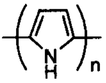

28

PPV

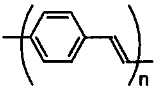

20

As already mentioned, an enhancement in the electronic and optical properties is anticipated with increasing π-conjugation length of the bridge. An important issue is to know at what chain length, saturation of the property occurs. To evaluate the saturation point of NLO effects, the first and second hyperpolarizabilities, β and γ, can generally be related by a power law (eqs. 2 and 3) to the number of repeat units, n, where z is a constant.[44,45,89] The exponent z represents the efficiency of an increase in β or γ with the increase of the system size. The exponent z itself depends on the chain length n. Saturation is reached when the exponent z tends to 1.

$$\beta \; or \; \gamma \propto n^{z} \tag{2}$$

$$\log \beta \; or \; \log \gamma \propto z \log n \tag{3}$$

Brédas and coworkers have found that the evolution of γ in PT **27** and PPy **28** can be divided into three regimes: Initially, the γ response picks up significantly with chain length. Then, for PT, at the ring numbers n = 3-6, the exponent stays nearly constant with z = 3.9. For PPy, the exponent z amounts to 4.9 for n = 3-7. Finally, from the ring number n = 6 for PT and n = 7 for PPy on, the exponent starts to decrease, indicating the beginning of the saturation regime.[98] In their studies, the second hyperpolarizabilities γ have been evaluated through the SOS approach. The γ values calculated for PPy are about three times smaller than those reported for PT. In oligopyrroles, the π-electrons are thus less easily delocalized along the chain axis than in oligothiophenes. This is in agreement with the observation that the larger the electronic delocalization along the chains, the slower the saturation regime is reached.[94,99]

Albert, *Morley*, and *Pugh* concentrated their research efforts on the donor-acceptor substituted polyenes **4**, polyynes **5**, and polyphenyls **6**. The dipole moments and transition energies of these conjugated systems were evaluated using a modified Complete Neglect of Differential Overlap (CNDO) method including singly and doubly excited configurations (SDCI) and the NLO properties were calculated using the correction vector approach.[73] They observed, on adding conjugation units, n, to the π-backbone of donor-acceptor substituted compounds (**4**-**6**), a dramatic red shift in the calculated longest wavelength absorption maximum λ_{max} accompanied with an increase of the ground state dipole moment μ_g. Analogous to the unsubstituted oligomers, the band gap E_g reached a limit upon increase of the π-conjugated chain length. The calculated λ_{max} and μ_g of the longer polyphenyls (**6**) and polyynes (**5**) tend to saturate at a smaller number of monomer units, n, than the corresponding polyenes (**4**). This originates from the fact that the resonance structures of the bridges of polyphenyls (**6**) and polyynes (**5**) are not isoenergetic, in contrast to the bridges of polyenes (**4**).

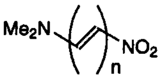

4

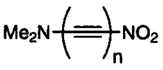

5

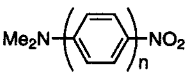

6

The magnitude of the calculated values for the considered properties, *i.e.* μ_g, λ_{max}, polarizability α, and hyperpolarizabilities β and γ, followed the order polyphenyls (**6**) < polyynes (**5**) < polyenes (**4**).[73] At short chain length n=1, the β and γ differences between the three molecules were not significant. However, on chain extension, β and γ of the donor-acceptor substituted polyynes (**5**) exceeded those calculated for the polyphenyls (**6**) by a factor of 2-3 at n=8. The β and γ values for the polyenes (**4**) exhibited the sharpest ascent with increasing chain length partly because of their large red shift in the λ_{max} values. Furthermore, the NLO responses in polyyne and polyphenyl architecture saturated rapidly at a shorter conjugation length compared to polyenes. This evolution was similar to the behavior of the experimental[96,97] and calculated[75] first hyperpolarizabilities β obtained for α.ω-diphenylpolyyne structures **8** containing one and two bridging triple bond units. There was only one dominant charge transfer state for the polyenes (**4**) and polyphenyls (**6**), whereas the polyynes (**5**) showed a clustering of multiple charge transfer states. The early saturation of the hyperpolarizabilities in donor-acceptor polyynes was attributed to the configuration mixing of in-plane and out-of plane $\pi \rightarrow \pi^*$ transitions, reducing the contribution of the lower excited states to the first hyperpolarizabilities β.[61]

Matsuzama and *Dixon* studied the nonlinear optical responses of a series of 4,4'-disubstituted α,ω-diphenylpolyenes **7**, as well as 4,4'-disubstituted α,ω-diphenylpolyynes **8**

(D=donor, A=acceptor) by a finite-field (FF) approach with the PM3-parametrization of the semiempirical Medium Neglect of Differential Overlap (MNDO) Hamiltonian and evaluated the exponents of the power law (eq. 2).[65] With n describing the number of carbon atoms, z-exponents of 2.0-2.6 and 0.03-0.04 were obtained for the β dependence in polyenes **7** and polyynes **8**, respectively. For γ, the ranges were 3.9-4.9 and 2.9-3.3 for polyenes **7** and polyynes **8**, respectively. The small z-exponent for β in polyynes **8** showed that the saturation region started already after one or two bridging units, whereas the z-exponent of the polyenes **7** exhibited a steeper ascent. These results confirmed the efficiency of enhancing the hyperpolarizabilities by having a polyene bridge.

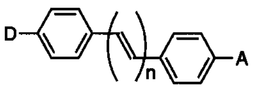

7

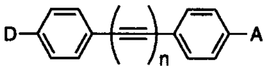

8

Conclusively, computational studies on oligomers and polymers, such as polyenes, polyynes, polythiophenes, and polypyrroles have shown that the variation of the nature of the conjugating bridge, the strength and position of donor and acceptor substituents, and the chain length, affect the extent and efficiency of π-conjugation. This ultimately has a tremendous effect on the molecular linear and nonlinear optical responses. Generally, the optical nonlinearities increase with increasing π-electron conjugation length up to an asymptotic intermediate chain length. The computations suggest that a judicious choice of bridges and donor/acceptor substituents, coupled with design principles like electron deficiency and richness, as well as aromaticity, can result in significantly enhanced molecular linear and nonlinear optical responses.

1.2.4 Bond Length Alternation as Structural Parameter for Trend Predictions

As proposed by *Marder* and coworkers, optimized NLO responses of a given molecular chromophore can be achieved by distorting the conjugated bridge from an unperturbed polyenic-like structure (**29**) toward a partially ionic cyanine-like fully delocalized structure (**30**), continuing toward the limit of a localized, but charge separated polymethine-like structure (**31**).[53-58] The distortion is controlled by adjusting the strength of the donor and acceptor substituents and solvent polarity. Indeed, solvent effects have profound influence on the structure and electronic properties of organic materials with extended π-conjugations.[100-104] A useful concept to quantify these effects is the bond length alternation (BLA), defined as the average difference in length between adjacent bonds in the conjugated pathway, or a closely related parameter, the average π-bond order alternation (BOA). As a consequence of strong bond length alternation, large changes in the linear and nonlinear response properties are found.

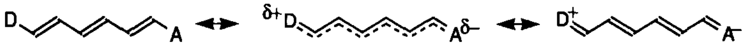

29 **30** **31**

Increasing Donor/Acceptor Strength, Solvent Polarity

In order to account for the medium influences on the molecular geometry and consequently on the optical properties, computational strategies follow the evolution of the molecular properties via application of an external field to modulate the ground state polarization and concomitantly BOA. *Brédas* and coworkers investigated the dependence of the first α, second- β, and third-order γ polarizabilities on ground-state polarization for a series of donor-acceptor polyenes donor-acceptor polyenes using the sum-over-states (SOS) technique.[58] It has been shown that distorting the BLA from a polyene-like structure **29** to a polymethine-like structure **30** tunes the electronic and NLO characteristics of the chromophore. The lowest first excited state experienced a red shift with the evolution from the neutral polyene structure **29** to the cyanine limit **30**, and then a blue shift occurred with the evolution from the cyanine **30** to the zwitterionic limit **31**. Analysis of the curves displaying the NLO responses *vs.* BLA gave the following predictions. The first polarizability α has a maximum at the cyanine limit **30**. Whereas β passes through zero at the cyanine limit **30**, γ shows a minimum. For an intermediate polyene/cyanine structure β has a maximum, while γ approaches zero. Numerous recent studies of several oligomeric and polymeric chromophores supported these evolutions.[100-105]

1.3 Acetylenic Carbon-Rich Compounds

Tetraethynylethene (TEE, 3,4-diethynylhex-3-ene-1,5-diyne, **32**) and its derivatives represent a class of two-dimensionally conjugated building blocks with established potential as precursors to carbon-rich nanometer-sized compounds with unusual structures, high stability, and useful electronic and nonlinear optical properties.[107,108] The first member of this class, tetrakis(phenylethynyl)ethene (**33**), was described in 1969 by *Hori* et al.[109] and was followed several years later by the persilylated derivative (**34**) synthesized by *Hauptmann*.[110-112] *Hopf* et al. later conveyed an alternative synthesis of **33**, as well as its X-ray crystal structure.[113] A synthesis of the parent unprotected molecule **32** was first reported by *Diederich* and coworkers in 1991.[114]

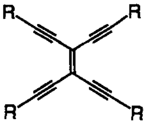

32 R=H
33 R=Ph
34 R=$SiMe_3$

Since then, the chemistry of TEEs has prospered considerably, so that now synthetic routes to virtually any desired protection and/or substitution pattern about the central ten carbon core have been achieved.[115-117] The synthetic flexibility inherent to these systems has allowed them to function as a "molecular construction kit" for the preparation of acyclic[118] and macrocyclic acetylenic compounds[119-122] as well as for polymerization into rod-like linear oligomers and polymers with the conjugated polytriacetylene (PTA) backbone like **35**.[123-129] PTA oligomers and polymers (**36**) have also been constructed starting from 1,2-diethynylethenes (DEEs, hex-3-ene-1,5-diynes).[128,130]

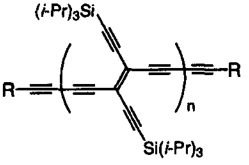

35

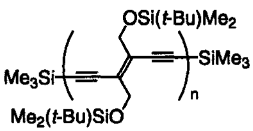

36

Moreover, these carbon-rich compounds have also attracted the interest of theoreticians and *ab initio* calculations have been carried out on the molecular and electronic structures of several acetylenic monomeric precursors. The equilibrium geometries of tetraethynylmethane (C_9H_4), tetraethynylethene ($C_{10}H_4$), tetraethynylallene ($C_{11}H_4$), tetraethynylbutatriene ($C_{12}H_4$), and hexaethynyl[3]radialene ($C_{18}H_6$) have been determined with the Hartree-Fock method using a double zeta plus polarization basis set.[131,132] Good agreement between experiment and the calculated geometries have been achieved for the known $C_{10}H_4$, $C_{12}H_4$, and $C_{18}H_6$. For C_9H_4, however, the experimental triple bonds are considerably shorter (by 0.05 Å) and the C(sp$_3$)–C(sp) single bonds are slightly longer. Crystal packing effects may be one of the reasons for the difference between theory and experiment. Furthermore, comparing the theoretical geometries, it has been noted that the C–C single bond of $C_{11}H_4$ (1.449 Å) is longer than that of both $C_{10}H_4$ and $C_{12}H_4$ (1.440 Å). The reason for this bond length difference has been attributed to the D_{2d} symmetry of $C_{11}H_4$, since π-electron delocalization between the acetylenic and the cumulenic groups is less effective in the nonplanar configuration.

In order to enhance the appeal of TEEs as potential materials for electronics and photonics, electron donating and electron accepting functionality have been attached to the planar TEE chromophore. A diverse library of monoarylated (**37**,**38**), *trans*-diarylated (**39**-**41**), *gem*-diarylated (**42**-**44**), tris- (**45**,**46**) and tetrakisarylated (**47**-**52**), as well as heteroaromatic (**53**-**55**) donor and/or acceptor functionalized TEEs have been prepared.

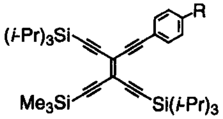

37 R = NO_2

38 R = NMe_2

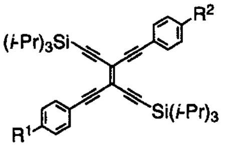

39 $R^1 = R^2 = NO_2$

40 $R^1 = R^2 = NMe_2$

41 $R^1 = NO_2$, $R^2 = NMe_2$

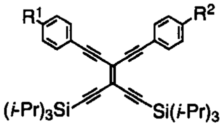

42 $R^1 = R^2 = NO_2$

43 $R^1 = R^2 = NMe_2$

44 $R^1 = NO_2$, $R^2 = NMe_2$

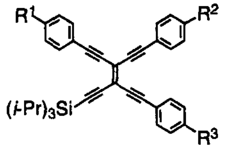

45 $R^1 = R^2 = R^3 = NO_2$

46 $R^1 = R^2 = OMe, R^3 = NO_2$

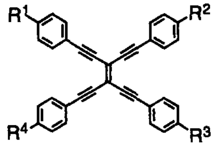

47 $R^1 = R^2 = R^3 = H, R^4 = NO_2$

48 $R^1 = R^3 = H, R^2 = R^4 = NO_2$

49 $R^1 = R^2 = H, R^3 = R^4 = NO_2$

50 $R^1 = R^2 = NO_2, R^3 = R^4 = NMe_2$

51 $R^1 = R^3 = NO_2, R^2 = R^4 = NMe_2$

52 $R^1 = R^4 = NO_2, R^2 = R^3 = NMe_2$

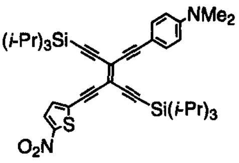

53

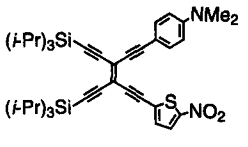

54

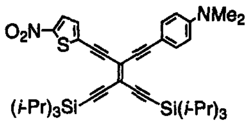

55

The expanded, conjugated eneyne carbon cores of functionalized TEEs are ideal for studying conjugation effects because, in contrast to similar structures such as *cis*-stilbenes[133-136] and tetraphenylethenes,[137,138] TEEs have a fully planar, sterically unencumbered framework. The aryl rings with the pendant donor and/or acceptor (D/A) functionalities are sufficiently remote from each other as to prevent unfavorable steric interactions, and thus electronic effects can be isolated from steric influences. X-ray structural analyses of several silyl- and D/A-substituted arylated TEEs have shown that nearly perfect planarity is maintained across the entire conjugated π skeleton including the aryl rings.[113-115,139-143]

By varying the attachment of the substituents to the planar TEE backbone, different conjugation pathways emerge. One-dimensional linear *trans*- or *cis*-donor-acceptor conjugation (Figure 1.2 pathways (a) and (b), respectively) is much more effective than geminal substitution cross conjugation (Figure 1.2 pathway (c)). With functional groups attached at all four ends, a total of six conjugation pathways provide a complete, two-dimensional conjugation combining two linear *trans*-conjugation (a), two linear *cis*-conjugation (b), and two geminal cross conjugation (c) paths (Figure 1.2).

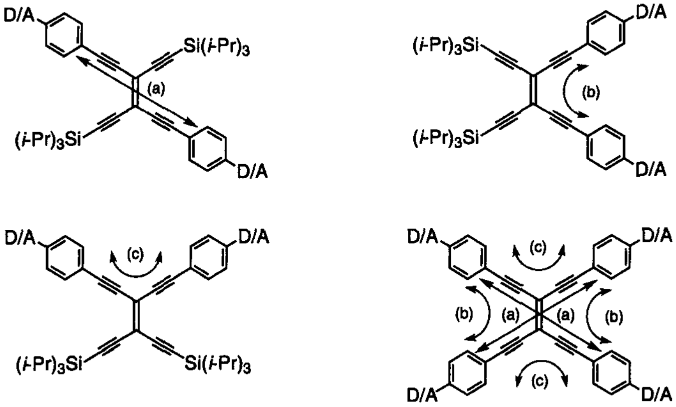

Figure 1.2. Schematic Representations of Possible Conjugation Paths in Donor and/or Acceptor (D/A) Substituted Tetraethynylethenes (TEEs).

The extent and mode of π-conjugation (linear, cross, or two-dimensional conjugation), the degree of functionalization (mono-, di-, tri-, or tetra-substitution), and the donor-acceptor strength govern molecular properties such as electronic absorption,[142,143] luminescence,[142,143] redox behavior,[144,145] and nonlinear optical responses[146-149] in these highly conjugated TEE chromophores. From systematic investigations of these properties, structure-property relationships have been established. The UV/Vis spectra of donor-acceptor substituted TEEs reveal a bathochromic shift of the longest wavelength band (λ_{max}) with (i) changing from geminal orientation of the substituents to *cis* and *trans* linear conjugation pathways, (ii) increasing conjugation length, and (iii) increasing the number of *trans*-donor-acceptor pathways upon tetrakisfunctionalization, *i.e.* generation of two-dimensional conjugation.[142,143] Furthermore, the third-order nonlinear optical coefficients γ are raised by increasing (i) the degree of donor substitution, (ii) the donor strength, (iii) the length of the conjugation path, and (iv) the number of linear donor-acceptor conjugation pathways in the molecules, *i.e.* full two-dimensional conjugation strongly enhances γ. Moreover, acentricity leads to larger γ-values than centrosymmetry, whereas cross conjugation is less favourable for realizing high γ-values.[146,149]

1.4 Objectives of the Present Work

Of great interest for the design and preparation of materials as candidates for applications in the emerging fields of electronics and photonics is the ability to predict the physical properties of these novel materials. Whereas a wide variety of new compounds based on the unique molecular construction units 1,2-diethynylethene (DEE) and tetraethynylethene (TEE) have been synthesized and characterized by UV/Vis spectroscopy, fluorescence, electrochemical analyses, and third harmonic generation (THG) measurements, very little has been probed by theoretical work.

To investigate the evolution of molecular properties in these acetylenic π-conjugated systems, the theoretical studies in this project focus on a series of molecules built from the conjugated, functionalized building blocks DEE and TEE. The determination of the molecular structures, electronic characteristics, and optical properties of functionalized DEEs and TEEs are targeted in the present work.

The molecular characteristics used as set of conformational descriptors are the mode of π-conjugation (linear *trans* and *cis*, and cross geminal conjugation), the extent of conjugation (DEE and TEE architecture), the nature of the building units (double bonds, triple bonds, aromatic moieties, and combinations of these), the type of substituent (π-donor or π-acceptor group), and the type of the end capped aromatic fragment (phenyl and thiophene ring). The set of properties investigated consists of the molecular geometry, the charge density, the electron affinity, and the electronic transition spectrum. The analysis of the obtained results provides the first step toward establishing structure-property relationships for these materials. Information gained from this study at the molecular level also targets to improve the understanding of the underlying observed properties in these extended acetylenic π-conjugated systems.

1.5 References

[1] For a book series of reviews and tutorials see: K. B. Lipkowitz, D. B. Boyd, *Reviews in Computational Chemistry*; Verlag Chemie: New York, 1990.

[2] H. P. Lüthi, G. Vacek, A. Hilger, W. Klopper, in *Computational Chemistry: Reviews of Current Trends*; World Scientific Publishing: Singapore, 1997; Vol. 2, Chapter 6. Practical Exercises in *Ab Initio* Quantum Chemistry - the World Wide Web as a Teaching Environment.

[3] P. Flükiger, G.Vacek, A. Hilger, H. P. Lüthi, *Chimia* **1997**, *51*, 100-106. Teaching *Ab Initio* Quantum Chemistry in a Networked Environment.

[4] J. Weber, P.-Y. Morgantini, *Chimia* **1995**, *49*, 77-83. Teaching Computational Chemistry Using Computers.

[5] J. H. Krieger, *Chem. & Eng. News* **1997**, *May 12*, 30-40. Computational Chemistry Impact.

[6] A. Szabo, N. S. Ostlund, *Modern Quantum Chemistry: Introduction to Advanced Electronic Structure Theory*; Macmillan Publishing: New York, 1982.

[7] W. J. Hehre, L. Radom, P. v. R. Schleyer, J. A. Pople, *Ab Initio Molecular Orbital Theory*; John Wiley & Sons: New York, 1986.

[8] Y. Yamaguchi, Y. Osamura, J. D. Goddard, H. F. Schaefer III, *A New Dimension to Quantum Chemistry: Analytic Derivative Methods in Ab Initio Molecular Electronic Structure Theory*; Oxford University Press, Inc.: New York, 1994.

[9] R. J. Bartlett, J. F. Stanton, in *Reviews in Computational Chemistry*; K. B. Lipkowitz, D. B. Boyd (Eds.), Verlag Chemie: New York, 1994; Vol. 5, Chapter 2. Applications of Post-Hartree-Fock Methods: A Tutorial.

[10] C. Møller, M. S. Plesset, *Phys. Rev.* **1934**, *46*, 618-622. Note on an Approximation Treatment for Many-Electron Systems.

[11] B. O. Roos, in *Methods in Computational Molecular Physics*; G. H. F. Diercksen, S. Wilson (Eds.), Reidel: Dordrecht, 1983; Vol 1. The Multiconfigurational (MC) SCF Method.

[12] I. Shavitt, in *Methods of Electronic Structure Theory*; H. F. Schaefer (Ed.), Ple-

num: NewYork, 1977. Chapter 6. The Method of Configuration Interaction.

[13] R. J. Bartlett, in *Modern Electronic Structure Theory*; D. R. Yarkony (Ed.), World Scientific: Singapore 1995; Chapter 16. Coupled-Cluster Theory: An Overview of Recent Developments.

[14] R. G. Parr, W. Yang, *Density Functional Methods in Atoms and Molecules*; Oxford University Press: New York, 1989.

[15] J. W. Labanowski, J. Andzelm, *Density Functional Methods in Chemistry*; Springer Verlag: New York, 1991.

[16] A. D. Becke, in *Modern Electronic Structure Theory*; D. R. Yarkony (Ed.), World Scientific: Singapore 1995; Chapter 15. Exchange-Correlation Approximations in Density-Functional Theory.

[17] W. Thiel, *Tetrahedron* **1988**, *44*, 7393-7408. Semiempirical Methods: Current Status and Perspectives.

[18] J. J. P. Stewart, in *Reviews in Computational Chemistry*; K. B. Lipkowitz, D. B. Boyd (Eds.), Verlag Chemie: New York, 1990; Vol. 1, Chapter 2. Semiempirical Molecular Orbital Methods.

[19] M. C. Zerner, in *Reviews in Computational Chemistry*; K. B. Lipkowitz, D. B. Boyd (Eds.), Verlag Chemie: New York, 1991; Vol. 2, Chapter 8. Semiempirical Molecular Orbital Methods.

[20] A. D. Becke, *J. Chem. Phys.* **1993**, *98*, 1372-1377. A New Mixing of Hartree-Fock and Local Density-Functional Theories.

[21] C. Lee, W. Yang, R. G. Parr, *Phys. Rev. B* **1988**, *37*, 785-789. Development of the Colle-Salvetti Correlation-Energy Formula into a Functional of the Electron Density.

[22] M. J. S. Dewar, E. G. Zoebisch, E. F. Healy, J. J. P. Stewart, *J. Am. Chem. Soc.* **1985**, *107*, 3902-3909. AM1: A New General Purpose Quantum Mechanical Molecular Model.

[23] J. Ridley, M. C. Zerner, *Theor. Chim. Acta* **1973**, *32*, 111-134. An Intermediate Neglect of Differential Overlap Technique for Spectroscopy: Pyrrole and the

Azines.

[24] J. Ridley, M. C. Zerner, *Theor. Chim. Acta* **1976**, *42*, 223-236. Triplet States via Intermediate Neglect of Differential Overlap: Benzene, Pyridine, and the Diazines.

[25] J. A. Pople, D. L. Beveridge, P. A. Dobosh, *J. Chem. Phys.* **1967**, *47*, 2026-2033. Approximate Self-Consistent Molecular-Orbital Theory. Intermediate Neglect of Differential Overlap.

[26] A. R. Katritzky, V. S. Lobanov, M. Karelson, *Chem. Soc. Rev.* **1995**, 279-287. QSPR: The Correlation and Quantitative Prediction of Chemical and Physical Properties From Structure.

[27] A. R. Katritzky, M. Karelson, V. S. Lobanov, *Pure Appl. Chem.* **1997**, *69*, 245-248. QSPR as a Means of Predicting and Understanding Chemical and Physical Properties in Terms of Structure.

[28] A. P. Bünz, B. Braun, R. Janowsky, *Ind. Eng. Chem. Res.* **1998**, *37*, 3043-3051. Application of Quantitative Structure-Performance Relationship and Neural Network Models for the Prediction of Physical Properties from Molecular Structure.

[29] G. Ceder, *Science* **1998**, *280*, 1099-1100. Predicting Properties from Scratch.

[30] G. B. Olson, *Science* **1997**, *277*, 1237-1242. Computational Design of Hierarchically Structured Materials.

[31] J. H. Burroughes, D. D. C. Bradley, A. R. Brown, R. N. Marks, R. H. Friend, P. L. Burn, A. B. Holmes, *Nature* **1990**, *347*, 539-541. Light-Emitting Diodes Based on Conjugated Polymers.

[32] P. L. Burn, A. Kraft, D. D. C. Bradley, A. R. Brown, R. H. Friend, R. W. Gymer, A. B. Holmes, R. W. Jackson, *J. Am. Chem. Soc.* **1993**, *115*, 10117-10124. Chemical Tuning of the Electronic Properties of Poly(*p*-phenylenevinylene)-Based Copolymers.

[33] D. A. Halliday, P. L. Burn, D. D. C. Bradley, R. H. Friend, O. M. Gelsen, A. B. Holmes, A. Kraft, J. H. F. Martens, K. Pichler, *Adv. Mat.* **1993**, *5*, 40-43. Large Changes in Optical Response Through Chemical Pre-ordering of Poly(*p*-phenylenevinylene).

[34] N. C. Greenham, S. C. Moratti, D. D. C. Bradley, R. H. Friend, A. B. Holmes, *Nature* **1993**, *365*, 628-630. Efficient Light-Emitting Diodes Based on Polymers

with High Electron Affinities.

[35] A. Heeger, J. Long, *Opt. Photonics News* **1996**, *8*, 24-30. Opto-Electronic Devices Fabricated from Semiconducting Polymers.

[36] M. G. Harrison, R. H. Friend, in *Electronic Materials: The Oligomer Approach*; K. Müllen, G. Wegner (Eds.), Wiley-VCH Verlag: Weinheim, 1998; Chapter 10. Optical Applications.

[37] S. R. Marder, J. E. Sohn, G. D. Stucky, *Materials for Nonlinear Optics: Chemical Perspective*; ACS Symposium Series 455; American Chemical Society: Washington, DC, 1991.

[38] P. N. Prasad, D. J. Williams, *Introduction to Nonlinear Optical Effects in Molecules and Polymers*; John Wiley: New York, 1991.

[39] P. N. Prasad, B. A. Reinhardt, *Chem. Mater.* **1990**, *2*, 669-669. Is There a Role for Organic Materials Chemistry in Nonlinear Optics and Photonics.

[40] S. R. Marder, J. W. Perry, *Science* **1994**, *263*, 1706-1707. Nonlinear Optical Polymers: Discovery to Market in 10 Years.

[41] A. Garito, R. F. Shi, M. Wu, *Phys. Today* **1994**, *47*, 51-57. Nonlinear Optics of Organic and Polymer Materials.

[42] R. F. Service, *Science* **1995**, *267*, 1918-1921. Nonlinear Competition Heats Up.

[43] K. Ziemelis, *Nature* **1998**, *393*, 619-620. Putting it on Plastic.

[44] D. R. Kanis, M. A. Ratner, T. J. Marks, *Chem. Rev.* **1994**, *94*, 195-242. Design and Construction of Molecular Assemblies with Large Second-Order Optical Nonlinearities. Quantum Chemical Aspects.

[45] J. L. Brédas, C. Adant, P. Tackx, A. Persoons, B. M. Pierce, *Chem. Rev.* **1994**, *94*, 243-278. Third-Order Nonlinear Optical Response in Organic Materials: Theoretical and Experimental Aspects.

[46] J. L. Brédas, *Adv. Mat.* **1995**, *7*, 263-274. Conjugated Polymers and Oligomers: Designing Novel Materials Using a Quantum-Chemical Approach.

[47] J. L. Oudar, D. S. Chemla, *J. Chem. Phys.* **1977**, *66*, 2664-2668. Hyperpolarizabil-

ities of the Nitroanilines and Their Relations to the Excited State Dipole Moment.

[48] J. L. Brédas, J. M. Toussaint, A. J. Heeger, *Mol. Cryst. Liq. Cryst.* **1990**, *189*, 81-91. The Coupling Between Electronic Structure, Geometric Structure, and Nonlinear Optical Properties in Conjugated Materials: The Case of Linear Polyenes.

[49] J. L. Brédas, *Science* **1994**, *263*, 487-488. Molecular Geometry and Nonlinear Optics.

[50] M. Blanchard-Desce, V. Alain, P. V. Bedworth, S. R. Marder, A. Fort, C. Runser, M. Barzoukas, S. Lebus, R. Wortmann, *Chem. Eur. J.* **1997**, *3*, 1091-1104. Large Quadratic Hyperpolarizabilities with Donor-Acceptor Polyenes Exhibiing Optimum Bond Length Alternation: Correlation Between Structure and Hyperpolarizability.

[51] H. S. Nalwa, *Adv. Mat.* **1993**, *5*, 341-358. Organic Materials for Third-Order Nonlinear Optics.

[52] S. R. Marder, C. B. Gorman, F. Meyers, J. W. Perry, G. Bourhill, J.-L. Brédas, B. M. Pierce, *Science* **1994**, *265*, 632-635. A Unified Description of Linear and Nonlinear Polarization in Organic Polymethine Dyes.

[53] S. R. Marder, J. W. Perry, G. Bourhill, C. B. Gorman, B. G: Tiemann, K. Mansour, *Science* **1993**, *261*, 186-189. Relation Between Bond-Length Alternation and Second Electronic Hyperpolarizabilities of Conjugated Organic Molecules.

[54] S. R. Marder, D. N. Beratan, L.-T. Cheng, *Science* **1991**, *252*, 103-106. Approaches for Optimizing the First Electronic Hyperpolarizability of Conjugated Organic Molecules.

[55] C. B. Gorman, S. R. Marder, *Chem. Mater.* **1995**, *7*, 215-220. Effects of Molecular Polarization on Bond-Length Alternation, Linear Polarizability, First and Second Hyperpolarizability in Donor-Acceptor Polyenes as a Function of Chain Length.

[56] F. Meyers, S. R. Marder, B. M. Pierce, J.-L. Brédas, *Chem. Phys. Lett.* 1994, 228, 171-176. Tuning of Large Second Hyperpolarizabilities in Organic Conjugated Compounds.

[57] F. Meyers, J.-L. Brédas, B. M. Pierce, S. R. Marder, *Nonlinear Opt.* **1995**, *14*, 61-71. Nonlinear Optical Properties of Donor-Acceptor Polyenes: Frequency-Dependent Calculations of the Relationship Among Molecular Polarizabilities, α, β, and

γ, and Bond-Length Alternation.

[58] F. Meyers, S. R. Marder, B. M. Pierce, J.-L. Brédas, *J. Am. Chem. Soc.* **1994**, *116*, 10703-10714. Electric Field Modulated Nonlinear Optical Properties of Donor-Acceptor Polyenes: Sum-Over-States Investigation of the Relationship between Molecular Polarizabilities (α, β, and γ) and Bond Length Alternation.

[59] J. M. André, J. Delhalle, J. L. Brédas, *Quantum Chemistry Aided Design of Organic Polymers*; World Scientific, Singapore, 1991.

[60] J. L. Brédas, *J. Chem. Phys.* **1985**, *82*, 3808-3811. Relationship Between Band Gap and Bond Length Alternation in Organic Conjugated Polymers.

[61] M. Jain, J. Chandrasekhar, *J. Phys. Chem.* **1993**, *97*, 4044-4049. Comparative Theoretical Evaluation of Hyperpolarizabilities of Push-Pull Polyenes and Polyynes. The Important Role of Configuration Mixing in the Excited States.

[62] L.-T. Cheng, W. Tam, S. H. Stevenson, G. R. Meridith, G. Rikken, S. R. Marder, *J. Phys. Chem.* **1991**, *95*, 10631-10643. Experimental Investigations of Organic Molecular Nonlinear Optical Polarizabilities. 1. Methods and Results on Benzene and Stilbene Derivatives.

[63] L.-T. Cheng, W. Tam, S. R. Marder, A. E. Steigman, G. Rikken, C. W. Spangler, *J. Phys. Chem.* **1991**, *95*, 10643-10652. Experimental Investigations of Organic Molecular Nonlinear Optical Polarizabilities. 2. A Study of Conjugation Dependences.

[64] N. Matsuzawa, D. A. Dixon, *J. Phys. Chem.* **1992**, *96*, 6232-6241. Semiempirical Calculations of Hyperpolarizabilities for Donor-Acceptor Molecules: Comparison to Experiment.

[65] N. Matsuzawa, D. A. Dixon, *Int. J. Quantum Chenistry* **1992**, *44*, 497-515. Semiempirical Calculations of Hyperpolarizabilities for Extenden π Systems: Polyenes, Polyynes, and Polyphenyls.

[66] J. O. Morley, V. J. Docherty, D. Pugh, *J. Chem. Soc., Perkin Trans 2* **1987**, 1351-1355. Non-linear Optical Properties of Organic Molecules. Part 2. Effect of Conjugation Length and Molecular Volume on the Calculated Hyperpolarizabilities.

[67] I. D. L. Albert, J. O. Morley, D. Pugh, *J. Chem. Soc., Faraday Trans 2* **1994**, *90*, 2617-2622. Further Studies on the Polarizabilities and Hyperpolarizabilities of the

Substituted Polyenes and Polyphenyls.

[68] G. Bourhill, J.-L. Brédas, S. R. Marder, F. Meyers, J. W. Perry, B. G. Tiemann, *J. Am. Chem. Soc.* **1994**, *116*, 2619-2620. Experimental Demonstration of the Dependence of the First Hyperpolarizability of Donor-Acceptor-Substituted Polyenes on the Ground-State Polarization and Bond Length Alternation.

[69] I. D. L. Albert, T. J. Marks, M. A. Ratner, *J. Am. Chem. Soc.* **1997**, *119*, 6575-6582. Large Molecular Hyperpolarizabilities. Quantitative Analysis of Aromaticity and Auxiliary Donor-Acceptor Effects.

[70] J. L. Brédas, B. Thémans, J. G. Fripiat, J. M. André, R. R. Chance, *Phys. Rev. B* **1984**, *29*, 6761-6773. Highly Conducting Polyparaphenylene, Polypyrrole, and Polythiophene Chains: An *Ab Initio* Study of the Geometry and Electronic-Structure Modifications upon Doping.

[71] K. Y. Wong, A. K. Y. Jen, V. P. Rao, K. J. Drost, *J. Chem. Phys.* **1994**, *100*, 6818-6825. Theoretical and Experimental Studies on the Molecular Second Order Nonlinear Optical Responses of Heteroaromatic Compounds.

[72] F. Meyers, J. L. Brédas, J. Zyss, *J. Am. Chem. Soc.* **1992**, *114*, 2914-2921. Electronic Structure and Nonlinear Optical Properties of Push-Pull Polyenes: Theoretical Investigation of Benzodithia Polyenals and Dithiole Polyenals.

[73] I. D. L. Albert, J. O. Morley, D. Pugh, *J. Phys. Chem. A* **1997**, *101*, 1763-1766. Comparative Study of Optical Nonlinearities in Substituted Polyynes versus the Corresponding Polyenes and Polyphenyls.

[74] J. O. Morley, *J. Chem. Soc. Faraday Trans.* **1991**, *87*, 3009-3013. Calculated Hyperpolarisabilities of Polythiophenes, Polyfurans, and Polypyrroles.

[75] C. Dehu, F. Meyers, J. L. Brédas, *J. Am. Chem. Soc.* **1993**, *115*, 6198-6206. Donor-Acceptor Diphenylacetylenes: Geometric Structure, Electronic Structure, and Second-Order Nonlinear Optical Properties.

[76] C. Dehu, J. L. Brédas, *Int. J. Quantum Chem.* **1994**, *52*, 89-96. Theoretical Study of the Conjugation Length Effect on the Electronic and Sedond-Order Nonlinear Optical Properies of Amino-Nitro Diphenylacetylenes.

[77] J. O. Morley, *Int. J. Quantum Chem.* **1993**, *46*, 19-26. Nonlinear Optical Properties of Organic Molecules. Calculations of the Hyperpolarizabilities of Donor-Accep-

tor Polyynes.

[78] V. P. Rao, A. K-Y. Jen, K. Y. Wong, K. J. Drost, *Tetrahedron Lett.* **1993**, *34*, 1747-1750. Novel Push-Pull Thiophenes for Second Order Nonlinear Optical Applications.

[79] V. P. Rao, A. K-Y. Jen, K. Y. Wong, K. J. Drost, *J. Chem. Soc., Chem. Commun.* **1993**, 1118-1120. Dramatically Enhanced Second-Order Nonlinear Optical Susceptibilities in Tricyanovinylthiophene Derivatives.

[80] A. K-Y. Jen, V. P. Rao, K. Y. Wong, K. J. Drost, *J. Chem. Soc., Chem. Commun.* **1993**, 90-92. Functionalized Thiophenes: Second-Order Nonlinear Optical Materials.

[81] K. Y. Wong, A. K-Y. Jen, V. P. Rao, *Phys. Rev. A* **1994**, *49*, 3077-3080. Experimental Studies of the Length Dependence of Second-Order Nonlinear Optical Responses of Conjugated Molecules.

[82] V. P. Rao, Y. Cai, Y.; A. K-Y. Jen, *J. Chem. Soc., Chem. Commun.* **1994**, 1689-1690. Ketene Dithioacetal as a π-Electron Donor in Second-Order Nonlinear Optical Chromophores.

[83] V. P. Rao, A. K.-Y. Jen, J. Chandrasekhar, I. N. N. Namboothiri, A. Rathna, *J. Am. Chem. Soc.* **1996**, *118*, 12443-12448. The Important Role of Heteroaromatics in the Design of Efficient Second-Order Nonlinear Optical Molecules: Theoretical Investigation on Push-Pull Heteroaromatic Stilbenes.

[84] T. L. Gilchrist, *Heterocyclic Chemistry*; John Wiley & Sons Inc.: New York, 1992.

[85] D. Beljonne, F. Meyers, J. L. Brédas, *Synth. Met.* **1996**, *80*, 211-222. Excited States in Bis-substituted Polyenes: Configuration Interaction Description of the Vertical Excitation Energies and Nonlinear Optical Properties.

[86] J.-L. Brédas, A. J. Heeger, *Chem. Phys. Lett.* **1994**, *217*, 507-512. Influence of Donor and Acceptor Substituents on the Electronic Characteristics of Poly(paraphenylene vinylene) and Poly(paraphenylene).

[87] J. Cornil, D. A. dos Santos, D. Beljonne, J.-L. Brédas, *J. Phys. Chem.* **1995**, *99*, 5604-5611. Electronic Structure of Phenylene Vinylene Oligomers: Influence of Donor/Acceptor Substitutions.

[88] J. Cornil, D. Beljonne, D. A. dos Santos, J.-L. Brédas, *Synth. Met.* **1996**, *76*, 101-

104. Poly(*p*-phenylene vinylene) as Active Layer in Light-Emitting Diodes: A Theoretical Investigation of the Effects of Derivatization.

[89] I. D. W. Samuel, I. Ledoux, C. Dhenaut, J. Zyss, H. H. Fox, R. R. Schrock, R. J. Silbey, *Science* **1994**, *265*, 1070-1072. Saturation of Cubic Optical Nonlinearity in Long-Chain Polyene Oligomers.

[90] J. L. Brédas, R. Silbey, D. S. Boudreaux, R. R. Chance, *J. Am. Chem. Soc.* **1983**, *105*, 6555-6559. Chain-Length Dependence of Electronic and Electrochemical Properties of Conjugated Systems: Polyacetylene, Polyphenylene, Polythiophene, and Polypyrrole.

[91] J. Cornil, D. Beljonne, J. L. Brédas, *J. Chem. Phys.* **1995**, *103*, 834-841. Nature of Optical Transitions in Conjugated Oligomers. I. Theoretical Characterization of Neutral and Doped Oligo(phenylenevinylene)s.

[92] J. Cornil, D. Beljonne, J. L. Brédas, *J. Chem. Phys.* **1995**, *103*, 842-849. Nature of Optical Transitions in Conjugated Oligomers. II. Theoretical Characterization of Neutral and Doped Oligothiophenes.

[93] D. Beljonne, J. Cornil, R. H. Friend, R. A. J. Janssen, J. L. Brédas, *J. Am. Chem. Soc.* **1996**, *118*, 6453-6461. Influence of Chain Length and Derivatization on the Lowest Singlet and Triplet States and Intersystem Crossing in Oligothiophenes.

[94] D. Beljonne, J. L. Brédas, *Phys. Rev. B* **1994**, *50*, 2841-2849. Theoretical Study of Pyrrole Oligomers: Electronic Excitations, Relaxation Energies, and Nonlinear Optical Properties.

[95] D. Beljonne, Z. Shuai, R. H. Friend, J. L. Brédas, *J. Chem. Phys.* **1995**, *102*, 2042-2049. Theoretical Investigation of the Lowest Singlet and Triplet States in Poly(paraphenylene vinylene)oligomers.

[96] A. E. Stiegman, V. M. Miskowski, J. W. Perry, D. R. Coulter, *J. Am. Chem. Soc.* **1987**, *109*, 5884-5886. A Series of Donor-Acceptor Molecules of the Form $NH_2(C_6H_4)(C{\equiv}C)_n(C_6H_4)NO_2$. Unusual Effects of Varying n.

[97] A. E. Stiegman, E. Graham, K. J. Perry, L. R. Khundkar, L.-T. Cheng, J. W. Perry, *J. Am. Chem. Soc.* **1991**, *113*, 7658-7666. The Electronic Structure and Second-Order Nonlinear Optical Properties of Donor-Acceptor Acetylenes: A Detailed

Investigation of Structure-Property Relationships.

[98] D. Beljonne, Z. Shuai, J. L. Brédas, *Int. J. Quant. Chem.* **1994**, *52*, 39-48. Theoretical Evolution of the Third-Order Molecular Polarizabilities as a Function of Chain Length in Thiophene and Pyrrole Oligomers.

[99] D. Beljonne, Z. Shuai, J. L. Brédas, *J. Chem. Phys.* **1993**, *98*, 8819-8828. Theoretical Study of Thiophene Oligomers: Electronic Excitations, Relaxation Energies, and Nonlinear Optical Properties.

[100] G. U. Bublitz, R. Ortiz, S. R. Marder, S. G. Boxer, *J. Am. Chem. Soc.* **1997**, *119*, 3365-3376. Stark Spectroscopy of Donor/Acceptor Substituted Polyenes.

[101] G. U. Bublitz, R. Ortiz, C. Runser, A. Fort, M. Barzoukas, S. R. Marder, S. G. Boxer, *J. Am. Chem. Soc.* **1997**, *119*, 2311-2312. Stark Spectroscopy of Donor-Acceptor Polyenes: Correlation with Nonlinear Optical Measurements.

[102] S. B. Allin, T. M. Leslie, R. S. Lumpkin, *Chem. Mater.* **1996**, *8*, 428-432. Solvent Effects in Molecular Hyperpolarizability Calculations.

[103] J. Gao, C. Alhambra, *J. Am. Chem. Soc.* **1997**, *119*, 2962-2963. Solvent Effects on the Bond Length Alternation and Absorption Energy of Conjugated Compounds.

[104] I. D. L. Albert, T. J. Marks, M. A. Ratner, *J. Phys. Chem.* **1996**, *100*, 9714-9725. Rational Design of Molecules with Large Hyperpolarizabilities. Electric Field, Solvent Polarity, and Bond Length Alternation Effects on Merocyanine Dye Linear and Nonlinear Optical Properties.

[105] G. Chen, S. Mukamel, *J. Phys. Chem.* **1996**, *100*, 11080-11085. Nonlinear Polarizabilities of Donor-Acceptor Substituted Conjugated Polyenes.

[106] J. L. Brédas, F. Meyers, *Nonlinear Opt.* **1991**, *1*, 119-123. On the Nature of the Ground State in Push-Pull Conjugated Molecules with Large Quadratic Optical Nonlinearites: From *p*-Nitroaniline to *p*-Nitro-*p*'-aminodiphenylhexatriyne.

[107] F. Diederich, Y. Rubin, *Angew. Chem.* **1992**, *104*, 1123-1146; *Angew. Chem. Int. Ed. Engl.* **1992**, *31*, 1101-1123. Synthetic Approaches toward Molecular and Polymeric Carbon Allotropes.

[108] F. Diederich, *Nature (London)* **1994**, *369*, 199-207. Carbon Scaffolding: Building

Acetylenic All-Carbon and Carbon-Rich Compounds.

[109] Y. Hori, K. Noda, S. Kobayashi, H. Taniguchi, *Tetrahedron Lett.* **1969**, 3563-3566. Synthesis and Properties of Tetrakis(phenylethynyl)ethylene.

[110] H. Hauptmann, *Angew. Chem.* **1975**, *87*, 490-491; *Angew. Chem. Int. Ed. Engl.* **1975**, *14*, 498-499. Tetraethynylethylenes.

[111] H. Hauptmann, *Tetrahedron Lett.* **1975**, 1931-1934. Untersuchungen zu Baseninduzierten Reaktionen an Tetraäthinyläthanen.

[112] H. Hauptmann, *Tetrahedron* **1976**, *32*, 1293-1297. Diäthinylcarbene und 2,4-Pentadiinylidene.

[113] H. Hopf, M. Kreutzer, P. G. Jones, *Chem. Ber.* **1991**, *124*, 1471-1475. Zur Darstellung und Struktur von Tetrakis(phenylethinyl)ethen.

[114] Y. Rubin, C. B. Knobler, F. Diederich, *Angew. Chem.* **1991**, *103*, 708-710; *Angew. Chem. Int. Ed. Engl.* **1991**, *30*, 698-700. Tetraethynylethene.

[115] R. R. Tykwinski, F. Diederich, *Liebigs Ann./Recueil* **1997**, 649-661. Tetraethynylethene Molecular Scaffolding.

[116] F. Diederich, in *Modern Acetylene Chemistry*; P. J. Stang, F. Diederich (Eds.), Verlag Chemie: Weinheim, 1995; Chapter 13. Oligoacetylenes.

[117] F. Diederich, L. Gobbi, *Top. Curr. Chem.* **1998**, in press. Cyclic and Linear Acetylenic Molecular Scaffolding.

[118] J.-D. van Loon, P. Seiler, F. Diederich, *Angew. Chem.* **1993**, *105*, 1235-1238; *Angew. Chem. Int. Ed. Engl.* **1993**, *32*, 1187-1189. Tetrakis(trialkylsilylethynyl)butatriene and 1,1,4,4-Tetrakis(trialkylsilylethynyl)-1,3-butadiene: Novel Cross-Conjugated Chromophores.

[119] J. Anthony, C. B. Knobler, F. Diederich, *Angew. Chem.* **1993**, *105*, 437-440; *Angew. Chem. Int. Ed. Engl.* **1993**, *32*, 406-409. Stable [12]- and [18]Annulenes Derived from Tetraethynylethene.

[120] A. M. Boldi, F. Diederich, *Angew. Chem.* **1994**, *106*, 482-485; *Angew. Chem. Int. Ed. Engl.* **1994**, *33*, 468-471. Expanded Radialenes: A Novel Class of Cross-Conjugated Macrocycles.

[121] J. Anthony, A. M. Boldi, C. Boudon, J.-P. Gisselbrecht, M. Gross, P. Seiler, C. B.

Knobler, F. Diederich, *Helv. Chim. Acta* **1995**, *78*, 797-817. Macrocyclic Tetraethynylethene Molecular Scaffolding: Perethynylated Aromatic Dodecadehydro[18]annulenes, Antiaromatic Octadehydro[12]annulenes, and Expanded Radialenes.

[122] T. Lange, V. Gramlich, W. Amrein, F. Diederich, M. Gross, C. Boudon, J.-P. Gisselbrecht, *Angew. Chem.* **1995**, *107*, 898-901; *Angew. Chem. Int. Ed. Engl.* **1995**, *34*, 805-809. Hexakis(trimethylsilyl)[3]radialene: A Carbon-Rich Chromophore with Unusal Electronic Properties.

[123] A. M. Boldi, J. Anthony, C. B. Knobler, F. Diederich, *Angew. Chem.* **1992**, *104*, 1270-1273; *Angew. Chem. Int. Ed. Engl.* **1992**, *31*, 1240-1242. Novel Cross-Conjugated Compounds Derived from Tetraethynylethene.

[124] J. Anthony, A. M. Boldi, Y. Rubin, M. Hobi, V. Gramlich, C. B. Knobler, P. Seiler, F. Diederich, *Helv. Chim. Acta* **1995**, *78*, 13-45. Tetraethynylethenes: Fully Cross-Conjugated π-Electron Chromophores and Molecular Scaffolds for All-Carbon Networks and Carbon-Rich Nanomaterials.

[125] A. M. Boldi, J. Anthony, V. Gramlich, C. B. Knobler, C. Boudon, J.-P. Gisselbrecht, M. Gross, F. Diederich, *Helv. Chim. Acta* **1995**, *78*, 779-796. Acyclic Tetraethynylethene Molecular Scaffolding: Multinanometer-Sized Linearly Conjugated Rods with the Poly(triacetylene) Backbone and Cross-Conjugated Expanded Dendralenes.

[126] J. Anthony, C. Boudon, F. Diederich, J.-P. Gisselbrecht, V. Gramlich, M. Gross, M. Hobi, P. Seiler, *Angew. Chem.* **1994**, *106*, 794-798; *Angew. Chem. Int. Ed. Engl.* **1994**, *33*, 763-766. Stable Soluble Conjugated Carbon Rods with a Persilylethynylated Polytriacetylene Backbone.

[127] J. Anthony, Ph. D. Thesis, University of California, Los Angeles, 1993. Cross-Conjugated Carbon-Rich Compounds.

[128] M. Schreiber, J. Anthony, F. Diederich, M. E. Spahr, R. Nesper, M. Hubrich, F. Bommerli, L. Degiorgi, P. Wachter, P. Kaatz, C. Bosshard, P. Günter, M. Colussi, U. W. Suter, C. Boudon, J.-P. Gisselbrecht, M. Gross, *Adv. Mater.* **1994**, *6*, 786-790. Polytriacetylenes: Conjugated Polymers with a Novel All-Carbon Backbone.

[129] M. Schreiber, R. R. Tykwinski, F. Diederich, R. Spreiter, U. Gubler, C. Bosshard, I. Poberaj, P. Günter, C. Boudon, J.-P. Gisselbrecht, M. Gross, *Adv. Mater.* **1997**, *9*,

339-343. Tetraethynylethene Molecular Scaffolding: Nonlinear Optical, Redox, and Amphiphilic Properties of Donor Functionalized Polytriacetylene and Expanded Radialenes.

[130] R. E. Martin, U. Gubler, C. Boudon, V. Gramlich, C. Bosshard, J.-P. Gisselbrecht, P. Günter, M. Gross, F. Diederich, *Chem. Eur. J.* **1997**, *3*, 1505-1512. Poly(triacetylene) Oligomers: Synthesis, Characterization, and Estimation of the Effective Conjugation Length by Electrochemical, UV/Vis, and Nonlinear Optical Methods.

[131] B. Ma, Y. Xie, H. F. Schaefer III, *Chem. Phys. Lett.* **1992**, *6*, 521-526. Tetraethynylethylene, A Molecule with Four Very Short C–C Single Bonds. Interpretation of the Infrared Spectrum.

[132] B. Ma, H. M. Sulzbach, Y. Xie, H. F. Schaefer III, *J. Am. Chem. Soc.* **1994**, *116*, 3529-3538. π Electron Delocalization and Compression in Acyclic Acetylenic Precursors to Multidimensional Carbon Networks: Comparison wSith Experiment for the Recently Synthesized Tris(trimethylsilyl)-Substituted Tetraethynylmethane. Structures, Thermochemistry, Infrared Spectra, Polarizabilities, and Hyperpolarizabilities.

[133] G. Hohlneicher, B. Dick, *J. Photochem.* **1984**, *27*, 215-231. Experimental Determination of the Low-Lying Excited A States of *trans*-Stilbene.

[134] G. Orlandi, W. Siebrand, *Chem. Phys. Lett.* **1975**, *30*, 352-354. Model for the Direct Photo-Isomerization of Stilbene.

[135] D. H. Waldeck, *Chem. Rev.* **1991**, *91*, 415-436. Photoisomerization Dynamics of Stilbenes.

[136] G. Hohlneicher, M. Müller, M. Demmer, J. Lex, J. H. Penn, L. Gan, P. D. Loesel, *J. Am. Chem. Soc.* **1988**, *110*, 4483-4494. 1,2-Diphenylcycloalkenes: Electronic and Geometric Structures in the Gas Phase, Solution, and Solid State.

[137] M. O. Wolf, H. H. Fox, M. A. Fox, *J. Org. Chem.* **1996**, *61*, 287-294. Reduction of Acetylated Tetraphenylethylenes: Electrochemical Behavior and Stability of the Related Reduced Anions.

[138] D. A. Shultz, M. A. Fox, *J. Org. Chem.* **1990**, *55*, 1047-1051. Structural Effects on the Disproportionation Equilibrium of Tethered Tetraphenylethylene Radical

Anions.

[139] F. Diederich, D. Philp, P. Seiler, *J. Chem. Soc., Chem. Commun.* **1994**, 205-208. π-Complexes Incorporating Tetraphenyltetraethynylethene.

[140] D. Philp, V. Gramlich, P. Seiler, F. Diederich, *J. Chem. Soc., Perkin Trans. 2* **1995**, 875-886. π-Complexes Incorporating Tetrakis(phenylethynyl)ethene.

[141] H. Taniguchi, K. Hayashi, K. Nishioka, Y. Hori, M. Shiro, T. Kitamura, *Chem. Lett.* **1994**, 1921-1924. A New Type of Inclusion Compounds Composed of a Charge-Transfer Complex between Tetrakis(phenylethynyl)ethene and 2,4,6-Trinitrofluorenone.

[142] R. R. Tykwinski, M. Schreiber, R. Pérez Carlón, F. Diederich, V. Gramlich, *Helv. Chim. Acta* **1996**, *79*, 2249-2281. Donor/Acceptor-Substituted Tetraethynylethenes: Systematic Assembly of Molecules for Use as Advanced Materials.

[143] R. R. Tykwinski, M. Schreiber, V. Gramlich, P. Seiler, F. Diederich, *Adv. Mater.* **1996**, *8*, 226-231. Donor-Acceptor Substituted Tetraethynylethenes.

[144] C. Boudon, J.-P. Gisselbrecht, M. Gross, J. Anthony, A. M. Boldi, R. Faust, T. Lange, D. Philp, J.-D. Van Loon, F. Diederich, *J. Electroanal. Chem.* **1995**, *394*, 187-197. Electrochemical Properties of Tetraethynylethenes, Fully Cross-Conjugated π-Chromophores, and Tetraethynylethene-Based Carbon-Rich Molecular Rods and Dehydroannulenes.

[145] A. Hilger, J.-P. Gisselbrecht, R. R. Tykwinski, C. Boudon, M. Schreiber, R. E. Martin, H. P. Luethi, M. Gross, F. Diederich, *J. Am. Chem. Soc.* **1997**, *119*, 2069-2078. Electronic Characteristics of Arylated Tetraethynylethenes: A Cooperative Computational and Electrochemical Investigation.

[146] C. Bosshard, R. Spreiter, P. Günter, R. R. Tykwinski, M. Schreiber, F. Diederich, *Adv. Mater.* **1996**, *8*, 231-234. Structure-Property Relationships in Nonlinear Optical Tetraethynylethenes.

[147] R. Spreiter, C. Bosshard, G. Knöpfle, P. Günter, R. R. Tykwinski, M. Schreiber, F. Diederich, *J. Phys. Chem. B* **1998**, *102*, 29-32. One- and Two-Dimensionally Conjugated Tetraethynylethenes: Structure versus Second-Order Optical Polarizabilities.

[148] U. Gubler, R. Spreiter, C. Bosshard, P. Günter, R. R. Tykwinski, F. Diederich,

Appl. Phys. Lett. **1998**, in press. Two-Dimensionally Conjugated Molecules: The Importance of Low Molecular Symmetry for Large Third-Order Nonlinear Optical Effects.

[149] R. R. Tykwinski, U. Gubler, R. E. Martin, F. Diederich, C. Bosshard, P. Günter, *J. Phys. Chem. B* **1998**, *102*, 4451-4465. Structure-Property Relationships in Third-Order Nonlinear Optical Chromophores.

2 Molecular Characteristics of Functionalized Diethynylethenes and Tetraethynylethenes

2.1 Introduction

In order to establish reliable structure-property relationships, the accurate determination of molecular structures is essential because of the strong correlation existing between the structure and the properties of molecules. Especially in π-conjugated organic compounds, any modification of the π electronic structure is connected to a geometric relaxation, involving changes in the overall molecular characteristics.[1] Hence, the first concern in theoretical examinations of a specific system is to obtain from the chosen calculation level a reliable estimation of the equilibrium geometry.

A broad library of organic chromophores based on the diethynylethene (DEE, hex-3-ene-1,5-diyne, **1**)[2-4] and tetraethynylethene (TEE, 3,4-diethynylhex-3-ene-1,5-diyne, **2**)[5,6] building blocks has been prepared in the laboratory of Prof. *F. Diederich*. The synthetic flexibility inherent to these systems allows the incorporation of electron donating and electron accepting functionality as shown by molecules **3** and **4**.[4,6,7] The extent and mode of π-conjugation (linear, cross, or two-dimensional conjugation) and the degree of functionalization (mono-, di-, tri-, or tetra-substitution) govern molecular properties such as electronic absorption,[4,7] luminescence,[4,7] redox behavior,[8,9] and nonlinear optical responses[9-12] in these highly conjugated organic systems. In order to selectively design molecules with optimal, specific properties, the theoretical calculations aim to achieve a better understanding of these particular structure-property relationships.

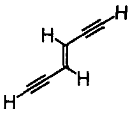

1

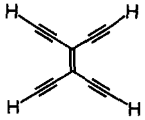

2

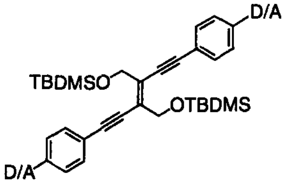

3

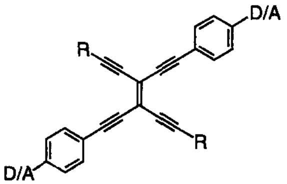

4

D = N(alkyl)$_2$
A = NO$_2$
R = Si(i-Pr)$_3$ or SiMe$_3$

Since the optimized molecular geometries play a vital role in the interpretation of electronic properties, the calculations first concentrate on the determination of the molecular characteristics of a series of functionalized DEEs and TEEs. Based on these predicted geometric structures, the electronic and optical characteristics are inspected and are discussed in the following chapters. The present study has thus been started by directing the research efforts towards the selection of the appropriate theoretical approach and basis set. The basis set evaluation performed on the parent TEE **2** and nitrobenzene in order to choose the optimal level of theory to be used for all the molecules considered in this investigation is described in Section 2.2. The main subject of the investigations presented in this Chapter is the examination of the structural features of the neutral and reduced forms of DEE and TEE derivatives and their evolution relative to a number of different topological criteria. Nitrophenyl substituents, *trans*-, *cis*-, and geminal substitution patterns, and acetylenic segments attached to the central olefinic bond of the DEE framework figure among those topological descriptors. The interest focuses first on the influence of nitrophenyl substituents on the bond length changes upon reduction. In order to study the structural changes in these substituted π-conjugated systems, the optimized neutral and anionic geometries of the mono- and bis(p-nitrophenyl) substituted TEEs are analyzed and compared to the parent TEE **2** and nitrobenzene in Section 2.3. Furthermore, in order to inspect the effects of linear and cross conjugation on the molecular structures, the neutral and reduced forms of the three bis(*p*-nitrophenyl) substituted DEE isomers (***trans***, ***cis***, and ***gem***) have been optimized. The comparison between the calculated bond lengths are used to relate the mode of conjugation (***trans*** and ***cis*** linear, and geminal cross conjugation) to the structural characteristics of these π-conjugated acetylenic chromophores. In addition, attention is turned toward evaluating the significance of the two additional acetylenic side chains in the extended TEE derived compounds (one- *vs.* two-dimensional conjugation). To this end, the optimized geometries and the σ- and π-charge populations of the three bis(*p*-nitrophenyl) DEE isomers are analyzed in comparison to the same features of their TEE homologues. The results of these examinations are detailed in Section 2.4.

2.2 Computational Details and Validation Studies

All calculations on the molecular structures were carried out using the restricted Hartree-Fock (RHF) and restricted open-shell Hartree-Fock (ROHF) schemes. Indeed, Hartree-Fock (HF) geometries are generally quite reliable for neutral systems and it is less common to see highly correlated post-Hartree-Fock calculations, like configuration interaction (CI) or Møller-Plesset (MP) many-body perturbation theory, on molecular structures.[13] Conventional wisdom implies that HF theory frequently gives bond lengths which are too short, whereas bond lengths obtained from MP2 and DFT methods are often too long relative to experiment.[14,15] From a systematic study carried out by ***Pople*** and coworkers on the molecular equilibrium structures of a subset of the G2 data set[16] with several methods using the 6-31G* basis set,[15] the geometries predicted with the HF, MP2, and BLYP (Becke's hybrid method with Lee-Yang-Parr correlation functional) methods are evaluated in order to examine and compare the accuracy of these levels of theory. For each method, the normal distribution (eq. 1) is calculated based on the mean error values $\bar{\Delta}$ and the standard deviations in errors Δ_{std}.

$$\rho(R_i) = \exp\left[-\frac{1}{2}\left(\frac{R_i - \bar{\Delta}}{\Delta_{std}}\right)^2\right] \qquad (1)$$

R_i is the error between the calculated bond distance R_i^{calc} and the corresponding experimental value R_i^{expm}.

$$R_i = R_i^{calc} - R_i^{expm} \qquad (2)$$

$$\bar{\Delta} = \frac{1}{n}\sum_{i=1}^{n} R_i \qquad (3)$$

$$\Delta_{std} = \sqrt{\frac{1}{n-1}\sum_{i=1}^{n}(R_i - \bar{\Delta})^2} \qquad (4)$$

Figure 2.1 shows the plotted normal distributions for the errors in the calculated bond distances for the HF, MP2, and BLYP approaches. HF exhibits a broad distribution centered left off the origin, indicating that the calculated bond lengths are too short relative to experiment. The distribution obtained from the BLYP bond distances has a peak right off the origin, showing the longer bond lengths compared to experiment. The MP2 bond distances are characterized by a sharper distribution, located between the HF and BLYP distributions and closer to the origin.

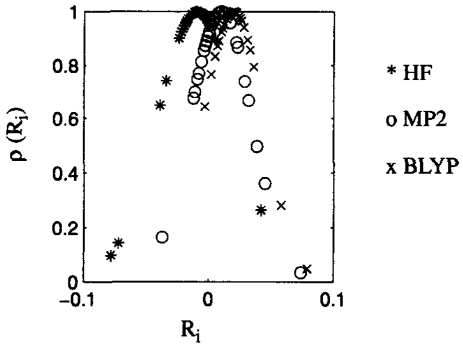

Figure 2.1. Normal distributions ρ(R) for the errors in the bond distances calculated by HF, MP2, and BLYP. The distributions have been calculated from the mean errors and the standard deviations in errors (see eq. 1)

Another criteria in determining the choice of the theory is that the Hartree-Fock self-consistent field (SCF) method, in contrast to post-SCF treatments, is applicable to the study of the substituted DEEs and TEEs, ranking as large-scale systems for the *ab initio* techniques. At the SCF level, basis sets of modest sizes are sufficient to provide molecular properties, whereas the post-SCF methods including high-level approximations for electron correlation, usually require larger basis sets. Therefore, the high-level *ab initio* approaches require substantial computational resources and are very expensive. The cost of the calculations is highly dependent on the number of atoms and basis functions in the molecule, which makes it impossible to study most of the systems in the present work at a high level of theory.

As a reference, and for the purpose of validating the methods and basis sets used, computations on the building blocks of mono- and bis-(*p*-nitrophenyl)-3,4-diethynylhex-3-en-1,5-diynes, namely tetraethynylethene **2** and nitrobenzene (NBZ) were conducted. Moreover, this examination serves to confirm the known performance of the HF method on neutral molecules and to ascertain the structural behavior of the anions. For the geometry optimization of TEE **2**, NBZ, and their respective anions, the basis set size has been systematically increased in order to assess the level of theory necessary to provide accurate results. The following standard Gaussian basis sets[17,18] as well as several polarized valence double-zeta correlation consistent basis sets of Dunning,[19] denoted PVDZ were employed: the split-valence plus polarization 6-31G** basis set, a modified 6-31+G* basis set, the PVDZ (9s4p1d/4s1p)[3s2p1d/2s1p], PVDZa (9s5p1d/4s1p)[3s3p1d/2s1p], and PVDZ+ (10s5p2d/5s2p)[4s3p2d/3s2p] basis sets. In order to determine the significance of diffuse functions in the structural description of the anions, the modified 6-31+G* and PVDZa basis sets were both augmented with a diffuse p-exponent (but no diffuse s- and d-functions) on the heavy atoms, whereas the PVDZ+ basis set had diffuse s-, p-, and d-functions on the heavy atoms, and a diffuse s- and p-exponent on the hydrogens. These correlation-consistent basis sets of Dunning have been designed to show systematic convergence to the complete basis set limit in the various theoretical methods.[19-21] The programs used were the Gaussian 94 package,[22] DISCO,[23] and TURBOMOLE.[24]

2.2.1 Validation Studies on Tetraethynylethene

The theoretical equilibrium geometries for neutral **2** obtained with different basis sets are compared in Table 2.1. All basis sets reproduce the same trends. The molecular structure calculated with the extended basis sets 6-31+G*, PVDZa, and PVDZ+ do not cause any variations from the geometry obtained at the HF/6-31G** level of theory, which is also in agreement with the results (at the HF/DZP level of theory) obtained by

Schaefer and coworkers.[25] The optimized structure **2** shows D_{2h} symmetry. The central bond *h* (Figure in Table 2.1) is calculated to be 1.345 Å, the triple bonds *f, f', q, q'* are 1.187 Å, the C–C single bonds *g, g', p,* and *p'* are 1.38 Å, and the C–H single bonds *e, e', r,* and *r'* are 1.057 Å. Thus, all bond lengths are close to the standard values for single, double, and triple bonds (1.43 Å for $C_{sp}{}^{2}$–C_{sp}, 1.34 Å for C=C, 1.182 Å for C≡C. and 1.06 Å for C_{sp}–H).[26] The calculated bond lengths are in good agreement with the experimental average values of the X-ray structure analysis of silylated **2**.[5] It should be pointed out that crystallographic data include some uncertainties. The reported structure is influenced by crystal packing effects,[5] and the theoretical results are therefore compared with the averaged experimental values. The largest bond length difference between calculated and experimental amounts to 0.02 Å. Between HF calculated and experimental data of neutral molecules, a ±0.02 Å bond distance reliability is generally reported.[13,15]

Upon reduction of **2** to the dianion $\mathbf{2}^{2-}$ (Table 2.2) the central bond *h* is substantially lengthened, whereas the C–C single bonds *g, g', p,* and *p'* and the triple bonds *f, f', q, q'* experience weaker bond length alternations. The differences between the distances found with the various basis sets are minimal.

Table 2.1. Bond lengths (in Å) and bond angles (in degrees) of the neutral TEE **2**.

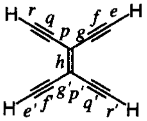

2

bond/angle[a]	HF/ 6-31G**	HF/ PVDZ	HF/ 6-31+G*	HF/ PVDZa	HF/ PVDZ+	exp[b]
e, e', r, r'	1.057	1.064	1.058	1.063	1.064	
f, f', q, q'	1.187	1.193	1.189	1.194	1.193	1.185
g, g', p, p'	1.438	1.440	1.438	1.439	1.440	1.451
h	1.345	1.348	1.347	1.348	1.348	1.324
$\varphi(h,g)$, $\varphi(h,p)$	121.9	121.9	121.9	121.9	121.9	121.7
$\varphi(g,f)$, $\varphi(p,q)$	178.0	178.2	178.4	178.4	178.4	178.9
$\varphi(f,e)$, $\varphi(q,r)$	179.4	179.4	179.5	179.6	179.5	

[a]Bond label according to Figure above. [b]Experimental average values of the silylated derivative (ref 5).

Table 2.2. Bond lengths (in Å) and bond angles (in degrees) of the TEE dianion **2**$^{2-}$.

bond/angle[a]	HF/ 6-31G**	HF/ PVDZ	HF/ 6-31+G*	HF/ PVDZa	HF/ PVDZ+
e, e', r, r'	1.053	1.060	1.055	1.061	1.061
f, f', q, q'	1.214	1.221	1.218	1.222	1.222
g, g', p, p'	1.400	1.402	1.400	1.400	1.399
h	1.527	1.527	1.512	1.508	1.513
$\varphi(h,g)$, $\varphi(h,p)$	121.9	122.0	122.2	122.3	122.2
$\varphi(g,f)$, $\varphi(p,q)$	178.9	179.2	178.0	178.3	178.7
$\varphi(f,e)$, $\varphi(q,r)$	179.1	179.4	178.6	179.2	179.1

[a] Bond label according to Figure in Table 2.1.

2.2.2 Validation Studies on Nitrobenzene

The theoretical equilibrium geometries for neutral NBZ and its radical anion obtained with different basis sets are given in Tables 2.3 and 2.4. All basis sets reproduce the same trends. The neutral and radical anion molecular structures calculated at the larger basis sets 6-31+G*, PVDZa, and PVDZ+ do not change significantly from the geometry obtained at HF/6-31G** level of theory. Nitrobenzene shows C_{2v} symmetry. The calculated neutral geometry is in good agreement with the experimentally determined molecular structure of NBZ.[27] The three aromatic carbon-carbon bonds *b*, *c*, and *d* in the ring (Figure in Table 2.3) have the same length and are very close to the value found for benzene (1.386 Å at HF/6-31G**). This shows that the electron withdrawing strength is mainly attributed to inductive effects within the σ-backbone resulting from the higher electronegativity of the nitrogen atoms, rather than resonance. The small mesomeric effect of the nitro group is also suggested by the low rotational barrier about bond *a* found experimentally[28,29] and theoretically.[30] In the radical anion NBZ$^{\bullet-}$ (Table 2.4), at HF/6-31G**, bond *a* shortens significantly by 0.075 Å, whereas the *N–O* bond elongates by 0.075 Å and bond *b* lengthens by 0.018 Å. The other two bonds *c* and *d* remain essentially unchanged.

Table 2.3. Bond lengths (in Å) and bond angles (in degrees) of nitrobenzene (NBZ).

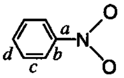

bond/angle[a]	HF/ 6-31G**	HF/ PVDZ	HF/ 6-31+G*	HF/ PVDZa	HF/ PVDZ+	exp[b]
a	1.459	1.464	1.461	1.464	1.465	1.467
b	1.383	1.385	1.384	1.386	1.385	1.387
c	1.383	1.386	1.385	1.387	1.387	1.386
d	1.386	1.389	1.388	1.389	1.389	1.389
N–O	1.194	1.188	1.194	1.189	1.191	1.227
φ*(CNO)*	117.7	117.6	117.7	117.7	117.7	118.4
φ*(ONO)*	124.6	124.8	124.6	124.6	124.6	123.2

[a]Bond label according to Figure above. [b]Experimental average values (ref 27).

Table 2.4. Bond lengths (in Å) and bond angles (in degrees) of the radical anion of nitrobenzene (NBZ$^{\bullet-}$).

bond/angle[a]	HF/ 6-31G**	HF/ PVDZ	HF/ 6-31+G*	HF/ PVDZa	HF/ PVDZ+
a	1.384	1.384	1.387	1.388	1.388
b	1.401	1.405	1.401	1.403	1.403
c	1.381	1.383	1.384	1.385	1.386
d	1.389	1.392	1.391	1.392	1.392
N–O	1.269	1.262	1.269	1.264	1.265
φ*(CNO)*	118.5	118.5	118.5	118.6	118.6

[a]Bond label according to Figure in Table 2.3.

The basis set study on the molecular structures of TEE and NBZ reveals that adding polarization functions has only a marginal effect on the predicted geometries. The presented comparisons show that the structures of TEE and NBZ computed at the HF/6-31G** level of theory are in good agreement with experimental results.[5,27] It appears that for the molecular structure computations of neutral and reduced species, the basis set requirements are less strict and that the HF/6-31G** level of theory is appropriate. Thus, the geometries of the series of substituted DEEs and TEEs examined in this study have been optimized using the 6-31G** basis set. C_s symmetry has been applied for all investigated systems.

2.3 Molecular Structures of Neutral and Reduced Forms of *p*-Nitrophenyl Tetraethynylethene Derivatives

The computations presented focus on the investigations of the molecular structure (ground state) of the neutral mono(*p*-nitrophenyl) TEE **5**, its radical anion $\mathbf{5}^{\bullet-}$, *trans*-bis(*p*-nitrophenyl) TEE **6**, its radical anion $\mathbf{6}^{\bullet-}$, and dianion $\mathbf{6}^{2-}$. The computed equilibrium geometries at the HF/6-31G** level of theory of the neutral compounds **5** and **6** and their anions are summarized in Tables 2.5 and 2.6.

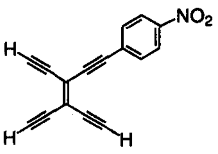

5

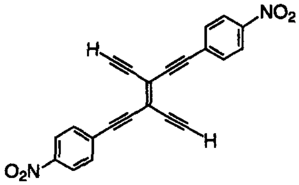

6

First, considering the computed structure of the carbon scaffold for the neutral species, the bond lengths found for the mono(*p*-nitrophenyl) compound **5** and the bis(*p*-nitrophenyl) derivative **6** lie in the same range as those predicted for the parent TEE **2** (Table 2.1), which means that all bond lengths are close to the standard values for single, double, and triple bonds (1.433 Å *vs.* 1.43 Å for $C_{sp}{}^2$–C_{sp}, 1.348 Å *vs.* 1.34 Å for C=C, and 1.190 Å *vs.* 1.182 Å for C≡C).[26] Comparison of the geometries predicted for NBZ (Table 2.3) and the nitrophenyl substituent of neutral **5** and **6** show disparity only in bond *d*. This slight lengthening is likely due to π-electron contributions of the TEE framework. Thus, the enediyne and benzoid character are dominant in the neutral compounds, and, as expected, little structural change upon substitution is observed for these molecules in the ground state.

These analyses demonstrate that the neutral structures, assuming the benzoid/acetylenic resonance form, show little evidence of ground state intramolecular charge transfer between the pendent substituents. Moreover, investigations of the calculated structures of the donor-acceptor system [*p*-(dimethylamino)phenyl]-(*p*-nitrophenyl)-substituted TEE and the donor-donor system bis[*p*-(*N*,*N*-dimethylamino)phenyl]-substituted TEE have also indicated that the benzoid/acetylenic resonance structure is dominant in the ground state. Likewise, X-ray structural analyses performed on a series of donor-acceptor substituted TEE derivatives have shown that the bond lengths and angles of their TEE cores are not affected by the pendant donor and/or acceptor groups.[4,7] Thus, the calculated predictions are in agreement with experimental findings. Similarly, the theoretical investigations by *Brédas* and coworkers[31-33] and *Stiegman* and coworkers[34,35] on donor-acceptor functionalized α,ω-diphenylacetylenes showed little distortion of the single and triple carbon-carbon bonds linking the donor and acceptor moieties, thus the ground state was dominated by the benzoid/acetylenic resonance form.

An examination of the bond length differences between the neutral and radical anion forms of **5** (Table 2.5), shows that the reduction process imparts little change on the core geometry. Whereas the central bond *h* (Figure in Table 2.5) of the parent TEE $\mathbf{2}^{\bullet-}$ and disubstituted $\mathbf{6}^{\bullet-}$ (Tables 2.6 and 2.7) lengthen by 0.084 Å and 0.073 Å, respectively, a change of merely 0.009 Å is observed for $\mathbf{5}^{\bullet-}$.

Upon reduction to $\mathbf{6}^{2-}$, the bond length changes observed in **6** (Table 2.6) reveal a strong tendency of the core geometry toward a cumulenic structure. The triple bonds *f* and *f'* along the conjugation path between the two aryl rings elongate by 0.048 Å from their neutral value of 1.190 Å, whereas the single bonds *g* and *g'* contract by 0.088 Å to a value of 1.345 Å, so that both types of bonds show significant double bond character. The central double bond *h* (Figure in Table 2.6) lengthens by as much as 0.130 Å from its neutral value in the dianion $\mathbf{6}^{2-}$, which indicates that this bond acquires strong single bond character. The bond length alternations of $\mathbf{6}^{2-}$ involve the entire substituted enediyne skeleton, whereas in the unsubstituted TEE $\mathbf{2}^{2-}$ (Table 2.7), only the central double bond is affected. This demonstrates that the presence of the two electron deficient nitrophenyl groups leads to a strong preference for a cumulenic resonance structure in the reduced chromophores of **6**. It is interesting to note that the lengths of the bonds *p*, *p'*, *q*, *q'*, *r*, and *r'*, which are outside the main conjugation path, are affected neither by the substituents nor by the reduction process.

Table 2.5. HF/6-31G** bond lengths and bond length differences (in Å) of **5** and radical anion $\mathbf{5}^{\bullet-}$.

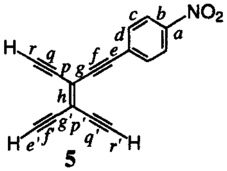

5

bond[a]	l_{ne}[b]	l_{ma}[c]	$\Delta l_{\mathrm{ma\,-\,ne}}$
a	1.458	1.368	–0.090
b	1.383	1.414	0.031
c	1.380	1.366	–0.014
d	1.394	1.409	0.015
δr[d]	0.009	0.046	
N–O	1.194	1.249	0.055
e	1.437	1.415	–0.022
f	1.190	1.201	0.011
g	1.434	1.415	–0.019
h	1.347	1.356	0.009
p	1.438	1.443	0.005
q	1.187	1.187	0.000
r	1.057	1.056	–0.001
e'	1.057	1.056	–0.001
f'	1.187	1.189	0.002
g'	1.437	1.437	0.000
p'	1.438	1.436	–0.002
q'	1.187	1.189	0.002
r'	1.057	1.056	–0.001

[a] Bond label according to Figure above. [b] ne Designates the neutral species. [c] ma Designates the monoanion. [d] δr as defined in eq. 5.

Table 2.6. HF/6-31G** bond lengths and bond length differences (in Å) of **6**, radical anion **6**$^{\bullet-}$, and dianion **6**$^{2-}$.

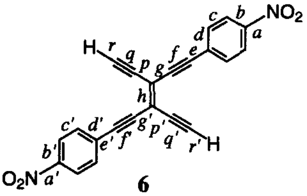

6

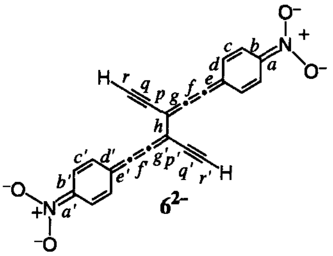

bond[a]	l_{ne}[b]	l_{ma}[c]	l_{da}[d]	$\Delta l_{\mathrm{ma-ne}}$	$\Delta l_{\mathrm{da-ma}}$	$\Delta l_{\mathrm{da-ne}}$
a, a'	1.459	1.440	1.383	−0.019	−0.057	−0.076
b, b'	1.383	1.389	1.416	0.006	0.027	0.033
c, c'	1.380	1.374	1.353	−0.006	−0.021	−0.027
d, d'	1.394	1.406	1.443	0.012	0.037	0.049
δr[e]	0.009	0.024	0.077			
N–O	1.193	1.200	1.220	0.007	0.020	0.027
e, e'	1.437	1.411	1.355	−0.026	−0.056	−0.082
f,f'	1.190	1.205	1.238	0.015	0.033	0.048
g, g'	1.433	1.399	1.345	−0.034	−0.054	−0.088
h	1.348	1.421	1.478	0.073	0.057	0.130
p, p'	1.438	1.429	1.435	−0.009	0.006	−0.003
q, q'	1.187	1.193	1.194	0.006	0.001	0.007
r, r'	1.057	1.055	1.055	−0.002	0.000	−0.002

[a]Bond label according to Figure above. [b]ne Designates the neutral species. [c]ma Designates the monoanion. [d]da Designates the dianion. [e]δr as defined in eq. 5.

Table 2.7. HF/6-31G** bond lengths and bond length differences (in Å) of **2**, radical anion $\mathbf{2}^{\bullet-}$, and dianion $\mathbf{2}^{2-}$.

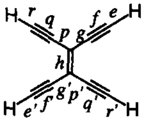

2

bond[a]	l_{ne}[b]	l_{ma}[c]	l_{da}[d]	Δl_{ma-ne}	Δl_{da-ma}	Δl_{da-ne}
e, e', r, r'	1.057	1.054	1.053	–0.003	–0.001	–0.004
f, f', q, q'	1.187	1.197	1.214	0.010	0.017	0.027
g, g', p, p'	1.438	1.421	1.399	–0.017	–0.022	–0.039
h	1.345	1.429	1.527	0.084	0.098	0.182

[a]Bond label according to Figure above. [b]ne Designates the neutral species. [c]ma Designates the monoanion. [d]da Designates the dianion.

As the monosubstituted species **5** is reduced to $\mathbf{5}^{\bullet-}$, bond *a* (Figure in Table 2.5) between the phenyl ring and the nitrogen atom contracts considerably ($\Delta l_{da-ne} = -0.090$ Å). Within the phenyl rings of **5**, the calculated bond lengths of the neutral molecule support the benzoid character, whereas in the radical anion a more quinoid-like structure is formed. Similar considerations apply for the dianion $\mathbf{6}^{2-}$. As **6** is reduced to $\mathbf{6}^{2-}$, the length of bond *a* (Figure in Table 2.6) between the phenyl ring and the nitrogen atom decreases considerably ($\Delta l_{da-ne} = -0.076$ Å). Analysis of the three computed structures (**6**, $\mathbf{6}^{\bullet-}$, $\mathbf{6}^{2-}$) shows that, when proceeding from the neutral to the dianion, the bond length alternation in the phenyl rings steadily increases so that the quinoid form dominates in the dianion. As an indicator for the extent of quinoid character in the phenyl rings, the degree of bond length alternation can be defined by the parameter in eq. 5 (bond labels from the Figure in Table 2.6).[31]

$$\delta r = \frac{(b-c)+(d-c)}{2} = \frac{(b'-c')+(d'-c')}{2} \tag{5}$$

In benzene, the δr value equals 0, whereas values between 0.08–0.14 are found in a fully quinoid ring, such as *p*-benzoquinone (δr=0.14).[36] In the analyses of **5** and $\mathbf{5}^{\bullet-}$, δr is

0.01 for the neutral species and 0.05 for the monoanion, whereas for **6** and its anions, δr is 0.01, 0.02, and 0.08, respectively, thus demonstrating the quinoid contribution to the anionic structures.

2.4 A Look at π-Conjugation in Functionalized Diethynylethenes and Tetraethynylethenes

The two additional acetylenic moieties appended to the central olefinic bond represent the main distinction between the DEE and the TEE skeletons. The aim of the present calculations is to evaluate the influence of these acetylenic moieties, *i.e.* to examine the impact of an extended π-conjugated carbon framework on the equilibrium structure of TEE based compounds. Additionally, the effects of the different substitution modes (*trans*, *cis*, and *gem*) on the molecular structures have been sought after. For this purpose, a series of bis(*p*-nitrophenyl) TEEs (**6**-**8**) and DEEs (**9**-**11**) are analyzed with respect to their structural differences.

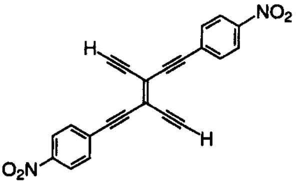

6

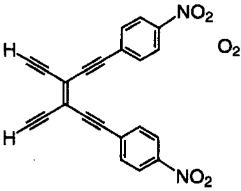

7

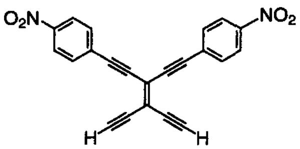

8

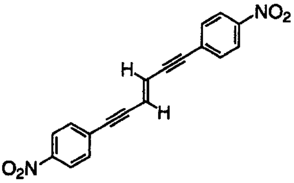

9

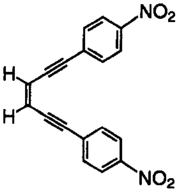

10

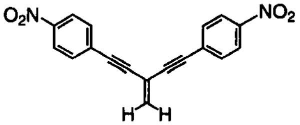

11

The consequence of attaching two additional acetylenic fragments onto the carbon framework is the formation of a fully two-dimensional π-conjugation system, combining four linear and two cross conjugated pathways, as illustrated in Figure 2.2. Whereas the TEE building block affords all six conjugation paths, the π-conjugation possibilities in the DEE based structures are limited to one-dimensional linear *trans*- or *cis*-conjugation, or one-dimensional geminal cross conjugation. Hence, the three bis(*p*-nitrophenyl) DEE isomers, *trans*-**9**, *cis*-**10**, and *gem*-**11**, are ideal for examining the effect of cross conjugation, as compared with linear conjugation on the structural characteristics, since the three potential conjugation paths can be inspected separately.

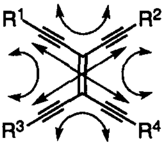

Figure 2.2. Linear and cross conjugation paths of tetrasubstituted TEE.

The computations concentrate on the investigations of the molecular ground state structure of the three neutral bis(*p*-nitrophenyl) TEEs, *trans*-**6**, *cis*-**7**, and *gem*-**8**, the three bis(*p*-nitrophenyl) DEEs, *trans*-**9**, *cis*-**10**, and *gem*-**11**, as well as their dianions. The computed equilibrium geometries at the HF/6-31G** level of theory of the neutral compounds and their dianions are summarized in Tables 2.8 and 2.9.

Table 2.8. HF/6-31G** bond lengths (Å) of **6**, **7**, **8**, and their dianions **6**$^{2-}$, **7**$^{2-}$, and **8**$^{2-}$.

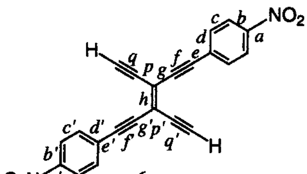
H
q
p
g
f
e
d
c
b
a
NO2
h
c'
d'
b'
a'
O2N
e'
f'
g'
p'
q'
H

6

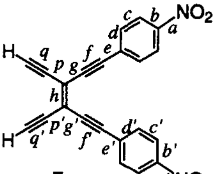
H
q
p
g
f
e
d
c
b
a
NO2
h
H
q'
p'
g'
f'
e'
d'
c'
b'
a'
NO2

7

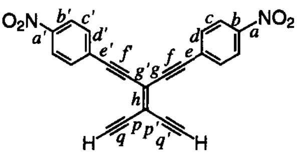
O2N
a'
b'
c'
d'
e'
f'
g'
g
f
e
d
c
b
a
NO2
h
H
q
p
p'
q'
H

8

bond[a]	l_{ne}[b](**6**)	l_{ne}(**7**)	l_{ne}(**8**)	l_{da}[c](**6**$^{2-}$)	l_{da}(**7**$^{2-}$)	l_{da}(**8**$^{2-}$)
a, a'	1.459	1.459	1.459	1.383	1.387	1.400
b, b'	1.383	1.383	1.383	1.416	1.414	1.407
c, c'	1.380	1.380	1.380	1.353	1.355	1.361
d, d'	1.394	1.393	1.394	1.443	1.441	1.428
δr[d]	0.009	0.009	0.009	0.077	0.073	0.056
N–O	1.193	1.193	1.193	1.220	1.219	1.214
e, e'	1.437	1.438	1.438	1.355	1.359	1.379
f, f'	1.190	1.190	1.190	1.238	1.236	1.220
g, g'	1.433	1.434	1.434	1.345	1.349	1.384
h	1.348	1.348	1.348	1.478	1.479	1.463
p, p'	1.438	1.437	1.437	1.435	1.435	1.410
q, q'	1.187	1.187	1.187	1.194	1.195	1.203

[a] Bond label according to Figure above. [b] ne Designates the neutral species. [c] da Designates the dianion. [d] δr as defined in eq. 5.

Table 2.9. HF/6-31G** bond lengths (Å) of **9**, **10**, **11**, and their dianions $\mathbf{9}^{2-}$, $\mathbf{10}^{2-}$, and $\mathbf{11}^{2-}$.

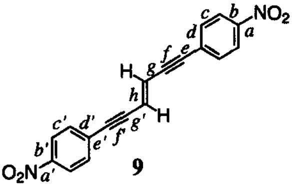

H
H
NO_2
O_2N
a
b
c
d
e
f
g
h
a'
b'
c'
d'
e'
f'
g'

9

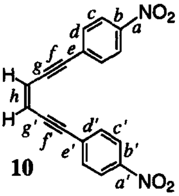

H
H
NO_2
NO_2
a
b
c
d
e
f
g
h
a'
b'
c'
d'
e'
f'
g'

10

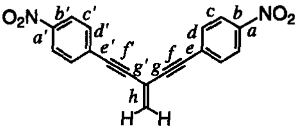

O_2N
NO_2
H
H
a
b
c
d
e
f
g
h
a'
b'
c'
d'
e'
f'
g'

11

bond[a]	$l_{ne}{}^{b}(\mathbf{9})$	$l_{ne}(\mathbf{10})$	$l_{ne}(\mathbf{11})$	$l_{da}{}^{c}(\mathbf{9}^{2-})$	$l_{da}(\mathbf{10}^{2-})$	$l_{da}(\mathbf{11}^{2-})$
a, *a'*	1.458	1.458	1.458	1.369	1.371	1.376
b, *b'*	1.383	1.383	1.383	1.424	1.422	1.419
c, *c'*	1.380	1.380	1.380	1.348	1.349	1.359
d, *d'*	1.394	1.394	1.394	1.453	1.452	1.429
δr^{d}	0.009	0.009	0.009	0.091	0.088	0.065
N–O	1.194	1.194	1.194	1.227	1.226	1.229
e, *e'*	1.438	1.438	1.439	1.344	1.347	1.390
f,*f'*	1.192	1.191	1.190	1.249	1.247	1.213
g, *g'*	1.431	1.430	1.443	1.332	1.334	1.416
h	1.330	1.330	1.329	1.450	1.452	1.371

[a] Bond label according to Figure above. [b] ne Designates the neutral species. [c] da Designates the dianion. [d] δr as defined in eq. 5.

The comparisons of the bond length variations between the different compounds, treated in the following, are outlined in Scheme 2.1 and illustrated graphically in Figure 2.3. In both series (DEEs and TEEs), the neutral and dianionic *cis*-geometries do not vary from the *trans*-geometries, and therefore the *cis*-systems are omitted in the discussion. The bond length differences between the neutral compounds **6**, **8**, **9**, **11**, and their dianions are reported in Table 2.10.

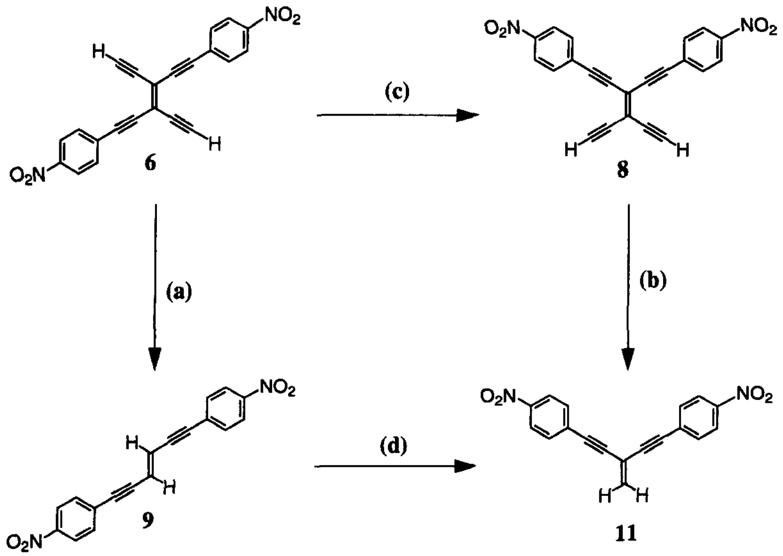

Scheme 2.1. Structural comparisons between compounds **6**, **8**, **9**, and **11**. Comparisons (a) and (b) illustrate the impact of the extent of conjugation, and (c) and (d) analyze the effects of linear and cross conjugation.

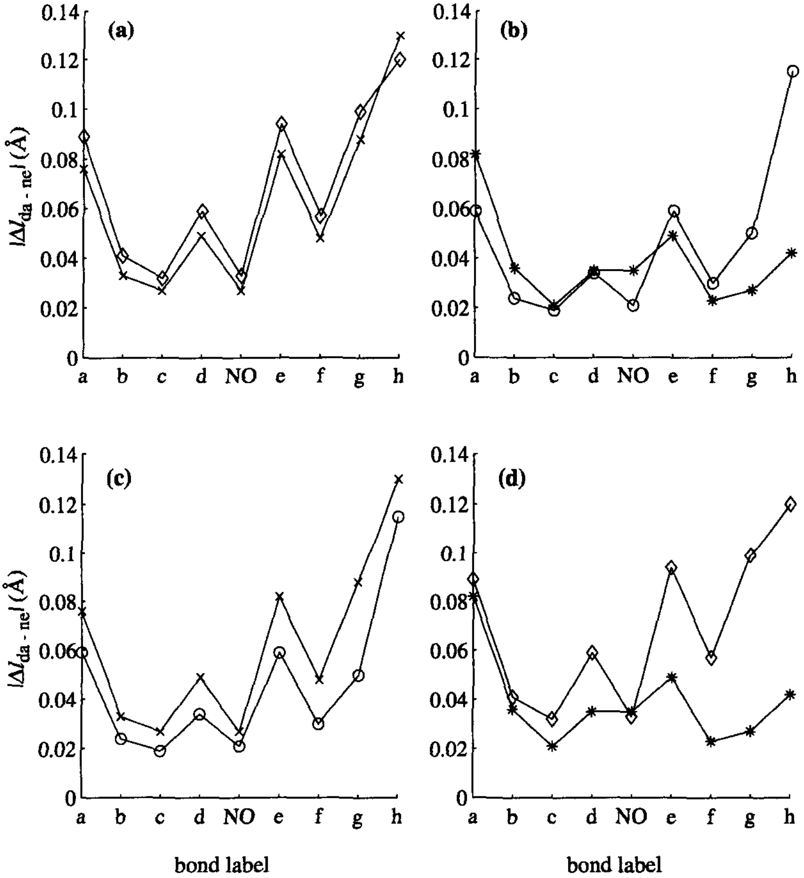

Figure 2.3. Comparison of the HF/6-31G** absolute bond length differences $|\Delta l_{da\,-\,ne}|$ (in Å) between the neutral and dianion of (a) **6**(×) *vs.* **9**(◊) and (b) **8**(o) *vs.* **11**(*), showing the effect of extension of the π-conjugated framework, and (c) **6**(×) *vs.* **8**(o), and (d) **9**(◊) *vs.* **11**(*), showing the effect of linear and cross conjugation.

Table 2.10. HF/6-31G** bond length differences $\Delta l_{\mathrm{da-ne}}$ (in Å) of **6**, **8**, **9**, **11**, and their dianions.

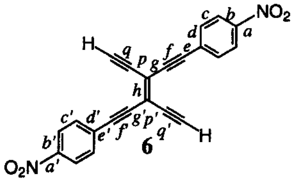
NO2
H
H
O2N
a b c d e f g h p q
a' b' c' d' e' f' g' p' q'

6

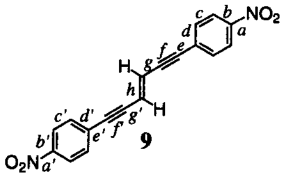
NO2
H
H
O2N
a b c d e f g h
a' b' c' d' e' f' g'

9

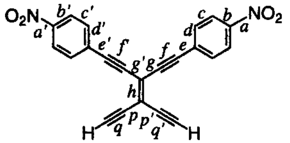
O2N
NO2
H
H
a b c d e f g h p q
a' b' c' d' e' f' g' p' q'

8

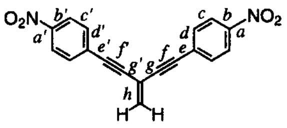
O2N
NO2
H
H
a b c d e f g h
a' b' c' d' e' f' g'

11

bond[a]	Δl (6^{2-}–6)[b]	Δl (8^{2-}–8)	Δl (9^{2-}–9)	Δl (11^{2-}–11)
a, a'	–0.076	–0.059	–0.089	–0.082
b, b'	0.033	0.024	0.041	0.036
c, c'	–0.027	–0.019	–0.032	–0.021
d, d'	0.049	0.034	0.059	0.035
N–O	0.027	0.021	0.033	0.035
e, e'	–0.082	–0.059	–0.094	–0.049
f, f'	0.048	0.030	0.057	0.023
g, g'	–0.088	–0.050	–0.099	–0.027
h	0.130	0.115	0.120	0.042
p, p'	–0.003	–0.027		
q, q'	0.007	0.016		

[a] Bond label according to Figures above. [b] Difference between the neutral species (ne) and its dianion (da).

2.4.1 Impact of the Extent of π-Conjugation: Comparison between Diethynylethene and Tetraethynylethene Architecture

The question whether the acetylenic side chains exert changes on the overall molecular structure is addressed by comparing the TEE/DEE pairs **6** and **9** (Figure 2.3 a) and **8** and **11** (Figure 2.3 b).

In the neutral species, the bond lengths predicted for *trans*-TEE **6** (Table 2.8) and for the corresponding DEE **9** (Table 2.9) are identical, with the exception of the central bond *h* (Figure in Table 2.8). Bond *h* is 0.018 Å shorter in the DEE **9**. This shows that in **6** a small charge delocalization to the acetylenic side chains occurs, inducing the elongation of the central olefinic bond. The same observations are found in the comparison of *gem*-compounds **8** and **11**, where bond *h* in the DEE derivative **11** is shorter by 0.019 Å than the corresponding bond in TEE **8**.

Upon reduction, the variations in bond length differences $\Delta l_{\text{da - ne}}$ become more distinct (Table 2.10). Looking first at the carbon cores of the *trans*-conjugated pair **6** and **9**, the single bonds *e*, *e'*, *g*, and *g'* are shorter and the triple bonds *f* and *f'* are longer in the DEE derivative $\mathbf{9}^{2-}$ compared to TEE $\mathbf{6}^{2-}$. Considering the δr values, the phenyl rings of the DEE system $\mathbf{9}^{2-}$ show a stronger quinoid character (δr = 0.09 (Table 2.9)) compared to the rings of TEE $\mathbf{6}^{2-}$ (δr = 0.08 (Table 2.8)). Thus, the DEE derivative **9** exhibits larger bond length differences upon reduction, resulting in a more pronounced cumulenic/quinoid resonance form in the DEE based dianion (Figure 2.3 a).

Different conclusions are drawn by inspecting the variations in bond length differences of the geminal molecules **8** and **11** (Table 2.10). The phenyl rings of *gem*-DEE $\mathbf{11}^{2-}$ have stronger quinoid character than *gem*-TEE $\mathbf{8}^{2-}$ (δr = 0.065 (Table 2.9) *vs*. 0.056 (Table 2.8)), and the largest bond length differences are found on bonds *a*, *a'*, *b*, *b*, and the *N–O* bond. On the other hand, the trend towards cumulenic structure decreases in $\mathbf{11}^{2-}$ compared to $\mathbf{8}^{2-}$ (in Figure 2.3 b: a crossing of $|\Delta l_{\text{da - ne}}|$ values at the carbon core bonds is noted). This observation seems to indicate that cross conjugation, which is the only conjugation pattern in the *gem*-DEE **11**, hinders delocalization throughout the whole molecule. Further evidence will be given in the next Section. Hence, in $\mathbf{11}^{2-}$, the incurred charge moves towards the acceptor substituents and mostly causes structural changes on the nitro groups. In the *gem*-TEE derivative $\mathbf{8}^{2-}$, on the other hand, the acetylenic moieties open additional π-conjugation possibilities, thus enabling a better overall charge distribution.

It is interesting to note, that in both pairs, the elongation of bond *h* is smaller for the DEE systems: this is found for the neutral compounds as well. In order to explain the origin of this lengthening, the analysis of the gross orbital populations has been carried out and is summarized in Tables 2.11 and 2.12. In the gross orbital population, the total number of electrons associated with a given atom in a molecule, is partitioned among the individual basis functions. This allows to divide the total charge into the π- and σ-charges by summing over all corresponding basis functions. Consideration of the carbon atoms C_1 and $C_{1'}$, respectively, to which the acetylenic side chains are attached, reveals that the total charges are significantly larger on the DEE derivatives (6.270 | e | and 6.428 | e |, respectively) than on the TEEs (6.151 | e | and 6.205 | e |, respectively). Separating the total charge into π-charge and σ-charge shows that the differences in the σ-contribution are somewhat larger than those of the π-contribution. The atoms C_1 and $C_{1'}$, respectively, of the TEE compounds accumulate less σ-charge than the corresponding atoms in DEEs, namely 4.950 | e | for TEE $\mathbf{6}^{2-}$ and 4.775 | e | for TEE $\mathbf{8}^{2-}$ *vs.* 5.150 | e | for DEE $\mathbf{9}^{2-}$ and 5.066 | e | for DEE $\mathbf{11}^{2-}$. Moving towards the nitrophenyl groups, no significant σ-charge differences in DEE and TEE are found. To corroborate the observations done for the dianions, the neutral species are examined. Similarly, the σ-charge accumulation on C_1 and $C_{1'}$, respectively, show values of 4.942 | e | for TEE **6** and 4.977 | e | TEE **8** *vs.* for 5.094 | e | for DEE $\mathbf{9}^{2-}$ and 5.136 | e | for DEE $\mathbf{11}^{2-}$. These findings prove that the inductive electron-withdrawing effect of the acetylenic moieties play an important role in the lengthening of the central bond.

It can be concluded that the introduction of acetylenic side chains into the DEE carbon framework controls the molecular geometry of the resulting TEEs by two distinguished effects. First, the structural characteristics are influenced by the generation of additional π-conjugation paths, enabling a better overall charge delocalization and thus provoking weaker structural rearrangement along the main conjugation axis in the TEE systems. Secondly, the inductive force of the acetylenic segments exerts considerable effects on the core geometry as well.

Table 2.11. HF/6-31G** Gross orbital populations (in | *e* |) on selected atoms of dianions **6**$^{2-}$ and **9**$^{2-}$ at equilibrium structure.

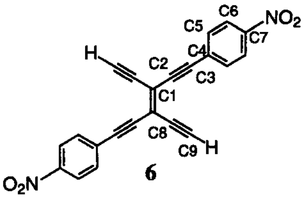

6

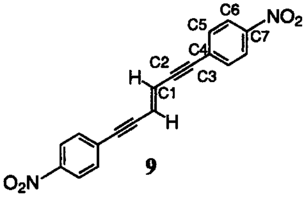

9

	TEE **6**$^{2-}$			DEE **9**$^{2-}$		
atom	total	π-charge	σ-charge	total	π-charge	σ-charge
C_1	6.151	1.201	4.950	6.270	1.121	5.150
C_2	5.921	0.901	5.020	6.005	0.962	5.043
C_3	6.242	1.185	5.057	6.138	1.151	4.987
C_4	6.003	0.884	5.118	6.035	0.916	5.119
C_5	6.177	1.100	5.077	6.177	1.106	5.071
C_6	6.085	0.907	5.178	6.086	0.912	5.173
C_7	5.949	1.273	4.676	5.954	1.281	4.673
N	6.525	1.057	5.468	6.535	1.069	5.466
O	8.579	1.607	6.973	8.600	1.631	6.969
C_8	5.704	0.916	4.788			
C_9	5.629	1.119	4.509			

Table 2.12. HF/6-31G** Gross orbital populations (in | *e* |) on selected atoms of dianions **8**$^{2-}$ and **11**$^{2-}$ at equilibrium structure.

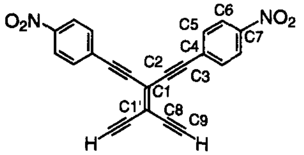

8

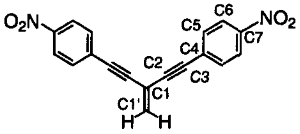

11

	TEE **8**$^{2-}$			DEE **11**$^{2-}$		
atom	total	π-charge	σ-charge	total	π-charge	σ-charge
$C_{1'}$	6.205	1.430	4.775	6.428	1.362	5.066
C_1	6.092	1.108	4.983	5.931	0.993	4.939
C_2	5.920	0.904	5.016	6.108	1.024	5.084
C_3	6.256	1.143	5.113	6.125	1.038	5.087
C_4	5.989	0.893	5.096	6.052	1.010	5.043
C_5	6.165	1.068	5.098	6.145	1.036	5.109
C_6	6.094	0.915	5.179	6.115	0.951	5.164
C_7	5.929	1.239	4.691	5.912	1.210	4.701
N	6.518	1.051	5.467	6.552	1.096	5.456
O	8.557	1.582	6.975	8.600	1.630	6.970
C_8	5.725	0.879	4.847			
C_9	6.705	1.263	5.442			

2.4.2 Impact of the Mode of Conjugation: Comparison between Linear and Cross Conjugation

Pairwise comparison of TEE isomers **6** and **8** (Figure 2.3 c) and DEE isomers **9** and **11** (Figure 2.3 d) illustrates the effect of cross conjugation on the molecular structures. Upon reduction, both *gem*-isomers **8** and **11** adopt less cumulenic/quinoid resonance character, demonstrating that cross conjugation is less efficient in delocalizing the incurred charge. For the DEE series (**9** and **11**), the bond length changes with respect to cross conjugation are less significant on the nitrophenyl ring than on the carbon core (Figure 2.3 d). This is consistent with the previous observation in Section 2.4.1 that the incurred charge in *gem*-**11** causes larger structural changes on the nitrophenyl groups (Table 2.10). Moreover, bond *h* undergoes a smaller elongation in the *gem* derivatives ($\Delta l_{\text{da - ne}}$ = 0.130 Å *vs.* 0.115 Å for the TEEs **6** and **8**, respectively, and 0.120 Å *vs.* 0.042 Å for the DEEs **9** and **11**, respectively), adopting therefore less single bond character. This results from the fact that, due to cross conjugation, bond *h* is less involved in the delocalization process.

In the TEE series, the bonds *p*, *p'*, and *q*, *q'* outside the main conjugation path are more affected in *gem*-**8** ($\Delta l_{\text{da - ne}}$ = –0.027 Å and 0.016 Å, respectively) than in *trans*-**6** ($\Delta l_{\text{da - ne}}$ = –0.003 Å and 0.007 Å, respectively). This has been explained by dividing the different delocalization pathways created by the acetylenic moieties into a *main* conjugation path, acting between pendent aryl substituents and a *secondary* conjugation path going along from the substituents to the unsubstituted acetylenic ends. In the *gem*-system **8**, a main *cross* conjugation path as well as all four possible secondary *linear* conjugation ways participate in the charge delocalization. In the *trans*-**6**, on the other hand, only the main *linear* conjugation way is predominantly effective, whereas the two secondary *cross*- and *cis-linear* conjugated paths do not seem to play an important role.

In summary, these findings clearly show that linear conjugation is dominant over cross conjugation, and, thus, illustrate nicely the relationships found experimentally between the mode of conjugation and molecular properties, namely the electronic absorption spectra[4,7] and the nonlinear responses.[10]

2.5 Conclusions

It can be concluded that in the ground state, the neutral compounds display a benzoid/acetylenic form. The geometric structure of the carbon core is not affected by the attachment of donor or acceptor groups. Therefore it can be stated that there is no intramolecular charge transfer between pendent aryl functionalities acting on the equilibrium geometries. In the anionic systems, the situation is different. Upon reduction of the monosubstituted **5**, only the nitrophenyl substituent is affected and adopts a quinoid-like form, whereas the TEE core remains unchanged. The reduction of the *trans*-bis(*p*-nitrophenyl) functionalized **6** to $\mathbf{6}^{2-}$, however, involves both the nitrophenyl groups and the TEE frame. The reduced species shows considerable changes in the bond lengths within both the phenyl rings and the TEE core, leading to cumulenic/quinoid structures. Most importantly, the central olefinic bond acquires significant single bond character. This dramatic change in the bond character in the reduced structures reflects the π-conjugation and charge delocalization patterns possible in these systems. Furthermore, the disubstituted compound retains planarity in all reduced states. This contrasts the behavior of similar compounds like tetraphenylethylenes[37-39] and tetracyanoethylene[40,41] where three-dimensional twisted induced charge transfer structures have been observed upon reduction.

The reduction of the bis(*p*-nitrophenyl) substituted DEE *trans*-**9** and *gem*-**11** predicts weaker bond length differences in *gem*-$\mathbf{11}^{2-}$. The changes in *gem*-$\mathbf{11}^{2-}$ concentrate on the nitrophenyl groups, showing that cross conjugation inhibits the overall charge delocalization. The addition of two acetylenic side chains to the central double bond of the DEE framework partially removes this hindrance in the resulting TEE. Indeed, the presence of the two acetylenic side chains has an impact on the molecular characteristics through both inductive and mesomeric effects. The consequence of these two intervening effects is reflected by a less pronounced cumulenic resonance form in the linear carbon arms and a stronger lengthening of the central bond in *trans*-TEE $\mathbf{6}^{2-}$ compared to *trans*-DEE $\mathbf{9}^{2-}$. The acetylenic moieties enable the formation of additional π-conjugation paths, *i.e.* a two-dimensional conjugation emerges. Upon reduction, these additional conjugation axes become active and permit charge distribution over a more extended π-system.

The changes of the unsubstituted acetylenic bonds in *trans*-TEE $\mathbf{6}^{2-}$ are less distinct than in the corresponding geminal compound $\mathbf{8}^{2-}$ and the chain along the main conjugation axis adopts a more pronounced cumulenic/quinoid like resonance form in $\mathbf{6}^{2-}$. This reveals that linear conjugation paths between the aryl substituents are dominant in delocalizing charge across the π-conjugated system. Hence, the attachment pattern (*trans*, *cis*, or *gem*) of the substituents, determining the conjugation mode, plays an important role for the structural characteristics and influences the overall electronic properties.

2.6 References

[1] J. L. Brédas, *Science* **1994**, *263*, 487-488. Molecular Geometry and Nonlinear Optics.

[2] M. Schreiber, J. Anthony, F. Diederich, M. E. Spahr, R. Nesper, M. Hubrich, F. Bommerli, L. Degiorgi, P. Wachter, P. Kaatz, C. Bosshard, P. Günter, M. Colussi, U. W. Suter, C. Boudon, J.-P. Gisselbrecht, M. Gross, *Adv. Mater.* **1994**, *6*, 786-790. Polytriacetylenes: Conjugated Polymers with a Novel All-Carbon Backbone.

[3] J. Anthony, Ph. D. Thesis, University of California, Los Angeles, 1993. Cross-Conjugated Carbon-Rich Compounds.

[4] R. R. Tykwinski, M. Schreiber, R. Pérez Carlón, F. Diederich, V. Gramlich, *Helv. Chim. Acta* **1996**, *79*, 2249-2281. Donor/Acceptor-Substituted Tetraethynylethenes: Systematic Assembly of Molecules for Use as Advanced Materials.

[5] Y. Rubin, C. B. Knobler, F. Diederich, *Angew. Chem.* **1991**, *103*, 708-710; *Angew. Chem. Int. Ed. Engl.* **1991**, *30*, 698-700. Tetraethynylethene.

[6] R. R. Tykwinski, F. Diederich, *Liebigs Ann./Recueil* **1997**, 649-661. Tetraethynylethene Molecular Scaffolding.

[7] R. R Tykwinski, M. Schreiber, V. Gramlich, P. Seiler, F. Diederich, *Adv. Mater.* **1996**, *8*, 226-231. Donor-Acceptor Substituted Tetraethynylethenes.

[8] A. Hilger, J.-P. Gisselbrecht, R. R. Tykwinski, C. Boudon, M. Schreiber, R. E. Martin, H. P. Lüthi, M. Gross, F. Diederich, *J. Am. Chem. Soc.* **1997**, *119*, 2069-2078. Electronic Characteristics of Arylated Tetraethynylethenes: A Cooperative Computational and Electrochemical Investigation.

[9] R. E. Martin, U. Gubler, C. Boudon, V. Gramlich, C. Bosshard, J.-P. Gisselbrecht, P. Günter, M. Gross, F. Diederich, *Chem. Eur. J.* **1997**, *3*, 1505-1512. Poly(triacetylene) Oligomers: Synthesis, Characterization, and Estimation of the Effective Conjugation Length by Electrochemical, UV/Vis, and Nonlinear Optical Methods.

[10] C. Bosshard, R. Spreiter, P. Günter, R. R. Tykwinski, M. Schreiber, F. Diederich, *Adv. Mater.* **1996**, *8*, 231-234. Structure-Property Relationships in Nonlinear Optical Tetraethynylethenes.

[11] R. Spreiter, C. Bosshard, G. Knöpfle, P. Günter, R. R. Tykwinski, M. Schreiber, F.

Diederich, *J. Phys. Chem. B* **1998**, *102*, 29-32. One- and Two-Dimensionally Conjugated Tetraethynylethenes: Structure Versus Second-Order Optical Polarizabilities.

[12] R. R. Tykwinski, U. Gubler, R. E. Martin, F. Diederich, C. Bosshard, P. Günter, *J. Phys. Chem. B* **1998**, *102*, 4451-4465. Structure-Property Relationships in Third-Order Nonlinear Optical Chromophores.

[13] H. F. Schaefer III, J. R. Thomas, Y. Yamaguchi, B. J. DeLeeuw, G. Vacek, in *Modern Electronic Structure Theory*; D. R. Yarkony (Ed.), World Scientific: Singapore 1995; Chapter 1. The Chemical Applicability of Standard Methods in *Ab Initio* Molecular Quantum Mechanics. pp. 21-23.

[14] T. Helgaker, J. Gauss, P. Jørgensen, J. Olsen, *J. Chem. Phys.* **1997**, *106*, 6430-6440. The Prediction of Molecular Equilibrium Structures by the Standard Electronic Wave Functions.

[15] B. G. Johnson, P. M. W. Gill, J. A. Pople, *J. Chem. Phys.* **1993**, *98*, 5612-5626. The Performance of a Family of Density Functional Methods.

[16] L. A. Curtiss, K. Raghavachari, G. W. Trucks, J. A. Pople, *J. Chem. Phys.* **1991**, *94*, 7221-7230. Gaussian-2 theory for molecular energies of first- and second-row compounds.

[17] W. J. Hehre, L. Radom, P. v. R. Schleyer, J. A. Pople, *Ab Initio Molecular Orbital Theory*; John Wiley & Sons: New York, 1986.

[18] E. R. Davidson, D. Feller, *Chem. Rev.* **1986**, *86*, 681-696. Basis Set Selection for Molecular Calculations.

[19] T. H. Dunning, *J. Chem. Phys.* **1989**, *90*, 1007-1023. Gaussian Basis Sets for Use in Correlated Molecular Calculations. I. The Atoms Boron through Neon and Hydrogen.

[20] R. A. Kendall, T. H. Dunning, R. J. Harrison, *J. Chem. Phys.* **1992**, *96*, 6796-6806. Electron Affinities of the First-Row Atoms Revisited. Systematic Basis Sets and Wave Functions.

[21] D. E. Woon, T. H. Dunning, *J. Chem. Phys.* **1993**, *98*, 1358-1371. Gaussian Basis Sets for Use in Correlated Molecular Calculations. III. The Atoms Aluminum

through Argon.

[22] Gaussian 94, M. J. Frisch, G. W. Trucks, H. B. Schlegel, P. M. W. Gill, B. G. Johnson, M. A. Robb, J. R. Cheeseman, T. A. Keith, G. A. Petersson, J. A. Montgomery, K. Raghavachari, M. A. Al-Laham, V. G. Zakrzewski, J. V. Ortiz, J. B. Foresman, J. Cioslowski, B. B. Stefanov, A. Nanayakkara, M. Challacombe, C. Y. Peng, P. Y. Ayala, W. Chen, M. W. Wong, J. L. Andres, E. S. Replogle, R. Gomperts, R. L. Martin, D. J. Fox, J. S. Binkley, D. J. Defrees, J. Baker, J. J. P. Stewart, M. Head-Gordon, C. Gonzalez, J.A. Pople, Gaussian, Inc. Pittsburgh, PA, 1995.

[23] DISCO, A Direct SCF and MP2 Code written by J. Almlöf, K. Faegri, M. W. Feyereisen, T. H. Fischer, H. P. Lüthi, ETH Zürich Version 3.0, 1994.

[24] R. Ahlrichs, M. Bär, M. Häser, H. Horn, C. Kölmel, *Chem. Phys. Lett.* **1989**, *162*, 165-169. Electronic Structure Calculations on Workstation Computers: The Program System Turbomole.

[25] B. Ma, Y. Xie, H. F. Schaefer III, *Chem. Phys. Lett.* **1992**, *6*, 521-526. Tetraethynylethylene, a Molecule with Four Very Short C–C Single Bonds. Interpretation of the Infrared Spectrum.

[26] F. A. Carey, R. J. Sundberg, *Advanced Organic Chemistry, Part A: Structure and Mechanisms*; Plenum Press: New York, 1990; Chapter 1. Chemical Bonding and Structure.

[27] R. Boese, D. Bläser, M. Nussbaumer, T. M. Krygowski, *Struct. Chem.* **1992**, *3*, 363-368. Low Temperature Crystal and Molecular Structure of Nitrobenzene.

[28] J. N. Høg, L. Nygaard, G. O. Sørensen, *J. Mol. Struct.* **1971**, *7*, 111-121. Microwave Spectrum and Planarity of Nitrobenzene.

[29] T. Correll, N. W. Larsen, T. Pedersen, *J. Mol. Struct.* **1980**, *65*, 43-49. Equilibrium Configuration and Barriers of Four Fluorine Substituted Nitrobenzenes, Obtained by Microwave Spectroscopy.

[30] M. Head-Gordon, J. A. Pople, *Chem. Phys. Lett.* **1990**, *173*, 585-589. Internal Rotation in Conjugated Molecules: Nitroethylene and Nitrobenzene.

[31] F. Meyers, J. L. Brédas, *Int. J. Quantum Chem.* **1992**, *42*, 1595-1614. Electronic Structure and Nonlinear Optical Properties of Push-Pull Conjugated Molecules.

[32] C. Dehu, F. Meyers, J. L. Brédas, *J. Am. Chem. Soc.* **1993**, *115*, 6198-6206. Donor-

Acceptor Diphenylacetylenes: Geometric Structure, Electronic Structure, and Second-Order Nonlinear Optical Properties.

[33] J. L. Brédas, F. Meyers, *Nonlinear Opt.* **1991**, *1*, 119-123. On the Nature of the Ground State in Push-Pull Conjugated Molecules with Large Quadratic Optical Nonlinearities: From *p*-Nitroaniline to *p*-Nitro-*p'*-aminodiphenylhexatriyne.

[34] A. E. Stiegman, V. M. Miskowski, J. W. Perry, D. R. Coulter, *J. Am. Chem. Soc.* **1987**, *109*, 5884-5886. A Series of Donor-Acceptor Molecules of the Form $NH_2(C_6H_4)(C{\equiv}C)_n(C_6H_4)NO_2$. Unusual Effects of Varying n.

[35] A. E. Stiegman, E. Graham, K. J. Perry, L. R. Khundkar, L.-T. Cheng, J. W. Perry, *J. Am. Chem. Soc.* **1991**, *113*, 7658-7666. The Electronic Structure and Second-Order Nonlinear Optical Properties of Donor-Acceptor Acetylenes: A Detailed Investigation of Structure-Property Relationships.

[36] K. Hagen, K. Hedberg, *J. Chem. Phys.* **1973**, *59*, 158-162. Reinvestigation of the Molecular Structure of Gaseous *p*-Benzoquinone by Electron Diffraction.

[37] M. A. Fox, D. A. Shultz, *J. Org. Chem.* **1988**, *53*, 4386-4390. Twisting in the Tetraphenylethylene Dianion.

[38] M. O. Wolf, H. H. Fox, M. A. Fox, *J. Org. Chem.* **1996**, *61*, 287-294. Reduction of Acetylated Tetraphenylethylenes: Electrochemical Behavior and Stability of the Related Reduced Anions.

[39] D. A. Shultz, M. A. Fox, *J. Org. Chem.* **1990**, *55*, 1047-1051. Structural Effects on the Disproportionation Equilibrium of Tethered Tetraphenylethylene Radical Anions.

[40] A. Zheludev, A. Grand, E. Ressouche, J. Schweizer, B. Morin, A. J. Epstein, D. A. Dixon, J. S. Miller, *J. Am. Chem. Soc.* **1994**, *116*, 7243-7249. Experimental Determination of the Spin Density in the Tetracyanoethenide Free Radical, $[TCNE]^{\bullet -}$, by Single-Crystal Polarized Neutron Diffraction. A View of a π* Orbital.

[41] D. A. Dixon, J. S. Miller, *J. Am. Chem. Soc.* **1987**, *109*, 3656-3664. Crystal and Molecular Structure of the Charge-Transfer Salt of Decamethylcobaltocene and Tetracyanoethylene (2:1): $\{[Co(C_5Me_5)_2]^+\}_2[(NC)_2CC(CN)_2]^{2-}$. The Electronic Structures and Spectra of $[TCNE]^n$ (n=0, 1-, 2-).

3 Electrochemical and Electronic Properties of Substituted Tetraethynylethenes

3.1 Introduction

In view of potential applications in electronics and photonics, π-conjugated systems must possess an optimal π-electron delocalization ability to allow the charges to move through the conjugated polymers. One approach to understand the underlying charge transfer processes of π-conjugated molecules is to explore their redox behavior. Hence, the interest in the electrochemical and electronic characteristics of conjugated oligomers has considerably grown and the evolution of the electrochemical properties of a number of conjugated monomeric and oligomeric systems has been analyzed by several groups.

Zhou and *Swager* have reported the redox behavior of alkyne linked bis(*p*-phenylenediamine) systems. If the two redox centers were separated by an ethynyl-para-phenylene-ethynyl bridge, the electrochemically generated radical cations and dications were highly localized and behaved essentially as individual redox centers.[1] These observations suggested an inability of the conjugated framework to participate in charge delocalization. However, if the centers were linked by a buta-1,3-diynediyl moiety, a slight potential difference existed between the different one-electron redox events, indicating that the redox centers may interact. This interaction was suggested to be principally electrostatic, since a considerably greater separation of the oxidation waves would be expected if the charge delocalization of the radical cation would include both of the aniline redox centers.

The electrochemistry of nitroaromatic molecules has been extensively studied.[2-8] The electrochemical behavior of a conjugated series of dinitroaromatic systems has been investigated by *Ammar* and *Savéant*.[8] The redox potential difference between the first and the second charge transfer decreased from 321 mV for *p*-dinitrobenzene, to 61 mV for 4-4'-dinitrobiphenyl, and to only 9 mV for 4-4'-dinitrostilbene. These results revealed that even in the presence of a conjugated bridge between two nitrophenyl groups, the difference between the first two reduction potentials rapidly decreased as the length of the bridge was increased. Comparably, the phenylacetylene endcapped tetraethynylethene (TEE) oligomers (up to pentamer) with a polytriacetylene (PTA) backbone, prepared in the laboratory of Prof. *F. Diederich*, underwent one reversible one-electron reduction per TEE unit. The difference between the first and second reduction potential decreased considerably with each monomer added to the chain.[9-12]

Schimanke and *Gleiter* have investigated the electrochemical properties of buta-1,3-diynediyl linked cyclopentadienylcobalt-cyclobutadiene complexes and reported two reversible one-electron oxidations at different potentials. According to the authors, these findings suggested that in the radical cation state, the two metal centers interacted through the butadiyne chain. Coulomb effects could be excluded, since both cobalt centers were far removed.[13]

Analogously, the cyclic voltammetry data of metal-capped μ-polyynediyl complexes reported by *Gladysz* and coworkers,[14-16] showed also two one-electron oxidation at different potentials, indicating that the two redox centers interacted via the acetylenic chain. However, with increasing carbon chain length, the redox potential difference between the first two oxidation steps decreased, and eventually, at a length of twenty carbon atoms, the two potentials merged to give a single two-electron oxidation. Similar behavior has been found for π-conjugated thienylenevinylene oligomers investigated by *Roncali* and coworkers.[17,18] With elongation of the chain, the difference between the two first peak potentials diminished, and the two one-electron processes finally coalesced into one two-electron wave. Chain extension led to an increase of the number of attainable redox states as well.

Partial charge delocalization in π-conjugated systems was confirmed through the electrochemical reduction of diphenyl stilbenes, demonstrating *cis-trans* isomerization as a result of reduced olefinic bond order.[19,20] Additionally, the electrochemical analyses and molecular orbital calculations of tetraphenylethenes also showed charge delocalization, resulting in both diminished bond order of the olefin and marked structural rearrangements to relieve steric and electrostatic interactions.[21-24]

In the following, the electrochemical and electronic properties of a series of tetraethynylethene (TEE) based systems are examined. The main objective of this joint theoretical and experimental study is to determine the ability of the conjugated enediyne TEE core to effectively promote electronic communication between pendent functionality in these π-conjugated acetylenic systems. Furthermore, the investigations aim at providing a better understanding of the impact of the extent of conjugation on the electronic properties of functionalized TEEs. In Section 3.2, the results of the electrochemical analysis of a series of acceptor substituted DEEs and TEEs, bearing one or two functional groups, are discussed. The obtained reduction potentials initially appeared to predict highly localized redox centers like in the reports of similar π-conjugated systems by *Zhou* and *Swager*,[1] and *Gladysz* and coworkers.[14,15] This observation initiated the interest in theoretical investigations on the electronic communication between the attached functional groups. The computational approach to determine electrochemical properties and the validation of the used level of theory are described in Section 3.3. Then, the electron affinities of the unsubstituted DEE, TEE, and of a series of functionalized TEE derivatives are compared in Section 3.4. The computed electronic features of the mono- and *trans*-dinitro substituted TEEs, presented in Section 3.4, reveal a much more complex picture than the electrochemical findings. A possible mechanism to reconcile the differing viewpoints between theory and electrochemistry is proposed in Section 3.5. Conclusions of these investigations and perspectives for further developments are addressed in Section 3.6.

3.2 Electrochemical Studies of Poly(*p*-nitrophenyl) Diethynylethenes and Tetraethynylethenes: The Experimental Findings

The description of the electrochemical reduction behavior of functionalized DEEs and TEEs has been limited to the unsubstituted systems and the mono- and bisnitro-substituted compounds that are of interest for the discussion of the electronic structures analyzed in the computational study. The reduction potentials of the entire series of donor and/or acceptor substituted TEEs can be referred to in published work.[25]

The electrochemical behavior of the entities nitrobenzene (NBZ), silylated DEE **1**, silylated TEE **2**, and arylated TEE **3**, as well as of their poly(*p*-nitrophenyl) derivatives **4**-**11** have been studied by cyclic voltammetry (CV) and steady state voltammetry (SSV) on a rotating disc electrode (RDE). The reduction properties obtained are summarized in Table 3.1.

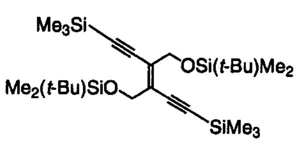
Me3Si
OSi(t-Bu)Me2
Me2(t-Bu)SiO
SiMe3

1

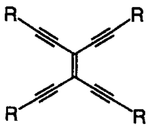

2 R = Me_3Si

3 R = Ph

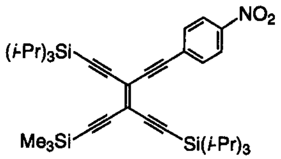
NO2
(i-Pr)3Si
Me3Si
Si(i-Pr)3

4

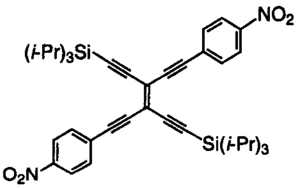
NO2
(i-Pr)3Si
O2N
Si(i-Pr)3

5

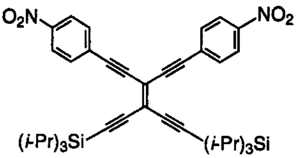
O2N
NO2
(i-Pr)3Si
(i-Pr)3Si

6

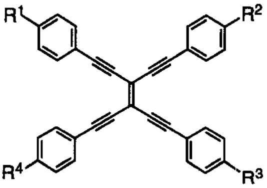

7 $R^1 = R^2 = R^3 = H, R^4 = NO_2$

8 $R^1 = R^3 = H, R^2 = R^4 = NO_2$

9 $R^1 = R^2 = H, R^3 = R^4 = NO_2$

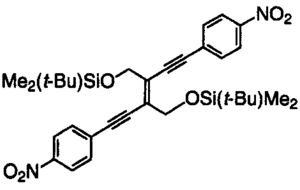
NO2
Me2(t-Bu)SiO
OSi(t-Bu)Me2
O2N

10

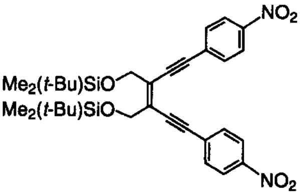
NO2
Me2(t-Bu)SiO
Me2(t-Bu)SiO
NO2

11

Table 3.1. Cyclic and steady state voltammetric reduction potentials for nitrobenzene (NBZ), diethynylethene **1**, tetraethynylethene **2**, functionalized tetraethynylethenes **3-9**, and the enediynes **10/11**.[a]

	Cyclic Voltammetry	Steady State Voltammetry	
compd	E° *vs.* Fc[b] (V)[c]	$E_{1/2}$ *vs.* Fc (V)[d]	no. of electrons
NBZ	−1.61 (80)		
1[e]	−2.68		
2[e]	−1.96 (320[f])	−2.02 (60)	1
		−2.50 (80)	
		−2.74 (160)	
3[e]	−1.76 (155[f])	−1.77 (60)	1
		−2.11 (70)	
		−2.32 (80)	
4	−1.36 (75)	−1.37 (68)	1
	−1.65 (75)	−1.68 (68)	1
5	−1.35 (85)	−1.37 (67)	2
	−1.73 (85)	−1.77 (62)	1
6	−1.38 (100)	−1.38 (92)	2
	−1.65 (73)	−1.71 (63)	1
7	−1.34 (90)	g	1
	−1.53 (85)		1
8	−1.29 (84)	−1.33 (61)	2
	−1.64 (100)	−1.71 (58)	1
9	−1.38 (150)	*ca.* −1.38[h]	2
	−1.57 (120)	*ca.* −1.57[h]	1
10	−1.42 (120)	−1.45 (100)	2
	−2.16	−2.12 (180)	1
11	−1.40 (100)	−1.44 (100)	2
	−2.09	−2.09 (115)	1

[a] Redox potentials observed in CH_2Cl_2 + 0.1 M Bu_4NPF_6 on glassy carbon. [b] Formal redox potential $E^\circ = (E_{pa} + E_{pc})/2$. [c] In parentheses: peak potential difference $\Delta E_p = E_{pc}$-E_{pa}, in mV, at scan rate = 100 mV s^{-1}. [d] In parentheses: slope of the wave in mV obtained by plotting E *vs.* log[I/Ilim−I)]. [e] Reduction potentials observed in THF + 0.1 M Bu_4NPF_6 at a Hg working electrode (ref. 11). [f] At scan rate = 10 V s^{-1}. [g] Not well defined. [h] Poorly resolved wave.

The electrochemical investigations were performed in the group of Prof. *M. Gross*, Université Louis Pasteur Strasbourg. The experiments were carried out at 20 ± 2 °C in CH_2Cl_2 containing 0.1 M Bu_4NPF_6 as the supporting electrolyte in a classical three electrode cell. The working electrode was either a glassy carbon (GC) or a Pt disk electrode. All potentials were referenced to the ferrocene/ferricinium (Fc/Fc+) couple which was used as an internal standard. The auxiliary electrode was a platinum wire, and a silver wire was used as a pseudo-reference electrode. The accessible range of potentials was +1.2 to –2.0 V *vs.* Fc/Fc+ on the Pt electrodes and +1.2 to –2.2 V *vs.* Fc/Fc+ on GC electrodes in CH_2Cl_2.

In the electrochemical investigations, CV and SSV gave concurring results. All species examined were electroactive within the available potential range, with the exception of **7** and **9** (Table 3.1). All species gave several reduction steps (Table 3.1).

Comparing the DEE **1** and TEE **2**, the reduction potentials clearly show that the addition of an electron to the TEE system is facilitated (occurring at less negative potentials). This behavior can be attributed to the two extra acetylenic branches, enabling a better stabilization of the incurred charge through inductive and mesomeric effects. It is known that isolated C≡C triple bonds are not reducible, but that they undergo electron reduction when they are embedded in π-electron conjugation with other multiple bonds.[26]

The *first* reduction step of **4-11** characteristically occurs at an average potential of –1.37 V/Fc. For the *trans*-bis(*p*-nitrophenyl) TEEs **5** and **8**, both SSV and CV confirm the presence of two overlapping and independent reduction events. This result suggests that the reduction occurs on the two nitrophenyl groups. Furthermore, the recently examined reduction behavior of a series of bis(*p*-nitrophenyl) endcapped DEE oligomers (up to the dodecamer) gave a first reversible reduction process, involving two electrons at a constant potential value of –1.39 V/Fc, independent of the chain length between the pendent end groups. These findings suggested as well, that the first reduction occurred at the terminal nitrophenyl groups.[27] For the *gem*-bis(*p*-nitrophenyl) TEEs **6** and **9**, on the other hand, SSV and CV indicate that the observed reduction involves two consecutive and overlapping charge transfers, the two reduction steps being separated by 70 mV and 75 mV, respectively. Spectroelectrochemical experiments on *gem*-**6** have also clearly shown that it is possible to electrogenerate either the radical anion or dianion due to the small potential difference existing between the two overlapping charge transfers. The absorption spectrum of the radical anion gives one band at 604 nm, whereas the dianion displays two bands at 572 nm and 612 nm.[25] This observation indicates that electronic communication exists between the two redox centers.

All mono- and bis(*p*-nitrophenyl) substituted TEEs **4-9** display a *second* reduction step at ca. –1.6 V/Fc, corresponding to a charge transfer to the TEE carbon framework. This reduction step to the TEE core is corroborated by comparison to the redox behavior of tetrakis(phenylethynyl)ethene **3**, where the absence of donor/acceptor functionality results in a reversible one-electron transfer at –1.68 V/Fc, very close to the second potentials observed for the nitrophenyl species.[11] Analysis of the *second* reduction potentials observed for the one-electron transfer to the TEE core of **4-9** reveals that the values for this redox step are dependent upon both orientation of the substituents about the TEE core and the nature of the other substituents present (*i.e.*, $(i\text{-Pr})_3\text{Si}$ *vs.* Ph).[25] The silylated dianionic species are more difficult to reduce than the analogous perarylated ones. This is in good agreement with the expectation that extension of the conjugated π-electron framework upon introduction of phenyl groups should lower the energy of the lowest unoccupied molecular orbital (LUMO).

In summary, for all mono- and bis(*p*-nitrophenyl) substituted TEEs, the first reduction wave has an amplitude proportional to the number of nitrophenyl groups present in the molecule, *i.e.* the electrons involved in the first reduction event are always equal the number of redox centers attached to the carbon core. The reduction potentials for bis(*p*-nitrophenyl) substituted TEEs suggest that the first reduction occur on both nitrophenyl end groups and, thus, the charges incurred are highly localized. The question whether both nitrophenyl groups behave essentially as independent two independent redox centers is now further addressed by theoretical investigations.

3.3 Computational Methodology and Validation Studies

All experimental reduction potentials reported in Section 3.2 have been measured against ferrocene and can be translated to electron affinities relative to vacuum by $EA_{vac} = -E_{red} - 5.32eV$.[28] This empirical formula relates computed electron affinities with redox potentials, although direct comparison of calculated and experimental data is not always straightforward. It should be pointed out that the theoretical data are single molecule (gas phase) values at 0 K with no counterions (electrolyte) involved. In the experiment, however, the charges can be stabilized via the presence of the electrolyte. The introduction of the counter charges in the theoretical model would change the situation dramatically, but the interaction between the counterions and the molecule can only be correctly described at a level including electron correlation. The corresponding computational effort is beyond the scope of this work.

The electron affinities are computationally determined as the difference of total energies. This study considers the adiabatic electron affinities, *i.e.* the total energies of the neutral compound and monoanion are investigated at their respective ***equilibrium*** structures.

$$EA_{ad} = E_{tot}^{ne} - E_{tot}^{ma} \tag{1}$$

Another way to determine the electron affinities is given by Koopmans' theorem. The theorem states that the ionization potential is equal to the energy of the highest occupied molecular orbital (HOMO) and that similarly, the electron affinity can be approximated by the energy of the lowest unoccupied molecular orbital (LUMO).[29] It has to be pointed out, that the electron affinities obtained by Koopmans' theorem are always smaller than those resulting from the adiabatic approach. This originates from the fact that, by Koopmans' theorem, the electrons in the anion are assumed to occupy the same orbitals than in the neutral molecule, *i.e.* no orbital relaxation upon adding an electron is taken into account.

All calculations were carried out using the restricted Hartree-Fock (RHF) and restricted open-shell Hartree-Fock (ROHF) schemes. Since electronic processes in organic systems lead to modifications of the molecular geometry, due to the strong correlation between the electronic structures and geometry,[30] it is essential that the electronic structure calculations are preceded by a geometry optimization. Validation studies on the TEE and NBZ geometries, reported in Chapter 2, have shown that for the molecular structure, computations at the HF/6-31G** level of theory appear to be appropriate. This is consistent with the general understanding that Hartree-Fock predicted geometries are quite reliable. However, the HF method is normally not sufficiently accurate for electronic properties like relative energies, binding energies, ionization potentials, electron affinities, *etc.* For energetic quantities, electron correlation effects must be taken into account.[31] Therefore, Density Functional Theory (DFT) employing Becke's three-parameter hybrid method[32] in conjunction with the Lee-Yang-Parr correlation functional[33], denoted B3LYP, was also used in the present study to investigate the electron affinities. This functional has proven to be among the most successful in providing reliable structures and energies.[34,35]

It is well know, that the basis set quality is very important in predicting the electronic properties of molecules. Therefore, analogous to the basis set study in Chapter 2, the electron affinities of TEE **12** and nitrobenzene (NBZ) are computed with the same group of basis sets, in order to determine the importance of larger basis sets for predicting accurate results. Details on the basis sets employed can be found in Section 2.2. The results of the validation study on the electron affinities are reported in Tables 3.2 and 3.3. For TEE, NBZ, and their respective monoanions, the geometries were optimized with all basis sets.

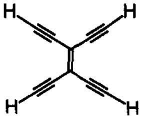

12

The results in Tables 3.2 and 3.3 show that the calculated electron affinities increase considerably using the B3LYP method. Moreover the HF and B3LYP calculated electron affinities increase with increasing basis set size. The addition of diffuse functions has tremendous effects on the calculated electron affinities.

Table 3.2. Total energy (in hartrees) and adiabatic energy difference (in eV) of **12** and radical anion $\mathbf{12}^{\bullet-}$.

level of theory	E_{tot} (ne)[a]	E_{tot} (ma)[b]	ΔE_{tot} (ne-ma)
HF/6-31G**	–380.729 714	–380.717 914	–0.321
HF/PVDZ	–380.748 649	–380.745 904	–0.075
HF/6-31+G*	–380.736 024	–380.738 997	0.080
HF/PVDZa	–380.753 479	–380.758 821	0.145
HF/PVDZ+	–380.756 380	–380.761 868	0.149
B3LYP/6-31G**	–383.169 746	–383.192 320	0.614
B3LYP/PVDZ	–383.189857	–383.221 806	0.869
B3LYP/PVDZa	–380.208 197	–383.252 897	1.216

[a]ne Designates the neutral species. [b]ma Designates the monoanion.

Table 3.3. Total energy (in hartrees) and adiabatic energy difference (in eV) of NBZ and NBZ$^-$.

level of theory	E_{tot} (ne)[a]	E_{tot} (ma)[b]	ΔE_{tot} (ne-ma)
HF/6-31G**	–434.184 268	–434.174 157	–0.275
HF/PVDZ	–434.212 263	–434.202 615	–0.262
HF/6-31+G*	–434.187 981	–434.196 345	0.227
HF/PVDZa	–434.223 327	–434.231 596	0.227
B3LYP/6-31G**	–436.758 512	–436.777 226	0.509
B3LYP/PVDZ	–436.782 994	–436.804 190	0.577
B3LYP/PVDZa	–436.813 513	–436.856 413	1.167

[a] ne Designates the neutral species. [b] ma Designates the monoanion.

According to the findings from the basis set evaluation on the molecular structures (Chapter 2), all geometries were optimized using the 6-31G** basis set. Single-point energy calculations of *trans*-bis(*p*-nitrophenyl) substituted TEE were then performed at the geometry obtained at the HF/6-31G** level using extended basis sets (*i.e.*, HF/PVDZa// HF/6-31G**). It clearly appeared from the studies on the electron affinities of TEE that a polarization function along with a diffuse p-type function are necessary to accurately determine the electronic structure of the anions. Additional diffuse s- and d-functions, however, did not seem to be critical components and were therefore omitted in the computations of the electron affinities of *trans*-bis(*p*-nitrophenyl) TEE. Thus, only the correlation consistent basis sets PVDZ and PVDZa were employed. C_s symmetry was applied for all investigated systems. The PDVZ (9s4p1d/4s1p)[3s2p1d/2s1p] and PVDZa (9s5p1d/4s1p) [3s3p1d/2s1p] working basis sets for *trans*-bis(*p*-nitrophenyl) TEE consisted of a total of 470 and 554 contracted basis functions, respectively. The programs used were the Gaussian 94 package,[36] DISCO,[37] and TURBOMOLE.[38] The molecular orbitals were visualized with the molecular graphics package MOLEKEL.[39]

3.4 Electronic Structures and Energetics of Tetraethynylethene Derivatives

3.4.1 Electronic Characteristics and Electron Affinities of Mono- and *trans*-Bis(*p*-nitrophenyl) Tetraethynylethenes

In order to predict and compare the redox characteristics of TEE derivatives, the computations focus on the investigation of the electronic structures (ground state) of neutral mono(*p*-nitrophenyl) TEE, **13**, its radical anion $\mathbf{13}^{\bullet-}$, *trans*-bis(*p*-nitrophenyl) TEE, **14**, as well as its radical anion $\mathbf{14}^{\bullet-}$ and dianion $\mathbf{14}^{2-}$.

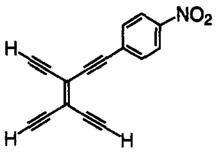

13

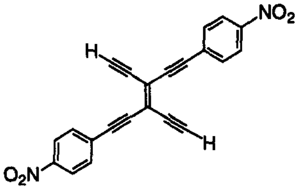

14

Optimization of the ground state geometries have predicted a transition from a benzoid/acetylenic like form to a quinoid/cumulenic form in the reduced state as discussed in Chapter 2. The changes in the molecular structures upon reduction can be qualitatively understood by inspecting the electronic structures of the different reduced states of **13** and **14**. For simplification, the present discussion is based on the shape of the molecular orbitals (MOs) (Figures 3.1 and 3.2) and the Mulliken charges (Table 3.4) for each compound at its respective equilibrium geometry.

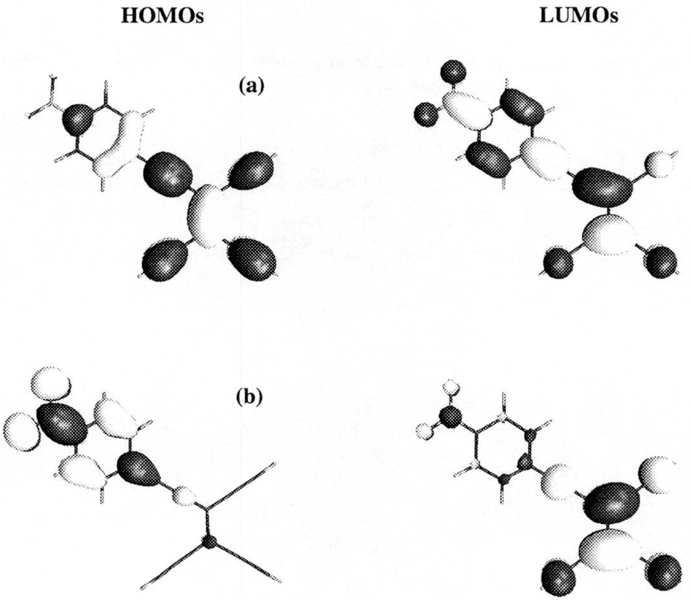

Figure 3.1. Highest occupied molecular orbitals (HOMOs; left) and lowest unoccupied molecular orbitals (LUMOs; right) of (a) neutral **13** and (b) radical anion **13**$^{\bullet -}$.

Figure 3.1 shows that in **13**$^{\bullet -}$ the additional charge localizes on the nitrophenyl ring as one would expect from chemical intuition. For disubstituted **14**, however, the first electron addition is strongly localized on the central ethylenic bond, and, somewhat surprisingly, very little charge is found on the nitrophenyl groups (Figure 3.2 b). Indeed, the highest occupied molecular orbital (HOMO) of the radical anion **14**$^{\bullet -}$ shows strong π^* antibonding character for the central bond, resulting in a lengthening of this bond. For the dianion **14**$^{2-}$, considerable charge is also now found on the nitrophenyl groups (Figure 3.2 c), and the charge is more evenly distributed throughout the molecule.

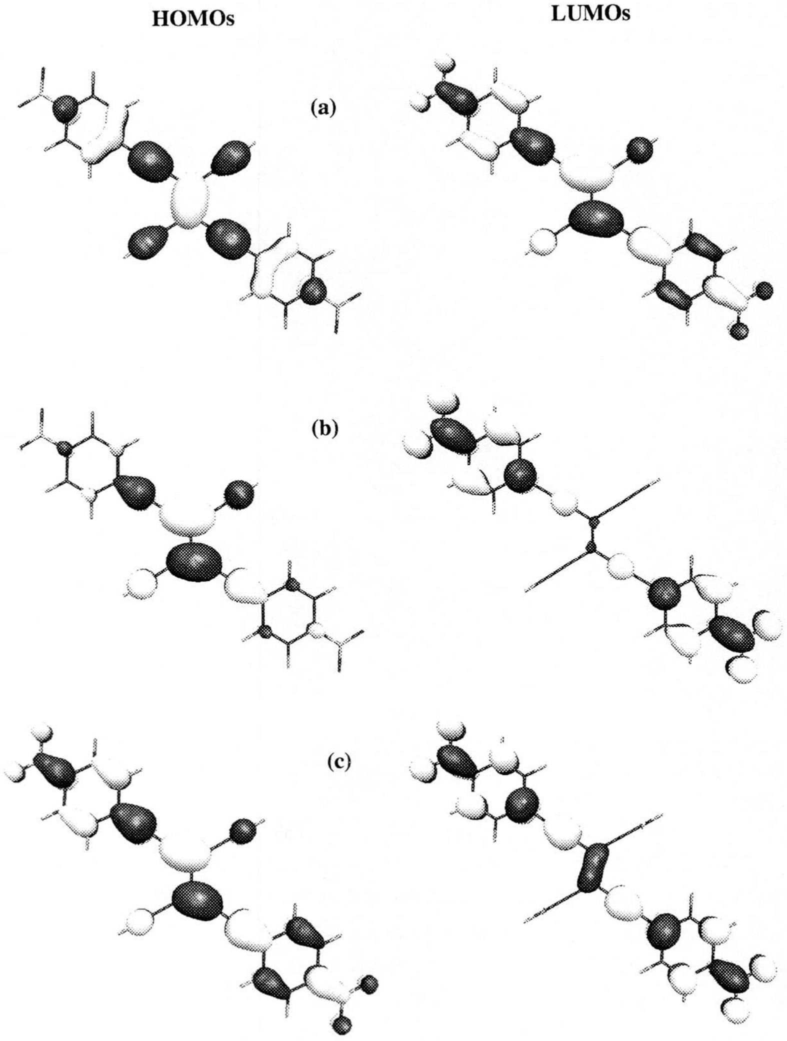

Figure 3.2. Highest occupied molecular orbitals (HOMOs; left) and lowest unoccupied molecular orbitals (LUMOs; right) of (a) neutral **14**, (b) radical anion $\mathbf{14}^{\bullet-}$, and (c) dianion $\mathbf{14}^{2-}$.

It seems that the nitrophenyl groups in **14** enhance the local electron affinity of the central ethylenic bond, thus in the first reduction step the charge does not migrate onto the nitrophenyl units, but is accommodated mainly by the central bond. Only in the second reduction step does charge accumulation on the nitrophenyl groups become significant (Table 3.4).

Table 3.4. HF/6-31G** Mulliken charges (in | *e* |) on selected atoms of **14**, its radical anion **14**$^{\bullet-}$, and dianion **14**$^{2-}$ at equilibrium structure.

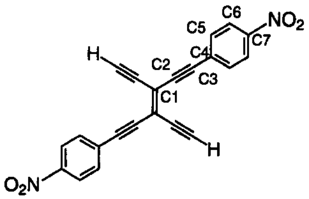

atom	ne[a]	ma[b]	da[c]
C_1	0.058	–0.075	–0.151
C_2	0.016	0.058	0.079
C_3	–0.233	–0.291	–0.242
C_4	0.036	0.054	–0.003
C_5	–0.122	–0.153	–0.177
C_6	–0.106	–0.098	–0.084
C_7	0.137	0.101	0.051
$-NO_2$	–0.416	–0.491	–0.685

[a]ne Designates the neutral species. [b]ma Designates the monoanion. [c]da Designates the dianion.

The different reduction behavior of compounds **13** and **14** can be illustrated in terms of the form and ordering of the molecular orbitals: the LUMOs of both molecules in their neutral states show strong delocalization (Figures 3.1 and 3.2). Once reduced (*i.e.*, the LUMO is half occupied and turns into the HOMO of the monoanion), a distinctly different situation is encountered. The HOMOs of both systems undergo localization, however, in opposite directions. The HOMO of **13**$^{\bullet-}$ localizes on the nitrophenyl unit, whereas the HOMO of **14**$^{\bullet-}$ localizes on the central ethylenic bond. Accordingly, the LUMOs of the respective monoanions show complementary behavior. The strong electronic relaxation effects and the concomitant structural relaxations involved make a prediction of properties based on inspection of the electronic structure of the neutral species very difficult, and thus the calculation and examination of the anions are essential. It should be pointed out that the MOs of the bis(*p*-nitrophenyl) DEEs calculated at the B3LYP//6-31G** level of theory have been analyzed as well, and give similar molecular orbital representations for the nitrosubstituted compounds **13** and **14**.

The electron affinities of *trans*-bis(*p*-nitrophenyl) TEE **14** computed at the HF and B3LYP level are presented in Table 3.5. For the first reduction step, an electron affinity of 1.267 eV is found (HF/PVDZa//HF/6-31G**) and for the second −1.607 eV. Using B3LYP/6-31G**// HF/6-31G**, the first electron affinity is determined to be 2.367 eV, whereas the second electron affinity is −0.582 eV. A direct comparison between the computed and experimental data (Section 3.2) for *trans*-bis(*p*-nitrophenyl) TEE **14** is difficult, particularly for the second reduction step. Whereas experiments have found little or no difference in the redox potentials for the first two electron transfer events, the computations would predict two distinct reduction potentials. The reason could lie in the fact that the calculated data are gas phase values, whereas the experiments have been carried out in CH_2Cl_2 containing Bu_4NPF_6 as the supporting electrolyte.

Table 3.5. Total energy (in hartrees) and adiabatic energy difference (in eV) of **14**, its radical anion $\mathbf{14}^{\bullet-}$, and dianion $\mathbf{14}^{2-}$.

level of theory	E_{tot} (ne)[a]	E_{tot} (ma)[b]	E_{tot} (da)[c]
HF/6-31G**	−1246.803 313	−1246.833 336	−1246.762 003
HF/PVDZ // HF/6-31G**	−1246.878 374	−1246.914 644	−1246.847 016
HF/PVDZa // HF/6-31G**	−1246.901 901	−1246.948 476	−1246.889 405
B3LYP/6-31G**// HF/6-31G**	−1254.301 835	−1254.388 869	−1254.367 474
B3LYP/6-31G**	−1254.320 283	−1254.406 064	−1254.384 492
level of theory	ΔE_{tot} (ne-ma)	ΔE_{tot} (ma-da)	ΔE_{tot} (ne-da)
HF/6-31G**	0.817	−1.940	−1.123
HF/PVDZ // HF/6-31G**	0.986	−1.839	−0.853
HF/PVDZa // HF/6-31G**	1.267	−1.607	−0.340
B3LYP/6-31G**// HF/6-31G**	2.367	−0.582	1.785
B3LYP/6-31G**	2.333	−0.587	1.746

[a]ne Designates the neutral species. [b]ma Designates the monoanion. [c]da Designates the dianion.

3.4.2 Modulation of Electron Affinities Through Extension of the π-Conjugation and Through Donor and/or Acceptor Substitution

In order to analyze the effects of conjugation and substitution on the electronic characteristics, the electron affinities of DEE **15**, TEE **12**, bisarylated TEE **16**, as well as of mono(*p*-nitrophenyl) TEE **13**, *trans*-bis(*p*-nitrophenyl) TEE **14**, *trans*-bis(*p*-aminophenyl) TEE **17**, and *trans*-bis(3,5-dimethoxyphenyl) TEE **18** are inspected. The results computed at HF/6-31G** level of theory are summarized in Table 3.6 and have to be viewed qualitatively.

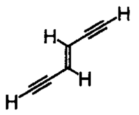

15

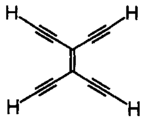

12

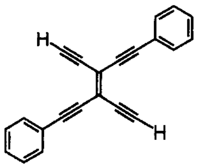

16

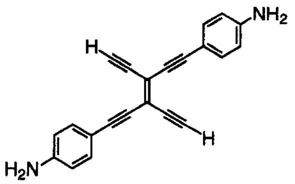

17

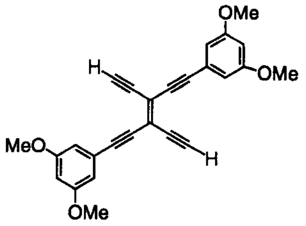

18

Table 3.6. HF/6-31G** Total energy (in hartrees) and adiabatic energy difference (in eV) of **12**-**17** and their radical anions.

compound	E_{tot} (ne)[a]	E_{tot} (ma)[b]	ΔE_{tot} (ne-ma)
DEE **15**	–229.391 646	–229.338 614	–1.442
TEE **12**	–380.729 714	–380.717 914	–0.321
bis(phenyl) TEE **16**	–839.866982	–839.863686	–0.090
mono(*p*-nitrophenyl) TEE **13**	–813.766 675	–813.774 765	0.220
bis(*p*-nitrophenyl) TEE **14**	–1246.803 313	–1246.833 336	0.817
bis(*p*-aminophenyl) TEE **17**	–949.935 138	–949.917 007	–0.493
bis(3,5-dimethoxyphenyl) TEE **18**	–1295.401 166	–1295.400 023	–0.031

[a]ne Designates the neutral species. [b]ma Designates the monoanion.

The EA of DEE **15** is the lowest in this series with a value of –1.442 eV. Reduction becomes more facile in TEE **12** (EA=–0.321 eV), and even easier in the arylated TEE **16** (EA=–0.090 eV). These findings show that the electron affinity increases with the extension of the π-conjugated framework by the acetylenic moieties and the phenyl rings. The same observations have been found in the electrochemically determined reduction potentials (Section 3.2). Comparisons between unsubstituted diarylated TEE **16**, donor-donor TEE **17**, and acceptor-acceptor TEE **14** illustrate that, whereas nitro groups increase the EA of diarylated TEE **16** by 0.907 eV (EA(**16**) = –0.090 eV and EA(**14**) = 0.817 eV), π-electron donating amino groups, as expected, decrease the EA by 0.403 eV (EA(**17**) = –0.493 eV). The methoxy groups do not seem to significantly alter the EA, since the EA difference between **16** and **18** amounts to merely 0.059 eV.

In Table 3.7 the frontier orbitals of DEE **15** and TEE **12**, as well as of the substituted TEEs are reported and the evolution of the highest occupied molecular orbital (HOMO) and the lowest unoccupied molecular orbital (LUMO) energies in the extended π-conjugated systems and with different substituents are analyzed.

Table 3.7. HF/6-31G** Frontier orbitals energy (in hartrees) and energy difference (in eV) of neutral DEE **15**, TEE **12**, and functionalized TEEs **13**, **14**, and **16-18**.

compound	HOMO	LUMO
DEE **15**	−8.886	2.509
TEE **12**	−8.481	1.381
bis(phenyl) TEE **16**	−7.530	1.168
mono(*p*-nitrophenyl) TEE **13**	−8.411	0.364
bis(*p*-nitrophenyl) TEE **14**	−8.393	0.135
bis(*p*-aminophenyl) TEE **17**	−6.694	1.630
bis(3,5-dimethoxyphenyl) TEE **18**	−7.893	1.266

Compared to DEE **15**, the LUMOs of the TEE **12** and bisarylated TEE **16** are stabilized upon introduction of the two acetylenic moieties and the phenyl rings, respectively. In accord with the electron affinities calculated in the adiabatic approach, the LUMOs also reflect that the extension of the π-conjugation carbon framework increases the reduction ability.

Taking bisarylated TEE **16** as a reference, the nitrophenyl substituted TEEs **13** and **14** exhibit an overall stabilization of the frontier orbitals. This is expected from the π-acceptor nature of the nitro group. The bis(aminophenyl) functionalized TEE derivative **17**, on the other hand, shows an overall destabilization of the frontier orbitals, due to the π-donating effect of the amino group. The LUMO energy of the bis(3,5-dimethoxyphenyl) TEE **18** is less destabilized than the one of the bis(aminophenyl) TEE **17** (1.266 eV *vs.* 1.630 eV, respectively). This indicates that, as expected, the donor substituents in meta position, as opposed to para position, have less influence on the electronic structure of the systems, due to smaller participation in the π-electron delocalization.

3.5 Formation of Charge States in Nitrophenyl Diethynylethene and Tetraethynylethene Oligomers

From the theoretical and experimental investigations on the reduction of the bis(*p*-nitrophenyl) substituted DEE and TEE systems, the following situation emerged: on one hand, the electrochemistry showed two closely spaced waves upon the first reduction, suggesting the terminal nitrophenyl groups to undergo reduction independently, and, on the other hand, HF calculations predicted strong structural modifications of the entire conjugated system, coupled with an even charge distribution throughout the molecule. In the following, the attempt to reconcile those two conflicting observations is outlined.

3.5.1 Polaron-like Radical Anions and Bipolaron-like Dianions as Charge Carriers in Bis(*p*-nitrophenyl) Substituted Tetraethynylethenes

Conductivity in doped polyacetylene and doped poly(*p*-phenylene) is associated with the propagation of local defects along the π-conjugated polymer chain, generating local relaxation of the polymer structure.[40,41] These defects can be classified into spinless charge carriers (charged solitons and bipolarons) and into charge states with spin (neutral solitons and polarons).[42-49] An example of these charge states on polyacetylene and poly(*p*-phenylene) is depicted in Figure 3.3. The doubly charged defects (bipolarons) are formed through combination of two radical ions or through a second ionization of the radical ion. A bipolaron is thus defined as a pair of identical charges associated with a strong local structural distortion. The migration of these diions is at the origin of the spinless conductivity in these polymers. Bipolarons in poly(*p*-phenylene) have been calculated to extend over four to five phenyl rings (without consideration of counter ions).[43] The quinoid form of poly(*p*-phenylene) has a higher electron affinity than the benzoid structure. However, calculations on oligomers of poly(*p*-phenylene), polypyrrole, and polythiophene have indicated that going from fully aromatic to fully quinoid structure cost about 15-20 kcal/mol per ring.[46] Thus, the formation of a bipolaron occurs when the energy gained by oxidation or reduction is larger than the one needed for the structural deformation.[46]

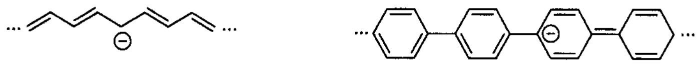

charged solitons

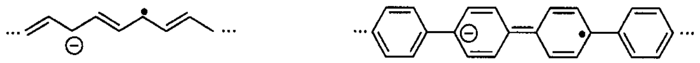

polarons

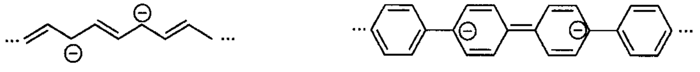

bipolarons

Figure 3.3. Negatively charged defects in polyacetylene and polyparaphenylene.

One possible explanation for the observed phenomena in the series of bis(*p*-nitrophenyl) DEEs and TEEs could be the result of a bipolaron mechanism. Upon reduction, compound **14** is ionized to produce a radical anion (polaron) **19** which will localize on the reduction site, *i.e.* the nitro group (Figure 3.4). The radical anion being easily reduced, a second electron immediately (or concurrently) enters the molecule and localizes on the other nitrogroup (**20**). The two independent polarons are not stable, and thus interact to form a dianion **21**, referred to as a bipolaron in terms of polymer physics. The recombination induces a large structural rearrangement to a cumulenic-like carbon core. The exceptional stability of the bis(*p*-nitrophenyl) DEE and TEE dianions can be explained by a significant stabilization through the inductive and mesomeric effect of the electron-withdrawing nitro groups. In the alternative structure **20** with two independent polarons, the enediyne structure of the TEE core is preserved, and only the nitrophenyl rings adopt a quinoid-like form. This two-polaron form **20** is not likely, since the molecular structure would not be consistent with the calculated cumulenic TEE core and with the low barrier to rotation about the central olefinic bond, found in this work and described in detail in Chapter 4. This bipolaron interpretation would explain the observed two-electron reduction process involving a strong molecular deformation as a result of the intramolecular recombination mechanism.

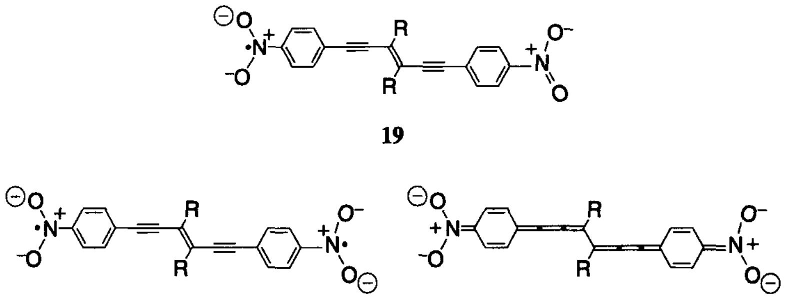

19

20 **21**

Figure 3.4. Proposed structures for radical anion **19**, biradical **20**, and dianion **21** of bis(*p*-nitrophenyl) substituted monomers. R=$OSi(t\text{-}Bu)Me_2$ or acetyl-$Si(alkyl)_3$.

The formation of highly stable bipolarons upon reduction may also explain the electrochemical behavior of a series of bis(*p*-nitrophenyl) endcapped DEE oligomers, recently investigated in the group of Prof. *M. Gross.*[27] Somewhat unexpected, for this series of DEE oligomers, the second reduction, *i.e.* the addition of the third electron on the π-conjugated carbon backbone, is even more facile than the first reduction event of the corresponding neutral silylated DEEs.[27] The ease of adding a third electron can be attributed to the high electron affinity of the cumulenic chain of the carbon framework, sketched in Figure 3.5 for dimer **22**. Comparing the electron affinities of the acetylenic (**23**) and cumulenic (**24**) alternatives of the central carbon chain, it can be deduced that it is easier to insert an electron to the cumulenic-like form. Indeed, the electron affinity of hexatriyne **23** is calculated at the HF/6-31G** level of theory to be –1.750 eV, whereas the cumulenic representative [5]cumulene **24** has yielded an electron affinity of –0.439 eV. These values are not to be considered quantitatively, but rather qualitatively for comparison purposes. Adding another electron to the cumulenic carbon chain will generate a charged radical, where the charge can migrate along the carbon axis and will cause a local geometry distortion, thus, reforming the original acetylenic structure.

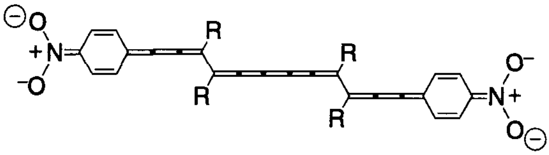

22

Figure 3.5. Proposed structure for dianion of bis(*p*-nitrophenyl) substituted dimer.

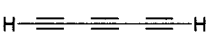

23

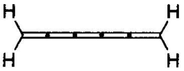

24

Figure 3.6. Acetylenic (**23**) and cumulenic (**24**) alternative structures for the central carbon entity of the doubly reduced form of bis(*p*-nitrophenyl) substituted dimer **22**.

With increasing chain length of the nitrophenyl substituted and silylated DEE oligomers, the difference between the reduction potentials diminishes and in both hexamers the reduction is observed at almost the same potential.[27] This indicates that at longer chain length, the end groups do not effect the electronic reduction process anymore. In the bipolaron language, this signifies that the propagation of the radicals through the carbon chain terminates at a certain covered distance. A suggested structure of the reduced hexamer is depicted in Figure 3.7. The radicals would localize on a carbon atom and the two radicals would not recombine anymore to form a bipolaron. Hence, the structural modifications are confined to two segments of the oligomer and the central part of the carbon chain remains unaffected, preserving the acetylenic-like resonance form. Additional experiments are required to verify and precisely elucidate these suggested process sequences.

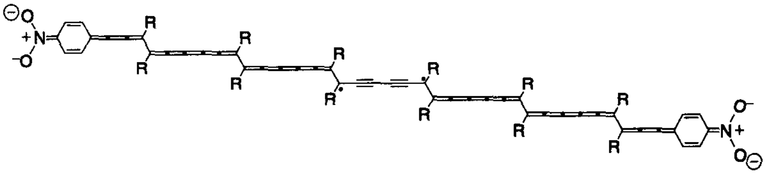

25

Figure 3.7. Proposed structure for dianion of bis(*p*-nitrophenyl) substituted hexamer.

3.5.2 Experimental Evidence of Bipolaron Formation Through Spectroelectrochemical Studies of Mono- and Bis(*p*-nitrophenyl) Substituted Tetraethynylethenes

The presence of a bipolaron can be monitored by investigation of the optical spectra upon reduction. Indeed, *Brédas* et al. have shown that polaron and bipolaron formation give rise to new electronic transitions within the optical gap appearing at higher wavelength, *i.e.* at lower energy.[49]

Spectroelectrochemical measurements, performed in the group of Prof. *M. Gross*, Université Louis Pasteur Strasbourg. were carried out in a thin layer cell (0.1 mm) through an optically transparent thin layer electrode (OTTLE) made of a Pt minigrid (1000 mesh). The auxiliary electrode was a Pt wire, and an aqueous Ag/AgCl electrode was used as the reference. The OTTLE cell was placed in a diode array UV/VIS spectrophotometer.

OTTLE studies of the first reduction steps for **4** and **5** give nice spectral evolutions with well defined isosbestic points. In each case, reversibility has been confirmed as the initial absorption spectrum could be quantitatively recovered through reoxidation. For the mono(*p*-nitrophenyl) derivative **4**, Figure 3.8 shows an absorption at 590 nm for the reduced species, a value characteristic of a reduced nitrophenyl moiety.[50]

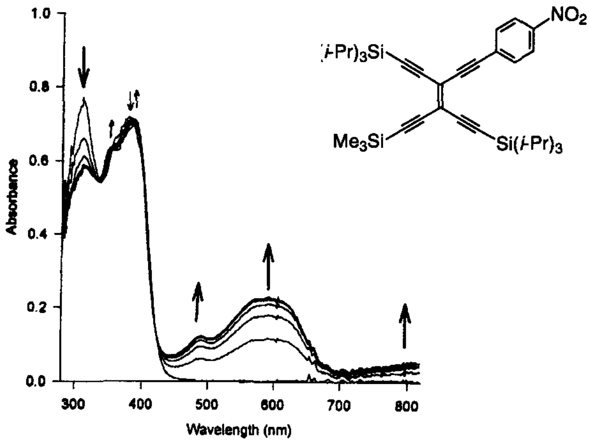

Figure 3.8. Time-resolved UV/Vis spectra for OTTLE reduction of **4** in CH_2Cl_2 + 0.1 M Bu_4NPF_6.

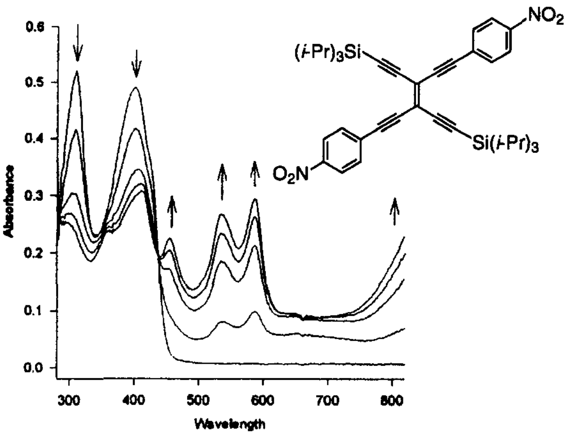

Figure 3.9. Time-resolved UV/Vis spectra for OTTLE reduction of **5** in CH_2Cl_2 + 0.1 M Bu_4NPF_6.

For **5** containing two nitrophenyl groups, Figure 3.9 shows that the reduced species gives rise to bands at 534 and 586 nm, as well as a low energy absorption above 820 nm. The electronic transition at 586 nm constitutes the new optical sign of the formed bipolaron. Similarly, for bis(*p*-nitrophenyl) substituted polyenes with a chain length of 12 carbon atoms, *Spangler* et al. have observed the maximum of the longest bipolaronic wavelength at 654 nm.[42] The presence of clear isosbestic points in Figure 3.9 indicates that both nitrophenyl groups are reduced concurrently and no intermediate species could be observed on the time scale of the OTTLE measurements, *i.e.* the two nitrophenyl groups in **5** behave as two independent redox centers. The perarylated **8** displays two bands at 560 and 606 nm, slightly lower in energy than those in **5**. This confirms the expectation that insertion of phenyl groups extends the π-electron skeleton and enables a better overall charge delocalization.

3.6 Concluding Remarks

Electrochemical analyses of acceptor functionalized tetraethynylethenes indicate that the conjugated carbon core is inefficient at delocalizing charges between redox centers. Thus, the first redox potentials of these molecules are essentially independent of the substitution pattern about the TEE core or the presence of other functionality. In particular, the first reduction potentials of mono- and bis(*p*-nitrophenyl) substituted TEEs occur at similar values, and the reduction waves have amplitudes proportional to the number of nitrophenyl groups present in the molecule. These results predict that the incurred charges are highly localized, and the nitrophenyl groups behave essentially as independent redox centers. Charge transfers at subsequent reduction potentials occur to the TEE core and are affected by other substituents and their orientation.

The computed electronic structures, however, clearly reveal that the incurred charges are effectively distributed by the enynes throughout the π-conjugated carbon framework. The calculated electronic structure of the singly reduced mono(*p*-nitrophenyl) substituted TEE $\mathbf{13}^{\bullet-}$ shows that the charge mainly localizes on the nitrophenyl ring, whereas in the bis(*p*-nitrophenyl) functionalized TEE radical anion $\mathbf{14}^{\bullet-}$, the charge is localized on the TEE core. Only in the dianion $\mathbf{14}^{2-}$ considerable charge accumulates on the two nitrophenyl ends. As a result of its electronic structure, the reduced species encounters strong structural changes.

A so-called bipolaron mechanism is suggested to rationalize the calculated and experimental observations. Indeed, the bipolaron formation accounts for the electrochemically observed first two-electron reduction, since two electrons enter almost concurrently (at the same potential) the system. Then, the two formed radical anions recombine, inducing strong structural rearrangement, to yield a dianion (bipolaron). This behavior is consistent with the strong cumulenic/quinoid character of bis(*p*-nitrophenyl) substituted TEE **14**$^{2-}$ predicted by the calculations. To further elucidate this proposed mechanism responsible for the two-electron process phenomena, the nitrophenyl DEE oligomers should be monitored spectroelectrochemically upon reduction. With increasing DEE chain length, the longest wave absorption of the nascent dianion should appear at lower energy as a result of the decreasing HOMO-LUMO gap. Indeed, with a decrease of the band gap, consequently, the energies of the bipolaronic levels generated within this gap will be lowered as well.

To confirm the cumulenic structure of the carbon chain in the bis(*p*-nitrophenyl) functionalized DEE and TEE oligomers, the molecular and electronic features of the neutral dimer, as well as of its radical anion, dianion, and trianion should be calculated. According to the delocalization scheme, the cumulenic type backbone should regain its acetylenic form in the trianion.

In order to gain a better understanding of the transport phenomena of polarons and bipolarons in these π-conjugated systems, calculations of the radical cations and dications of the diamino functionalized TEEs should be performed. It is known, that electron affinities are more difficult to calculate than ionization potentials and, therefore, it might be less demanding in terms of required theory and basis sets to calculate accurate ionization potentials and compare them to the experimentally determined oxidation potentials. By analyzing the electronic structures of the oxidized donor substituted TEEs, observations similar to those for the reduced acceptor functionalized TEEs should emerge.

3.7 References

[1] Q. Zhou, T. M. Swager, *J. Org.Chem.* **1995**, *60*, 7096-7100. Probing Delocalization across Alkyne-Containing Linkages: Synthesis and Cyclic Voltammetry of Bridged Phenylenediamines.

[2] W. Kemula, T. M. Krygowski, in *Encyclopedia of Electrochemistry of the Elements, Organic Section*; A. J. Bard, H. Lund (Eds.), M. Dekker: New York, 1979; Vol. XIII, Chapter 2. Nitro Compounds.

[3] A. H. Maki, D. H. Geske, *J. Am. Chem. Soc.* **1961**, *83*, 1852-1860. Electron Spin Resonance and Polarographic Investigation of Substituted Nitrobenzene Negative Ions.

[4] D. H. Geske, A. H. Maki, *J. Am. Chem. Soc.* **1960**, *82*, 2671-2676. Electrochemical Generation of Free Radical and Their Study by Electron Spin Resonance Spectroscopy; the Nitrobenzene Anion Radical.

[5] B. S. Jensen, V. D. Parker, *J. Chem. Soc., Chem. Commun.* **1974**, 367-368. Reversible Anion Radical-Dianion Redox Equilibria Involving Ions of Simple Aromatic Compounds.

[6] T. M. Krygowski, M. Stencel, Z. Galus, *J. Electroanal. Chem.* **1972**, *39*, 395-405. Polarographic and Voltammetric Study of Mono-Nitro Derivatives of Benzenoid Hydrocarbons in DMF-Interpretation within Hammett-Streitwieser Equation and HMO-Theory.

[7] D. H. Geske, J. L. Ragle, M. A. Bambenek, A. L. Balch, *J. Am. Chem. Soc.* **1964**, *86*, 987-1002. Study of Steric Effects by Electron Spin Resonance Spectroscopy and Polarography. Substituted Nitrobenzenes and Nitroanilines.

[8] F. Ammar, J. M. Savéant, *J. Electroanal. Chem.* **1973**, *47*, 115-125. Thermodynamics of Successive Electron Transfers. Internal and Solvation Enthalpy and Entropy Variations in a Series of Polynitro Compounds.

[9] J. Anthony, C. Boudon, F. Diederich, J.-P. Gisselbrecht, V. Gramlich, M. Gross, M. Hobi, P. Seiler, *Angew. Chem.* **1994**, *106*, 794-798; *Angew. Chem. Int. Ed. Engl.* **1994**, *33*, 763-766. Stable Soluble Conjugated Carbon Rods with a Persilylethynylated Polytriacetylene Backbone.

[10] J. Anthony, Ph. D. Thesis, University of California, Los Angeles, 1993. Cross-

Conjugated Carbon-Rich Compounds.

[11] C. Boudon, J.-P. Gisselbrecht, M. Gross, J. Anthony, A. M. Boldi, R. Faust, T. Lange, D. Philp, J.-D. Van Loon, F. Diederich, *J. Electroanal. Chem.* **1995**, *394*, 187-197. Electrochemical Properties of Tetraethynylethenes, Fully Cross-Conjugated π-Chromophores, and Tetraethynylethene-Based Carbon-Rich Molecular Rods and Dehydroannulenes.

[12] M. Schreiber, J. Anthony, F. Diederich, M. E. Spahr, R. Nesper, M. Hubrich, F. Bommerli, L. Degiorgi, P. Wachter, P. Kaatz, C. Bosshard, P. Günter, M. Colussi, U. W. Suter, C. Boudon, J.-P. Gisselbrecht, M. Gross, *Adv. Mater.* **1994**, *6*, 786-790. Polytriacetylenes: Conjugated Polymers with a Novel All-Carbon Backbone.

[13] H. Schimanke, R. Gleiter, *Organometallics* **1998**, *17*, 275-277. Synthesis and Electrochemical Properties of Butadiyne-Bridged Cyclopentadienylcobalt-Cyclobutadiene Complexes.

[14] T. Bartik, B. Bartik, M. Brady, R. Dembinski, J. A. Gladysz, *Angew. Chem.* **1996**, *108*, 467-469; *Angew. Chem., Int. Ed. Engl.* **1996**, *35*, 414-417. A Step-Growth Approach to Metal-Capped One-Dimensional Carbon Allotropes: Syntheses of C_{12}, C_{16}, and C_{20} μ-Polyynediyl Complexes.

[15] M. Brady, W. Weng, J. A. Gladysz, *J. Chem. Soc., Chem. Commun.* **1994**, 2655-2656. New Families of Coordinated Carbon: Oxidative Coupling and Cross-coupling of a Transition Metal Butadiynyl Complex to Bimetallic M–C≡CC≡CC≡CC≡C–M and M–C≡CC≡CC≡C–M Adducts.

[16] M. Brady, W. Weng, Y. Zhou, J. W. Seyler, A. J. Amoroso, A. M. Arif, M. Böhme, G. Frenking, J. A. Gladysz, *J. Am. Chem. Soc.* **1997**, *119*, 775-788. Consanguineous Families of Coordinated Carbon: A ReC_4Re Assembly That Is Isolable in Three Oxidation States, Including Crystallographically Characterized ReC≡CC≡CRe and $^+Re=C=C=C=Re^+$ Adducts and a Radical Cation in Which Charge Is Delocalized between Rhenium Termini.

[17] I. Jestin, P. Frère, N. Mercier, E. Levillain, D. Stievenard, J. Roncali, *J. Am. Chem. Soc.* **1998**, *120*, 8150-8158. Synthesis and Characterization of the Electronic and Electrochemical Properties of Thienylenevinylene Oligomers with Multinanometer Dimensions.

[18] E. H. Elandaloussi, P. Frère, P. Richomme, J. Orduna, J. Garin, J. Roncali, *J. Am.*

Chem. Soc. **1997**, *119*, 10774-10784. Effect of Chain Extension on the Electrochemical and Electronic Properties of π-Conjugated Soluble Thienylenevinylene Oligomers.

[19] C. K. Chien, H. C. Wang, M. Szwarc, A. J. Bard, K. Itaya, K. *J. Am. Chem. Soc.* **1980**, *102*, 3100-3104. Electron Transfer Induced Isomerization of *cis*-4,4'-Diphenylstilbene into Its Trans Form.

[20] H. C. Wang, G. Levin, M. Szwarc, *J. Am. Chem. Soc.* **1977**, *99*, 2642-2647. Kinetics of Isomerization of the Free *cis*-Stilbene Radical Anion into Its Trans Isomer in Hexamethylphosphoric Triamide. Spectroscopic and Electron Spin Resonance Identification of *cis*-Stilbene Radical Anion in Tetrahydrofuran.

[21] M. O. Wolf, H. H. Fox, M. A. Fox, *J. Org. Chem.* **1996**, *61*, 287-294. Reduction of Acetylated Tetraphenylethylenes: Electrochemical Behavior and Stability of the Related Reduced Anions.

[22] D. A. Shultz, M. A. J. Fox, *Org. Chem.* **1990**, *55*, 1047-1051. Structural Effects on the Disproportionation Equilibrium of Tethered Tetraphenylethylene Radical Anions.

[23] M. A. Fox, D. A. Shultz, *J. Org. Chem.* **1988**, *53*, 4386-4390. Twisting in the Tetraphenylethylene Dianion.

[24] J. L. Muzyka, M. A. Fox, *J. Org. Chem.* **1991**, *56*, 4549-4552. Effect of Substituents on the Electrochemistry of Substituted Tetraphenylethylenes.

[25] A. Hilger, J.-P. Gisselbrecht, R. R. Tykwinski, C. Boudon, M. Schreiber, R. E. Martin, H. P. Luethi, M. Gross, F. Diederich, *J. Am. Chem. Soc.* **1997**, *119*, 2069-2078. Electronic Characteristics of Arylated Tetraethynylethenes: A Cooperative Computational and Electrochemical Investigation.

[26] J. Perichon, M. Herlem, F. Bobilliart, A. Thiebault, K. Nyberg, in *Encyclopedia of Electrochemistry of Elements*; A. J. Bard, H. Lund (Eds.), M. Dekker: New York, 1978; Organic Section, Vol. XI, Chapter 1. Hydrocarbons.

[27] J.-P. Gisselbrecht, C. Boudon, M. Gross, unpublished results, 1998.

[28] A. J. Bard, L. R. Faulkner, *Electrochemical Methods, Fundamentals and Applications*; John Wiley & Sons: New York, 1980. Chapter 14. Spectrometric and Photo-

chemical Experiments.

[29] A. Szabo, N. S. Ostlund, *Modern Quantum Chemistry: Introduction to Advanced Electronic Structure Theory*; Macmillan Publishing: New York, 1982.

[30] J. L. Brédas, *Science* **1994**, *263*, 487-488. Molecular Geometry and Nonlinear Optics.

[31] W. J. Hehre, L. Radom, P. v. R. Schleyer, J. Pople, *Ab Initio Molecular Orbital Theory*; John Wiley & Sons: New York, 1986.

[32] A. D. Becke, *J. Chem. Phys.* **1993**, *98*, 1372-1377. A New Mixing of Hartree-Fock and Local Density-Functional Theories.

[33] C. Lee, W. Yang, R. G. Parr, *Phys. Rev. B* **1988**, *37*, 785-789. Development of the Colle-Salvetti Correlation-Energy Formula into a Functional of the Electron Density.

[34] J. Baker, M. Muir, J. Andzelm, *J. Chem. Phys.* **1995**, *102*, 2063-2079. A Study of Some Organic Reactions Using Density Functional Theory.

[35] B. G. Johnson, P. M. W. Gill, J. A. Pople, *J. Chem. Phys.* **1993**, *98*, 5612-5626. The Performance of a Family of Density Functional Methods.

[36] Gaussian 94, M. J. Frisch, G. W. Trucks, H. B. Schlegel, P. M. W. Gill, B. G. Johnson, M. A. Robb, J. R. Cheeseman, T. A. Keith, G. A. Petersson, J. A. Montgomery, K. Raghavachari, M. A. Al-Laham, V. G. Zakrzewski, J. V. Ortiz, J. B. Foresman, J. Cioslowski, B. B. Stefanov, A. Nanayakkara, M. Challacombe, C. Y. Peng, P. Y. Ayala, W. Chen, M. W. Wong, J. L. Andres, E. S. Replogle, R. Gomperts, R. L. Martin, D. J. Fox, J. S. Binkley, D. J. Defrees, J. Baker, J. J. P. Stewart, M. Head-Gordon, C. Gonzalez, J.A. Pople, Gaussian, Inc. Pittsburgh, PA, 1995.

[37] DISCO, A Direct SCF and MP2 Code written by J. Almlöf, K. Faegri, M. W. Feyereisen, T. H. Fischer, H. P. Lüthi, ETH Zürich Version 3.0, 1994.

[38] R. Ahlrichs, M. Bär, M. Häser, H. Horn, C. Kölmel, *Chem. Phys. Lett.* **1989**, *162*, 165-169. Electronic Structure Calculations on Workstation Computers: The Program System Turbomole.

[39] MOLEKEL 2.6, Peter F. Flükiger, University of Geneva and CSCS Manno, Swit-

zerland, 1997.

[40] L. M. Tolbert, *Acc. Chem. Res.* **1992**, *25*, 561-568. Solitons in a Box: The Organic Chemistry of Electrically Conducting Polyenes.

[41] M. Peo, S. Roth, K. Dransfield, B. Tieke, J. Hocker, H. Gross, A. Grupp, H. Sisel, *Solid State Commun.* **1980**, *35*, 119-121. Apparent Absence of Pauli Paramagnetism in Metallic Polyparaphenylene.

[42] C. W. Spangler, P.-K. Liu, K. O. Havelka, in *Molecular Electronics and Molecular Electronic Devices*, K. Sienicki, Ed.; CRC Press: Boca Raton, 1992; Vol. 3, Chapter 5. The Formation of Charge States in Organic Molecules, Oligomers, and Polymers for Applications in Molecular Electronic and Photonic Devices.

[43] J. L. Brédas, R. R. Chance, R. Silbey, *Phys. Rev. B* **1982**, *26*, 5843-5854. Comparative Theoretical Study of the Doping of Conjugated Polymers: Polarons in Polyacetylene and Polyparaphenylene.

[44] J. L. Brédas, J. C. Scott, K. Yakushi, G. B. Street, *Phys. Rev. B* **1984**, *30*, 1023-1025. Polarons and Bipolarons in Polypyrrole: Evolution of the Band Structure and Optical Spectrum upon Doping.

[45] D. S. Boudreaux, R. R. Chance, J. L. Brédas, R. Silbey, *Phys. Rev. B* **1983**, *28*, 6927-6936. Solitons and Polarons in Polyacetylene: Self-Consistent-Field Calculations of the Effect of Neutral and Charged Defects on Molecular Geometry.

[46] J. L. Brédas, B. Thémans, J. G. Fripiat, J. M. André, R. R. Chance, *Phys. Rev. B* **1984**, *29*, 6761-6773. Highly Conducting Polyparaphenylene, Polypyrrole, and Polythiophene Chains: An *Ab Initio* Study of the Geometry and Electronic-Structure Modifications upon Doping.

[47] R. R. Chance, D. S. Boudreaux, J. L. Brédas, R. Silbey, in *Handbook of Conducting Polymers*; T. A. Skotheim, Ed.; Marcel Dekker: New York, 1986; Vol. 2, Chapter 24. Solitons, Polarons, and Bipolarons in Conjugated Polymers.

[48] J. L. Brédas, in *Handbook of Conducting Polymers*; T. A. Skotheim, Ed.; Marcel Dekker: New York, 1986; Vol. 2, Chapter 25. Electronic Structure of Highly Conducting Polymers.

[49] J. L. Brédas, G. B. Street, *Acc. Chem. Res.* **1985**, *18*, 309-315. Polarons, Bipolar-

ons, and Solitons in Conducting Polymers.

[50] E. Constantinescu, M. Hillebrand, E. Volanschi, H. Wendt, *J. Electroanal. Chem.* **1988**, *256*, 95-109. Cyclic Voltammetric and Spectral Studies of the Electronic Structure and Relative Reactivities of *ortho*-, *meta*-, and *para*-Nitrobenzaldehyde Radical Anions.

4 *Cis-Trans* Isomerization of Functionalized Diethynylethenes and Tetraethynylethenes

4.1 Introduction

The *cis-trans* isomerization reactions of olefins can be initiated thermally, catalytically, electrochemically, or photochemically. The activation energies of the *cis-trans* isomerization of ethene derivatives in the ground state are usually very large. The calculated barrier to rotation for the ground state of ethene is 63.2 kcal/mol from double configuration (DC) SCF calculations[1] and 63.7 kcal/mol using an extensive configuration interaction (CI) procedure.[2] These values are in very good agreement with the experimentally determined activation barrier of 64.9 kcal/mol.[3]

Electron transfer induced isomerization reactions of olefins have been less intensively studied than photochemical *cis-trans* isomerizations. *Szwarc* and coworkers have shown that *cis*-stilbene and *cis-p,p'*-diphenylstilbene are reduced to their radical anion or dianion, followed by a spontaneous isomerization to the respective *trans*-radical anion or -dianion.[4,5]

The photoinduced *cis-trans* isomerizations of ethene,[6-8] as well as of stilbene and stilbene-like molecules[9-18] on the other hand, represent some of the most thoroughly investigated photochemical reactions. An excellent theoretical description of the two-electron two-orbital model for ethene and other biradical-like compounds is given by Bonacic-Koutecky, Koutecky, and Michl.[19] Details on the mechanistic characteristics of *cis-trans* isomerization of stilbenes are surveyed by Saltiel and Charlton[20], and Görner and Kuhn.[21]

Hence, these reactions can serve as benchmark for studies on arylated diethynylethenes (DEEs) and tetraethynylethenes (TEEs). In contrast to *cis*-stilbene or tetraphenylethene derivatives, the DEE and TEE systems are planar. Therefore, in the functionalized DEE and TEE compounds, the aryl rings with the pendant donor and/or acceptor groups are sufficiently remote from each other to prevent unfavorable steric hindrance during the course of *cis-trans* isomerizations, and thus, electronic effects can be separated from steric effects.

The potential energy surfaces of ethene as a function of the rotation angle θ about the central C=C bond (Figure 4.1a) reveal that the minimum of the ground state S_0 is located at θ = 0°, *i.e.* at a planar geometry. The excited states T, S_1 (S in Figure 4.1a) and S_2 (D in Figure 4.1a), on the other hand, exhibit a minimum at θ = 90°. At the perpendicular geometry, the two lowest states S_0 and T are very close in energy and the two highest S_1 and S_2 state energies are nearly the same as well. [8]

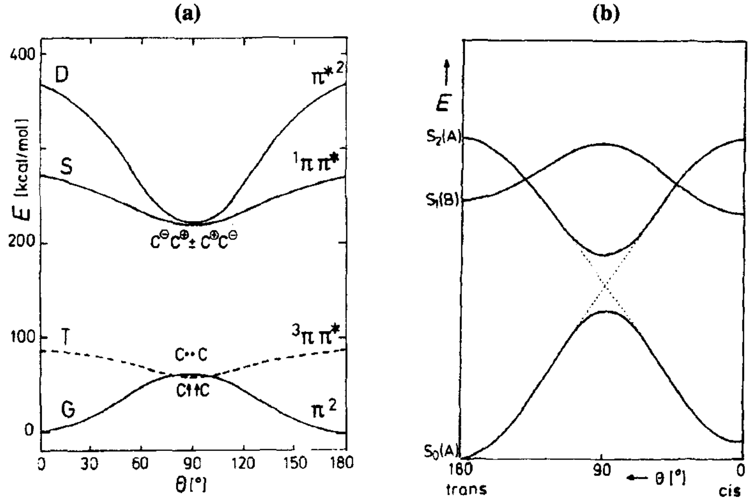

Figure 4.1. Schematic representation of the *cis-trans* isomerization of (a) ethene and (b) stilbene as a function of the rotation angle θ. Figures adopted from ref. 8.

In contrast to ethene, stilbene with its extended π-electron delocalization over the ethylenic bond and the phenyl rings, shows a maximum at $\theta = 90°$ in the potential energy curve for the singly excited S_1 (Figure 4.1b). This differentiating behavior is attributed to the fact that in stilbene the first excited state is stabilized in the planar configuration ($\theta = 0°$ and $\theta = 180°$) through conjugation, an option unavailable for ethene. The potential energy surface for the doubly excited S_2 state follows the same pattern in both ethene and stilbene, *i.e.* it shows a minimum at $\theta = 90°$.[8] For stilbene, the minimum of the potential energy surface of the S_2 state lies energetically below that of the S_1 state. The theoretically proposed model for the isomerization process involves excitation to the lowest excited singlet state S_1 and then a twisting reaction that follows a nonadiabatic mechanism consisting of an avoided crossing of the singlet state S_1 with the doubly excited state S_2.[9]

Theoretical investigations on the molecular and electronic structures of neutral and reduced bis(*p*-nitrophenyl) substituted TEEs (Chapters 2 and 3) have shown strong structural rearrangement and charge delocalization throughout the entire molecule. These calculations suggest a significant reduction of the central olefinic bond order upon reduction, which would decrease drastically the barriers to rotation about this bond and ultimately facilitate isomerization. The goal of the present study is to further investigate this prediction by calculating the torsional potentials of the neutral and reduced species of bis(*p*-nitrophenyl) substituted TEE. The results are reported in Section 4.3. The expected facile rotation has been subsequently examined by electrochemical reduction and reoxidation of the model compound bis(*p*-nitrophenyl) substituted DEE. The electrochemical process, which has been monitored by absorption spectroscopy, is described in Section 4.4.

The electrochemically observed *cis-trans* isomerization of the reduced DEE compound has initiated a study on the photolytic behavior of a series of substituted DEEs and TEEs, since bond length alternations in the functionalized DEEs and TEEs are also expected upon excitation. Section 4.5 outlines the attempts to explore by means of calculations the excited state behavior of the acceptor-acceptor (A/A) **1**, donor-acceptor (A/D) **2**, and donor-donor (D/D) **3** substituted TEEs.

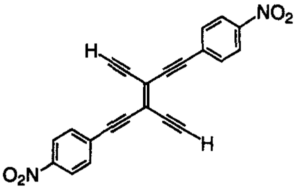

1

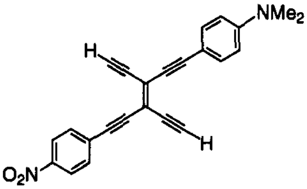

2

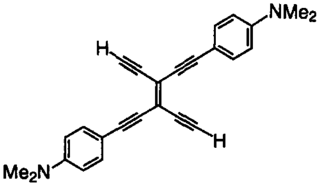

3

4.2 Computational Details

All calculations were carried out using the restricted Hartree-Fock (RHF) and restricted open-shell Hartree-Fock (ROHF) schemes. The geometry optimizations and the calculations of the barriers to rotation of **1** were performed at the HF/6-31G** level of theory starting from the planar equilibrium structure.

In Section 4.5, the calculations on the potential energy surfaces of **1**, **2**, and **3** were performed at the semiempirical AM1 (Austin Model 1) level using the configuration interaction (CI) technique as implemented in AMPAC.[22] The electronic states considered were the ground state S_0 and the two lowest excited singlet states, S_1 and S_2. The active space for the CI consisted of the HOMO and LUMO. Full relaxation of the geometries along the reaction coordinate (*i.e.* the rotation about the central ethylenic bond) in all electronic states was allowed (adiabatic approach). Validation studies were performed at the *ab initio* level using the single-excitation configuration interaction (CI-Singles) technique implemented in the Gaussian 94 package.[23] This technique however, is limited to singly excited states. Calculations at the AM1/CI level with an active space consisting of two orbitals, on the potential energy curves of stilbene yield a maximum at $\theta = 90°$ for the ground state S_0 and for the singly excited S_1, and a minimum at $\theta = 90°$ for the doubly excited S_2. This is in accordance with the extrema found by Orlandi and Siebrand.[9] However, in contrast to their results, S_1 shows only a shallow maximum and the S_2 curve lies always above S_1. This difference is explained by the fact that extensive CI-calculations need to be carried out in order to describe accurately excited state potential energy curves.[9] However, an extension of the considered configurations has been disregarded, since the present investigations intend to explain with a simple and fast computational approach the experimentally observed differences in the photochemical behavior of **1**, **2**, and **3** by comparing the three energy potential curves, and not to explore in detail the photochemical reaction pathways of the *cis-trans* isomerization. Hence, the AM1/CI method including two orbitals has been estimated to be appropriate for the fixed purpose. Considering the large size of the investigated systems, more elaborate calculations would have been too time consuming.

The programs used were the Gaussian 94 package[23] and AMPAC.[22] The molecular structures and molecular orbitals were represented with the molecular graphics package MOLEKEL.[24]

4.3 Study of the Barriers to Rotation in Bis(*p*-nitrophenyl) Substituted Tetraethynylethene

Investigations done on the molecular equilibrium geometries of a series of donor and/or acceptor substituted TEEs predict that these functionalized chromophores undergo strong structural rearrangement upon reduction. The reduced species show considerable alternation in the bond lengths within both the phenyl rings and the carbon core (Chapter 2 and ref. 25). A reduced bond length alternation of the conjugated segment is also predicted based on a wealth of information derived from doping studies of polymers such as polydiacetylene or poly(phenylene)vinylene and from other theoretical investigations.[26-29]

The study of torsional potentials provides information about the molecular bonding and electronic effects. To determine the bond character and the extent of conjugation and charge delocalization, the barrier to rotation about the central bond *h* of TEE (see Figure of Table 4.1), as well as the barrier to rotation of the nitrophenyl rings about bond *e* connecting the TEE with the nitrophenyl group (see Figure of Table 4.2) is computed for **1**. Tables 4.1 and 4.2 show the calculated total and relative energies.

From these calculations, two conclusions can be drawn. First, it appears that the twisted (D_{2d}) form represents a saddle point between *cis*- and *trans*-isomers. Attempts to locate a twisted form lower in energy than the planar structures, by relaxation of all geometrical constraints, have failed. Therefore, in contrast to similar systems such as tetraphenylethylene[30-32] and tetracyanoethylene[33,34], which show twisted equilibrium structures in their reduced states, compound **1** retains planarity in all reduced states.

Secondly, the decrease of the torsion potential about the TEE central bond from 85.9 kcal/mol (this value is a Hartree Fock artifact for the rotational barrier about a double bond[35,36]) to 5.9 kcal/mol upon reduction, illustrates that the central double bond in the TEE frame acquires significant single bond character as the dianion (Table 4.1).

Table 4.1. HF/6-31G** Barriers to rotation E_{rot} (in kcal/mol) about the central bond of **1**, radical anion $\mathbf{1}^{\bullet -}$, and dianion $\mathbf{1}^{2-}$.

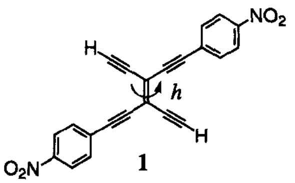

1

angle[a] (deg.)	E_{rot} (ne)[b]	E_{rot} (ma)[c]	E_{rot} (da)[d]
0	0.000	0.000	0.000
30	10.501	4.286	1.673
60	40.717	16.258	4.687
90	85.922[e]	25.194	5.925[f]

[a] All geometry parameters were kept at the values optimized for the planar equilibrium structures. [b] ne Designates the neutral species. [c] ma Designates the monoanion. [d] da Designates the dianion. [e] This value is a Hartree Fock artifact. [f] The relaxation of the geometry in the dianion at 90° reduces the barrier to rotation by 0.5 kcal/mol.

Table 4.2. HF/6-31G** Barriers to rotation E_{rot} (in kcal/mol) about bond *e* between the nitrophenyl rings and the TEE core of **1**, radical anion $\mathbf{1}^{\bullet-}$, and dianion $\mathbf{1}^{2-}$.

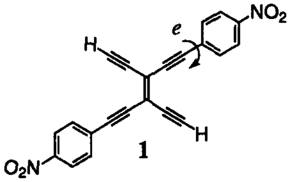

1

angle[a] (deg.)	E_{rot} (ne)[b]	E_{rot} (ma)[c]	E_{rot} (da)[d]
0	0.000	0.000	0.000
30	0.188	1.454	4.664
60	0.610	4.321	17.161
90	0.829	5.792	28.857

[a]All geometry parameters were kept at the values optimized for the planar equilibrium structures. [b]ne Designates the neutral species. [c]ma Designates the monoanion. [d]da Designates the dianion.

Torsion about the sp-sp^2 carbon-carbon single bond (bond *e*) in **1** is very low with a value of 0.829 kcal/mol (Table 4.2). The molecular structure of **1** is similar to neutral diphenylacetylene, which has an experiment activation energy for torsional rotation of 0.6 kcal/mol.[37] Consistent with the observation of a transition toward a cumulenic structure is the increase of the torsional potential from 0.829 kcal/mol (neutral) to 28.9 kcal/mol (dianion) for the rotation about bond *e* connecting the TEE with the nitrophenyl ring in $\mathbf{1}^{2-}$ (Table 4.2). For the corresponding DEE **5** (Scheme 4.1), the torsional potential about bond *h* is calculated to be 34.0 kcal/mol. This is in accord with the predicted geometry of the reduced DEE. The central bond *h* acquires less single bond character upon reduction in bis(*p*-nitrophenyl) substituted DEE than in the analogous TEE (Chapter 2) and, thus, rotation becomes a little more difficult.

Based on these important findings, a mechanism is developed, involving the *cis-trans* isomerization of the reduced compound as outlined in Scheme 4.1 for the *cis-* and *trans*-enediyne model compounds **4a** and **4b**. According to the results on the torsional potential, the *cis*-enediyne **4a** is predicted to undergo a lowering of the bond length alternation in the TEE core following a one-electron transfer to each of the two nitrophenyl moieties, and the species tends toward dianion **5** with a cumulenic/quinoid structure. This pathway allows the nitrophenyl moieties to function as independent centers since the conjugation between the cumulenic 'halves' in **5** and **6** is effectively impeded by the central single bond. Again, a key consideration in this mechanism is the loss of the central double bond of the enediyne framework of **4a** and **4b**, and the potential for subsequent rotation about the ensuing single bond. Rotation would then allow for isomerization of **5** to **6**, and following reoxidation, formation of **4b**.

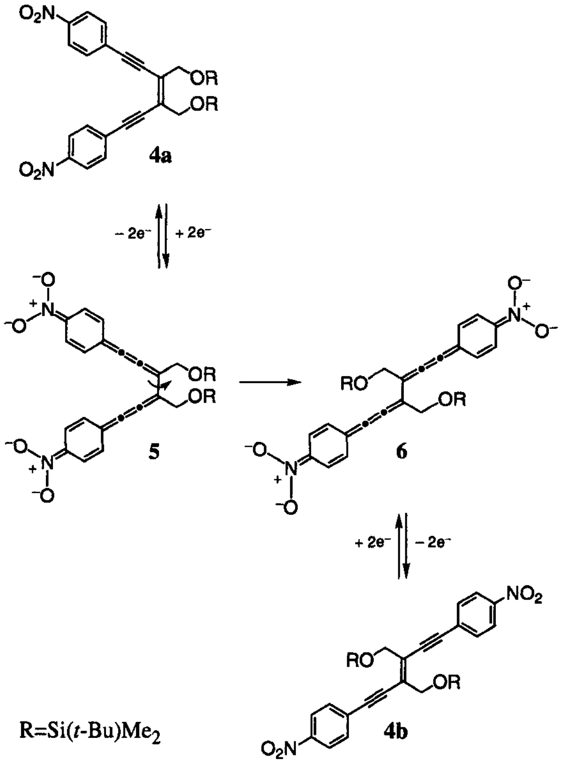

Scheme 4.1. Proposed mechanism for *cis-trans* isomerization of enediynes **4a** and **4b**.

4.4 Electrochemical Isomerization: The Experimental Evidence

Experimental support for the outlined redox pathway and the formation of a cumulenic type intermediate has been provided through independent analysis of the electrochemical behavior of isomerically pure substituted DEEs **4a** and **4b**. The bis(*p*-nitrophenyl)-substituted TEE is not used for the experimental validation, since the *cis*-bis(*p*-nitrophenyl) TEE isomer could not be obtained isomerically pure.

The electrochemical investigations were performed in the group of Prof. *M. Gross*, Université Louis Pasteur Strasbourg. Spectroelectrochemical measurements were carried out in a thin layer cell (0.1 mm) through an optically transparent thin layer electrode (OTTLE) made of a Pt minigrid (1000 mesh). The auxiliary electrode was a Pt wire, and an aqueous Ag/AgCl electrode was used as the reference. The OTTLE cell was placed in a diode array UV/VIS spectrophotometer.

Both species **4a** and **4b** give two reductions. The first is a two-electron reversible charge transfer as expected for reduction of the nitrophenyl groups, and the second is an irreversible one-electron charge transfer. Since **4a** and **4b** have different UV/VIS absorption spectra (Figure 4.2c), the spectral evolution of **4a** is monitored during CV through OTTLE measurements to detect *cis-trans* isomerization. Initially, the spectrum of **4a** shows characteristic absorption bands at 314 and 368 nm (Figure 4.2a). As the species is electrochemically reduced, these absorptions are lost, and a broad intensive band between 700 and 800 nm appears. Reoxidation of the sample to a neutral species results in a spectrum with only one absorption band at 372 nm, characteristic of the *trans*-species, **4b** (Figure 4.2b). The possibility of photochemical isomerization[38,39,40] is disregarded, as running the spectroscopy without electrolysis results in no change in the spectrum of **4a**. Analogous OTTLE studies of **4b** show that during the course of reduction and oxidation, this species remains isomerically pure.

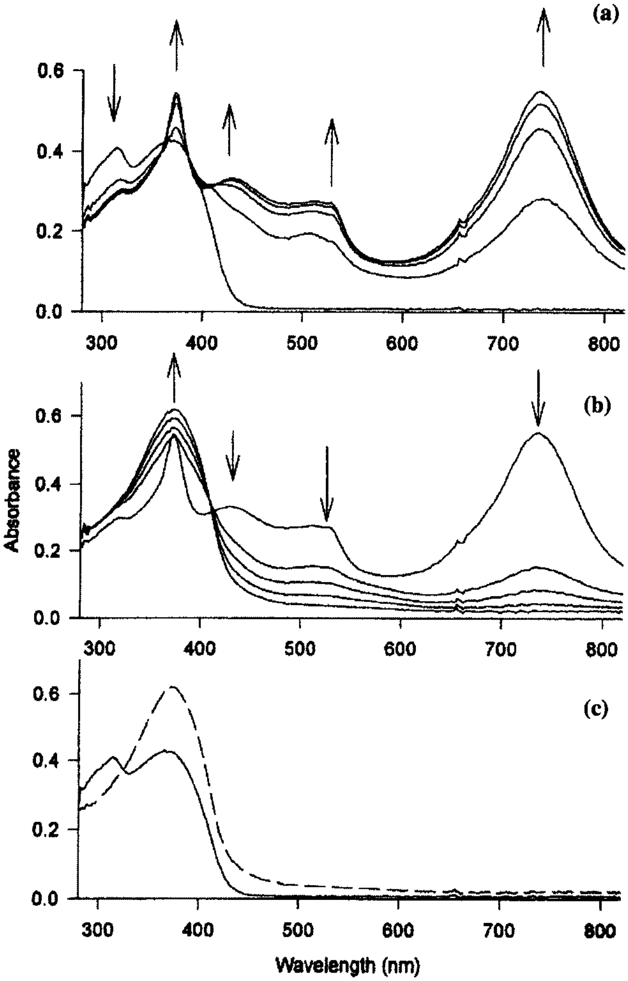

Figure 4.2. Time-resolved UV/Vis spectra for OTTLE in CH_2Cl_2 + 0.1 M Bu_4NPF_6 for (a) reduction of **4a** to dianion **5** and (b) oxidation of **6** to **4b**. (c) UV/Vis spectra of **4a** (—) and **4b** (- - -).

4.5 Photochemical Isomerization of (*p*-Dimethylaminophenyl) and/or (*p*-Nitrophenyl) Substituted Tetraethynylethenes

The experimentally performed *trans-cis* photoisomerization, carried out in the laboratory of Prof. *F. Diederich*, found that the type of donor/acceptor (D/A) functionalization drastically affects the total quantum yields and partial quantum yields of isomerization $\Phi_{t\rightarrow c}$ and $\Phi_{c\rightarrow t}$. The total quantum yields are highest for the A/A substituted derivative, followed by the D/D and finally the D/A compounds.[38]

The calculations presented in this Section describe the attempt to rationalize the experimentally observed differences in the *trans-cis* photochemical behavior of TEEs, functionalized with electron-donating (*p-N,N*-dimethylaminophenyl) and/or electron-accepting (*p*-nitrophenyl) groups. The goal has been to explain with a simple and fast computational approach the effects of the type of functionalization on the photolytic behavior. For this purpose, first the electronic structure of a series of A/A, D/D, and D/A TEEs **1**-**3** are analyzed and secondly, the potential energy curves for the ground state S_0, and the two singlet excited states S_1 and S_2 are computed at the AM1/CI level of theory.

Due to the strong coupling between electronic structure and geometry, the consideration of the electron density on the π bonds gives a good indication on the geometric modifications occurring upon excitation.[41] Inspection of the wavefunction shows that the first excited state in the A/A, the D/D, and the D/A TEEs **1**-**3** originates mainly from an electron transition between the highest occupied molecular orbital (HOMO) and the lowest unoccupied molecular orbital (LUMO), and therefore those molecular orbitals are of main interest in the investigation of the photochemical isomerization process.

The HOMO of the A/A TEE **1** reveals strong π bonding character and is concentrated about the central double bond on the TEE core. The LUMO displays strong π* antibonding character for the central double bond and some delocalization into the nitrophenyl groups of the TEE is observed (Figure 4.3a). The HOMO of the D/A TEE **2** exhibits the same type of π bonding character and is delocalized over the TEE core and the donor substituent. In the LUMO, delocalization over the TEE core into the acceptor moiety is observed (Figure 4.3b). In the D/D TEE **3**, however, the HOMO is strongly delocalized throughout the whole π system. The LUMO, on the other hand, mainly shows localization on the central olefinic bond, *i.e.* strong π* antibonding character, and only weak delocalization into the phenyl rings (Figure 4.3c).

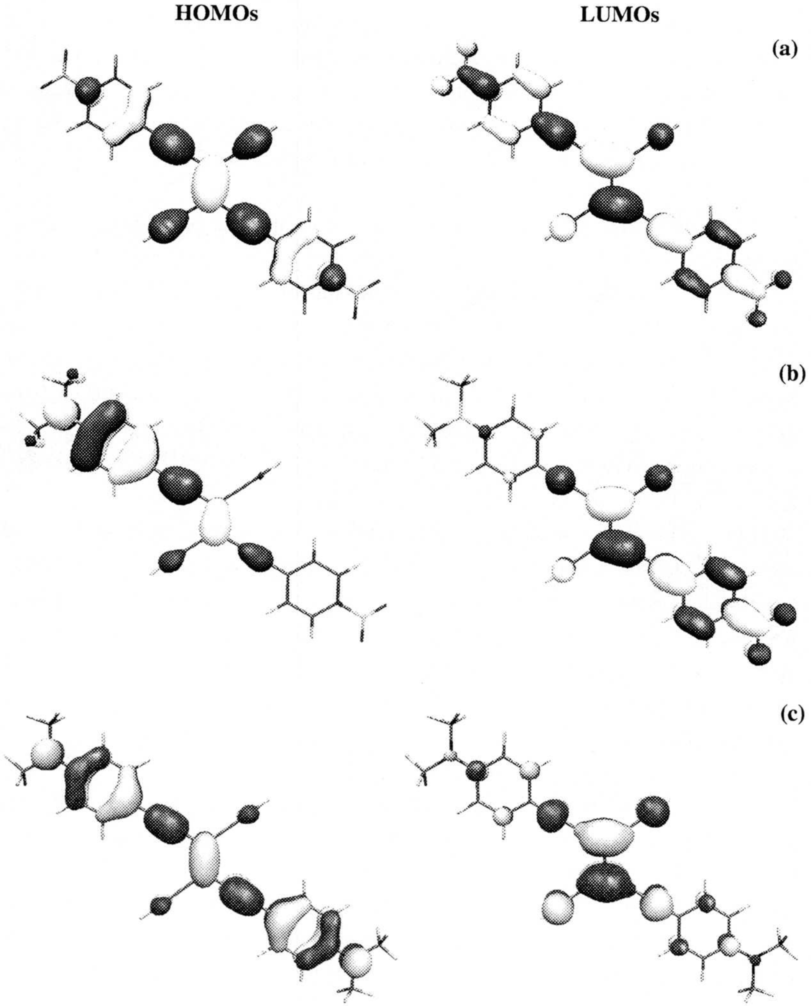

Figure 4.3. Highest occupied molecular orbitals (HOMOs; right) and lowest unoccupied molecular orbitals (LUMOs; left) of (a) A/A **1**, (b) D/A **2**, and (c) D/D **3**.

In all the considered systems, an electron is promoted upon excitation from a π-type to a π*-type antibonding orbital, strongly localized on the central olefinic bond. The effect of this electron transition is an elongation of this particular bond. Thus the barrier to rotation is strongly reduced, enabling facile isomerization.

In order to verify the anticipated structural modifications upon excitation, the ground state S_0 and the two singlet excited states S_1 and S_2 of the A/A **1**, D/A **2**, and D/D **3** TEEs have been optimized at the AM1/CI level of theory. The singly excited state S_1 experiences strong structural changes mainly on the TEE core. In the doubly excited state S_2, these variations become even more significant. Especially the central bond elongates from 1.37 Å in the ground state S_0 to 1.58 Å in the S_2 state.

Calculations of photoinduced isomerization entail the determination and exact ordering of excited states and analysis of their behavior during the twisting process about the CC bond, *i.e.* the determination of the different potential energy curves along the reaction coordinate which is the rotation angle.[8] The potential energy curves for the computed S_0, S_1, and S_2 states are presented in Figure 4.4.

For all three compounds, the energy surfaces of the doubly excited state S_2, calculated at the AM1-CI level of theory, show a minimum at $\theta = 90°$ as observed for the case of stilbene and ethene (Figure 4.1).[8] Somewhat surprisingly, the S_1 potential energy curve shows a shallow minimum at $\theta = 90°$ for the D/A **2** and an almost flat curve for A/A **1** and D/D **3**. This behavior is in contrast to stilbene and corresponds more closely to the one observed for ethene. The same flat curvature is also obtained at the *ab initio* single-excitation configuration interaction (CIS) level. At the AM1-CI level of theory, the doubly excited state S_2 is always higher in energy than the S_1 state. Nevertheless, for A/A **1** and D/D **3** both surfaces nearly fall together at $\theta = 90°$ (Figures 4.4a and 4.4c), and a crossing of the S1 and S2 surfaces, similar to that of stilbene, cannot be ruled out.

From the differing S_1 surfaces, it becomes clear that the A-A and D/D end group pairs interact differently with the π-conjugated system than the D/A combination, and thus other mechanisms may be implicated in the isomerization process and change the isomerization barrier heights. Unfortunately this simple theoretical approach yields only minor dissimilarities between the potential energy surfaces of the A/A **1**, D/A **2**, and D/D **3** functionalized TEEs, and the expected explanation with regard to different behaviors in the isomerization process for the three substituted TEEs could not be obtained.

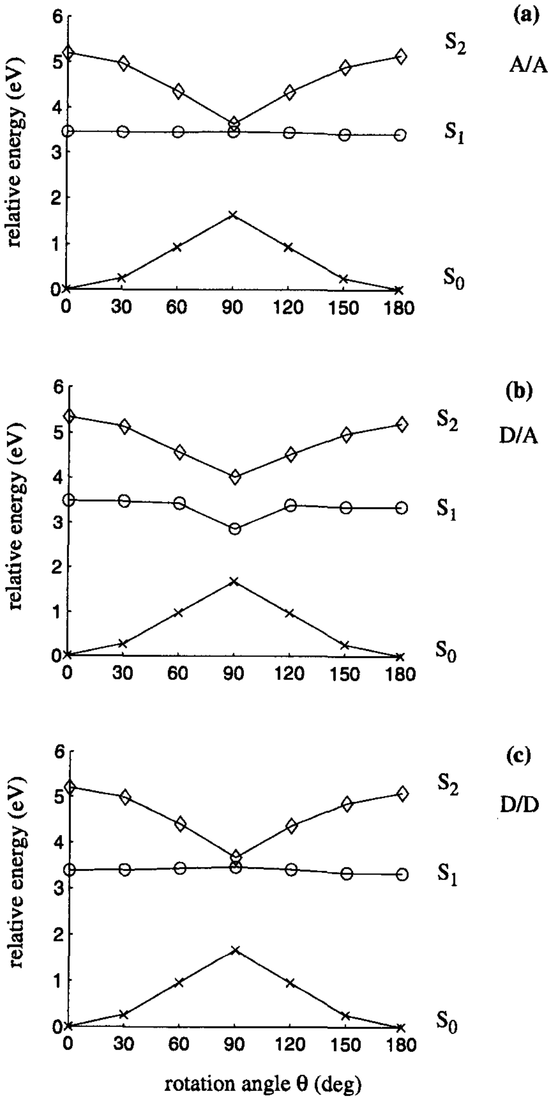

Figure 4.4. Potential energy surfaces for the S_0 (×), S_1 (o), and S_2 (◊) states of (a) A/A **1**, (b) D/A **2**, and (c) D/D **3**.

As has been shown experimentally[15-18] and theoretically,[13,42-44] the determination of the exact reaction pathway of a light-induced *cis-trans* isomerization is a rather complex problem. A possibly more revealing description of the potential energy curves requires more elaborate calculations, at the MCSCF level for example. For locating the surface crossings, it is essential to take into account a full geometry optimization upon rotation in the calculations of the potential energy curves of the excited states, as has been shown for styrene in a complete active space (CAS) SCF study.[42] CASSCF geometry optimization are not yet practical for large systems like the functionalized TEEs with two phenyl rings because of the large number of electrons and orbitals which form the π-system of TEE derivatives and which have to be included in the active space.

4.6 Concluding Remarks

One of the most revealing observations from the calculations on bis(*p*-nitrophenyl) substituted TEE **1** has been that upon reduction the molecule experiences considerable bond length alternation. The reduced species adopts a cumulenic/quinoid structure, and, more importantly, the central olefinic bond acquires significant single bond character. This dramatic change in bond character in the dianion reflects the π conjugation and charge delocalization patterns that are possible in this system. Accordingly, the barriers to rotation within the molecule also experience major changes: torsion of the nitrophenyl group about the bond to the TEE core becomes more difficult, whereas torsion about the central olefinic bond assumes a value expected for a single bond. The theoretical prediction of a cumulenic/quinoid structure for the reduced species has been subsequently validated experimentally by the irreversible electrochemical isomerization of a *cis*-1,6-bis(4-nitrophenyl)hex-3-ene-1,5-diyne derivative to its *trans*-isomer during cyclic voltammetric reduction. The outcome of this experiment shows that alkynes are clearly effective in facilitating charge delocalization into the conjugated framework.

Furthermore, theoretical investigations on a series of (*p*-*N*,*N*-dimethylaminophenyl) and/or (*p*-nitrophenyl) substituted tetraethynylethenes **1**-**3** have been carried out in order to explain their different experimentally observed photochemical behavior. The calculated electronic structure shows localization of the HOMOs and LUMOs about the central olefinic bond. These calculations suggest a significant reduction of the olefinic bond order upon excitation, which ultimately facilitates isomerization. Calculations on the molecular geometries of the ground state S_0, and the two singlet excited states S_1 and S_2 confirm this prediction. Unfortunately, the AM1/CI calculated potential energy curves of S_0, S_1, and S_2 do not yield any explanation for the effect of the type of donor/acceptor (D/A) functionalization on the photolytic behavior. On the other hand, more sophisticated methods like CASSCF (complete active space self consistent field) or CASPT2 (complete active space second order perturbation theory) are very time consuming for molecules of this size and the corresponding computational effort is beyond the scope of the intended investigation.

The behavior of functionalized TEEs under irradiation is of great interest in respect of utilization of these molecules for device construction and practical applications. Currently, in the laboratory of Prof. *F. Diederich*, the synthetic methodology is worked out to introduce molecular switches into poly(triacetylene) (PTA) oligomers in order to influence with light the delocalization paths.[45] The switchable system consists of two possible conjugation ways: the longest linear π-electron conjugation way along the PTA backbone and the donor-acceptor conjugation path orthogonal to the former. If the switch is turned off, the donor and acceptor groups are not activated and the horizontal conjugation along the PTA backbone determines the molecular properties. If the switch is turned on through light irradiation, the orthogonal donor-acceptor conjugation path becomes dominant and controls largely the molecular properties. The switching process is monitored by UV/Vis spectroscopy. With *p*-nitrophenyl- and *p*-methoxyphenyl-substituted compounds the switching process works instantly, but does not operate with the [*p*-dimethylamino)phenyl]-substituted system, except if protonated. In order to explain these findings, it would be interesting to pursue the theoretical investigations on this photochemical switching mechanism by calculating the structural characteristics and molecular properties of the ground and excited states of these switchable systems. Moreover, one major problem in the preparation of these TEE based switchable systems is the *cis-trans* isomerization occurring under exposure to daylight. In view of excluding the undesired *cis-trans* isomerization process, more elaborate calculations on the excited state properties and behavior could yield guidelines for a better design of the chromophores by suggesting specific organization of the substituents around the two-dimensional core.

4.7 References

[1] R. J. Buenker, S. D. Peyerimhoff, H. L. Hsu, *Chem. Phys. Lett.* **1971**, *11*, 65-70. A New Interpretation for the Structure of the V–N Bands of Ethylene.

[2] M. H. Wood, *Chem. Phys. Lett.* **1974**, *24*, 239-242. The Barrier To Rotation for the Ground State of Ethylene: A DC SCF Approach.

[3] W. von E. Doering, W. R. Roth, F. Bauer, R. Breuckmann, T. Ebbrecht, M. Herbold, R. Schmidt, H. W. Lennartz, D. Lenoir, R. Boese, *Chem. Ber.* **1989**, *122*, 1263-1275. Rotationsbarrieren gespannter Olefine.

[4] C. K. Chien, H. C. Wang, M. Szwarc, A. J. Bard, K. Itaya, K. *J. Am. Chem. Soc.* **1980**, *102*, 3100-3104. Electron Transfer Induced Isomerization of *cis*-4,4'-Diphenylstilbene into Its Trans Form.

[5] H. C. Wang, G. Levin, M. Szwarc, *J. Am. Chem. Soc.* **1977**, *99*, 2642-2647. Kinetics of Isomerization of the Free *cis*-Stilbene Radical Anion into Its Trans Isomer in Hexamethylphosphoric Triamide. Spectroscopic and Electron Spin Resonance Identification of *cis*-Stilbene Radical Anion in Tetrahydrofuran.

[6] R. J. Buenker, S. D. Peyerimhoff, *Chem. Phys.* **1976**, *9*, 75-89. All-Valence-Electron Configuration Mixing Calculations for the Characterization of the $^1(\pi,\pi^*)$ States of Ethylene.

[7] A. J. Merer, R. S. Mulliken, *Chem. Rev.* **1969**, *69*, 639-656. Ultraviolet Spectra and Excited States of Ethylene and Its Alkyl Derivatives.

[8] M. Klessinger, J. Michl, *Excited States and Photochemistry of Organic Molecules*, ed. VCH Publishers, Inc., New York, 1995; Chapter 4. Potential Energy Surfaces: Barriers, Minima, and Funnels; Chapter 5. Photophysical Processes; Chapter 7. *Cis-Trans* Isomerization of Double Bonds.

[9] G. Orlandi, W. Siebrand, *Chem. Phys. Lett.* **1975**, *30*, 352-354. Model for the Direct Photo-Isomerization of Stilbene.

[10] G. Hohlneicher, B. Dick, *J. Photochem.* **1984**, *27*, 215-231. Experimental Determination of the Low-Lying Excited A States of *trans*-Stilbene.

[11] G. Hohlneicher, M. Müller, M. Demmer, J. Lex, J. H. Penn, L.-X. Gan, P. D, Loesel, *J. Am. Chem. Soc.* **1988**, *110*, 4483-4494. 1,2-Diphenylcycloalkenes: Elec-

tronic and Geometric Structures in the Gas Phase, Solution, and Solid State.

[12] V. Molina, M. Merchán, B.O. Ross, *J. Phys. Chem. A* **1997**, *101*, 3478-3487. Theoretical Study of the Electronic Spectrum of *trans*-Stilbene.

[13] M. J. Bearpark, F. Bernardi, S. Clifford, M. Olivucci, M. A. Robb, T. Vreven, *J. Phys. Chem. A* **1997**, *101*, 3841-3847. Cooperating Rings in *cis*-Stilbene Lead to an S_0/S_1 Conical Intersection.

[14] D. Schulte-Frohlinde, H. Blume, H. Güsten, *J. Phys. Chem.* **1962**, *66*, 2486-2491. Photochemical *cis-trans* Isomerization of Substituted Stilbenes.

[15] D. H. Waldeck, *Chem. Rev.* **1991**, *91*, 415-436. Photoisomerization Dynamics of Stilbenes.

[16] H. Meier, *Angew. Chem.* **1992**, *104*, 1425-1446; *Angew. Chem. Int. Ed. Engl.* **1992**, *31*, 1399-1420. The Photochemistry of Stilbenoid Compounds and Their Role in Materials Technology.

[17] A. A. Heikel, J. S. Baskin, L. Bañares, A. H. Zewail, *J. Phys. Chem. A* **1997**, *101*, 572-590. Structural Effects on the Isomerization Dynamics of *trans*-Stilbenes: IVR, Microcanonical Reaction Rates, and the Nature of the Transition State.

[18] B. B. Champagne, J. F. Pfanstiel, D. F. Plusquellic, D. W. Pratt, W. M. van Herpen, W. L. Meerts, *J. Phys. Chem.* **1990**, *94*, 6-8. *Trans*-Stilbene: A Rigid, Planar Asymmetric Top in the Zero-Point Vibrational Levels of Its S_0 and S_1 Electronic States.

[19] V. Bonacic-Koutecky, J. Koutecky, J. Michl, *Angew. Chem.* **1987**, *99*, 216-236; *Angew. Chem. Int. Ed. Engl.* **1987**, *26*, 170-189. Neutral and Charged Biradicals, Zwitterions, Funnels in S_1, and Proton Translocation: Their Role in Photochemistry, Photophysics, and Vision.

[20] J. Saltiel, J. L. Charlton, in *Rearrangements in Ground and Excited States*; P. de Mayo, (Ed.), Academic Press: New York, 1980; Chapter 14. Cis-Trans Isomerization of Olefins.

[21] H. Görner, H. J. Kuhn, in *Advances in Photochemistry*; D. C. Neckers, D. H. Volman, G. von Bünau, (Eds.), John Wiley & Sons, Inc.: New York, 1995; Vol. 19.

Cis-Trans Photoisomerization of Stilbenes and Stilbene-Like Molecules.

[22] AMPAC 5.0, Semichem, 7128 Summit, Shawnee, KS 66216, 1994.

[23] Gaussian 94, M. J. Frisch, G. W. Trucks, H. B. Schlegel, P. M. W. Gill, B. G. Johnson, M. A. Robb, J. R. Cheeseman, T. A. Keith, G. A. Petersson, J. A. Montgomery, K. Raghavachari, M. A. Al-Laham, V. G. Zakrzewski, J. V. Ortiz, J. B. Foresman, J. Cioslowski, B. B. Stefanov, A. Nanayakkara, M. Challacombe, C. Y. Peng, P. Y. Ayala, W. Chen, M. W. Wong, J. L. Andres, E. S. Replogle, R. Gomperts, R. L. Martin, D. J. Fox, J. S. Binkley, D. J. Defrees, J. Baker, J. J. P. Stewart, M. Head-Gordon, C. Gonzalez, J.A. Pople, Gaussian, Inc. Pittsburgh, PA, 1995.

[24] MOLEKEL 2.6, Peter F. Flükiger, University of Geneva and CSCS Manno, Switzerland, 1997.

[25] A. Hilger, J.-P. Gisselbrecht, R. R. Tykwinski, C. Boudon, M. Schreiber, R. E. Martin, H. P. Lüthi, M. Gross, F. Diederich, *J. Am. Chem. Soc.* **1997**, *119*, 2069-2078. Electronic Characteristics of Arylated Tetraethynylethenes: A Cooperative Computational and Electrochemical Investigation.

[26] C. W. Spangler, P.-K. Liu, K. O. Havelka, in *Molecular Electronics and Molecular Electronic Devices*, K. Sienicki, Ed.; CRC Press: Boca Raton, 1992; Vol. 3, Chapter 5. The Formation of Charge States in Organic Molecules, Oligomers, and Polymers for Applications in Molecular Electronic and Photonic Devices.

[27] J. L. Brédas, G. B. Street, *Acc. Chem. Res.* **1985**, *18*, 309-315. Polarons, Bipolarons, and Solitons in Conducting Polymers.

[28] J. L. Brédas, J. C. Scott, K. Yakushi, G. B. Street, *Phys. Rev. B* **1984**, *30*, 1023-1025. Polarons and Bipolarons in Polypyrrole: Evolution of the Band Structure and Optical Spectrum upon Doping.

[29] J. L. Brédas, R. R. Chance, R. Silbey, *Phys. Rev. B* **1982**, *26*, 5843-5854. Comparative Theoretical Study of the Doping of Conjugated Polymers: Polarons in Polyacetylene and Polyparaphenylene.

[30] M. O. Wolf, H. H. Fox, M. A. Fox, *J. Org. Chem.* **1996**, *61*, 287-294. Reduction of Acetylated Tetraphenylethylenes: Electrochemical Behavior and Stability of the Related Reduced Anions.

[31] D. A. Shultz, M. A. Fox, *J. Org. Chem.* **1990**, *55*, 1047-1051. Structural Effects on

the Disproportionation Equilibrium of Tethered Tetraphenylethylene Radical Anions.

[32] M. A. Fox, D. A. Shultz, *J. Org. Chem.* **1988**, *53*, 4386-4390. Twisting in the Tetraphenylethylene Dianion.

[33] A. Zheludev, A. Grand, E. Ressouche, J. Schweizer, B. Morin, A. J. Epstein, D. A. Dixon, J. S. Miller, *J. Am. Chem. Soc.* **1994**, *116*, 7243-7249. Experimental Determination of the Spin Density in the Tetracyanoethenide Free Radical, $[TCNE]^{\bullet -}$, by Single-Crystal Polarized Neutron Diffraction. A View of a π^* Orbital.

[34] D. A. Dixon, J. S. Miller, *J. Am. Chem. Soc.* **1987**, *109*, 3656-3664. Crystal and Molecular Structure of the Charge-Transfer Salt of Decamethylcobaltocene and Tetracyanoethylene (2:1): $\{[Co(C_5Me_5)_2]^+\}_2[(NC)_2CC(CN)_2]^{2-}$. The Electronic Structures and Spectra of $[TCNA]^n$ (n=0, 1-, 2-).

[35] W. J. Hehre, L. Radom, P. v. R. Schleyer, J. Pople, *Ab Initio Molecular Orbital Theory*; John Wiley & Sons: New York, 1986.

[36] M. Head-Gordon, J. A. Pople, *J. Phys. Chem.* **1993**, *97*, 1147-1151. Internal Rotation in Conjugated Molecules: Substituted Ethylenes and Benzenes.

[37] J. K. Young, J. S. Moore, in *Modern Acetylene Chemistry*; P. J. Stang, F. Diederich (Eds.), Verlag Chemie: Weinheim, 1995; Chapter 12. Acetylenes in Nanostructures.

[38] R. E. Martin, J. Bartek, F. Diederich, R. R. Tykwinski, E. Meister, A. Hilger, H. P. Lüthi, *J. Chem. Soc., Perkin Trans. 2* **1998**, 233-241. Photochemical ***trans-cis*** Isomerisation of Donor/Acceptor-Substituted (*E*)-Hex-3-en-1,5-diynes (1,2-Diethynylethenes, DEEs) and 3,4-Diethynylhex-3-ene-1,5-diynes (Tetraethynylethenes, TEEs).

[39] J. Anthony, C. B. Knobler, F. Diederich, *Angew. Chem.* **1993**, *105*, 437-440; *Angew. Chem. Int. Ed. Engl.* **1993**, *32*, 406-409. Stable [12]- and [18]Annulenes Derived from Tetraethynylethene.

[40] B. König, E. Schofield, P. Bubenitschek, P. G. Jones, *J. Org. Chem.* **1994**, *59*, 7142-7143. Synthesis and Photoinduced *cis-trans* Isomerization of Diaryl Enediyne Chromophores.

[41] J. L. Brédas, *Science* **1994**, *263*, 487-488. Molecular Geometry and Nonlinear

Optics.

[42] M. Bearpark, M. Olivucci, S. Wilsey, F. Bernardi, M. A. Robb, *J. Am. Chem. Soc.* **1995**, *117*, 6944-6953. A MC-SCF Study of Styrene Singlet-State Photoisomerization.

[43] M. Garavelli, P. Celani, N. Yamamoto, F. Bernardi, M. A. Robb, M. Olivucci, *J. Am. Chem. Soc.* **1996**, *118*, 11656-11657. The Structure of the Nonadiabatic Photochemical *Trans-Cis* Isomerization Channel in *All-Trans* Octatetraene.

[44] M. Olivucci, I. N. Ragazos, F. Bernardi, M. A. Robb, *J. Am. Chem. Soc.* **1993**, *115*, 3710-3721. A Conical Intersection Mechanism for the Photochemistry of Butadiene. A MC-SCF Study.

[45] L. Gobbi, F. Diederich, P. Seiler, **1998**, manuscript in preparation.

Leer - Vide - Empty

5 Design of Nitrosubstituted Conjugated Systems with High Electron Affinities

5.1 Introduction

Polymeric light emitting diodes (LEDs) have been extensively studied recently due to their promise for practical applications.[1-4] Light emission is produced in the luminescent polymer layer via recombination of electrons and holes injected from the two electrodes. It is known that balanced charge injection from both electrodes and comparable mobility of both charge carrier types inside the polymer are crucial for high device efficiencies.[5-7] The ease of charge injection depends on the energy gap between the molecular frontier orbitals of the polymer (HOMO for hole injection and LUMO for electron injection) and the work function of the contact metal electrodes. In general, polymer LEDs have smaller hole injection barriers than electron injection barriers. Thus, one approach towards facilitating electron injection and enhancing the device efficiency is to increase the electron affinity of the compound.[8-12]

The objective of the present investigation has been to design molecular structures with high electron affinities. For this purpose, the electron affinities of a series of nitrosubstituted carbon-rich systems have been determined. Indeed, the electrochemical analysis of a series of nitrofunctionalized diethynylethenes (DEEs) and tetraethynylethenes (TEEs) has shown that the reduction potentials are dependent on the extent of the conjugated π-electron framework. The DEE based nitro systems were more difficult to reduce than the corresponding TEEs.[13]

In order to establish a structure-electron affinity relationship, the electron affinities of π-conjugated systems are modulated by systematic changes of the molecular topology. The investigated molecules are composed from the following building blocks: double bonds, triple bonds, aromatic rings (benzene, thiophene, pyridine), and nitro groups. The nitro group has been chosen as acceptor substituent, since, as shown in Chapter 3, attachment of nitro groups lowered the LUMO level significantly and thus, facilitates the electron addition. In Section 5.2, the computational approach for the calculation of the electron affinities is described and then, in Section 5.3, the computed electron affinities are discussed as a function of substitution, chain elongation, and nature of the π-conjugated chain.

5.2 Computational Details

All calculations were carried out using the restricted Hartree-Fock (RHF) and restricted open-shell Hartree-Fock (ROHF) schemes. All geometries were optimized using the 6-31G** basis set. Conventional wisdom implies that electron affinity calculations usually require methods to account for electron correlation and basis sets including diffuse functions to model the charge density distribution of the anions correctly.[14,15] The size of the more extended systems considered in this study, whose calculations necessitated large amounts of computer time and/or disk storage, prevented the use of larger basis sets or more sophisticated methodologies, since the entire series of molecules had to be treated on equal level of theory for proper comparisons. The results should therefore be viewed qualitatively. The errors are expected to be systematic, so that the trends of the obtained results remain internally consistent.

The adiabatic electron affinity (EA) of a system has been determined by calculating the energy difference between the anion and the corresponding neutral molecule. The EA is positive when the energy gained by reduction is larger than that needed for the structural deformation, *i.e.* if the monoanion is more stable than the neutral.

$$EA_{ad} = E_{tot}^{ne} - E_{tot}^{ma} \qquad (1)$$

with E_{tot} total energy of ground state at equilibrium geometry
ne designates the neutral species
ma designates the monoanion

The total energies of the neutral compounds and their radical anions at their respective equilibrium structure, as well as the adiabatic electron affinities are summarized in the Appendix A at the end of this Chapter.

For the purpose of comparison, the EA of some of the investigated compounds were calculated with the Becke's three-parameter hybrid method[21] in conjunction with the Lee-Yang-Parr correlation functional,[22] denoted B3LYP. The B3LYP calculated EA values are generally about 1 eV higher than those predicted with HF. Density Functional Theory (DFT) has been shown in several other studies to yield quite accurate predictions of energies and electron affinities.[16-20] The better performance of B3LYP in the EA accuracy lies in the fact that DFT, in contrast to HF, accounts for electron correlation energy. This is particularly important in the current context, as the error introduced in the calculation of the radical anion by neglecting the electron correlation inevitably leads to an underestimation of the EA of the compound. Importantly however, the trends remain the same for both approaches. The results obtained with B3LYP are summarized in Appendix B.

C_s symmetry was retained for all systems. The computations were performed using the Gaussian 94 package.[23] The molecular structures and molecular orbitals were visualized with the molecular graphics package MOLEKEL.[24]

5.3 Results and Discussion

Several topological parameters are selected to analyze the electron affinities (EAs) of carbon-rich π-conjugated systems as a function of the molecular structure. Among those variables are:

- the type of substituents, *i.e.* amino and nitro substituents (Section 5.3.1),
- the number of substituents (Section 5.3.1),
- the chain length (Section 5.3.2),
- the nature of the building units of the π-conjugated chain (double bonds, triple bonds, aromatic rings like benzene, thiophene, pyridine) (Section 5.3.3), and

the incorporation of acetylenic side chains to the central olefinic bond in the conjugation path (one- *vs.* two-dimensional architecture) (Section 5.3.4).

In the following schemes, the adiabatic EA is reported for each compound.

5.3.1 Donor- or Acceptor-Substituted TEEs

Comparisons in Scheme 5.1 between parent TEE **1**, bisamino TEE **2**, and bisnitro TEE **4** illustrate that, as expected, nitro groups increase the EA of TEE **1** by 1.964 eV (EA(**1**) = –0.321 eV and EA(**4**) = 1.643 eV) and π-electron donating amino groups decrease the EA.

The number of nitro groups attached to the carbon core also plays a role on the EA. The EA rises considerably by 1.964 eV with the attachment of *two* nitro groups to the TEE core (EA(**1**) = –0.321 eV and EA(**4**) = 1.643 eV), compared to an increase of 1.111 eV in mononitrosubstituted TEE **3** (EA(**3**) = 0.790 eV). This behavior has been confirmed by the EA analysis of several other mono- and bisnitrosubstituted compounds listed in Appendix A.

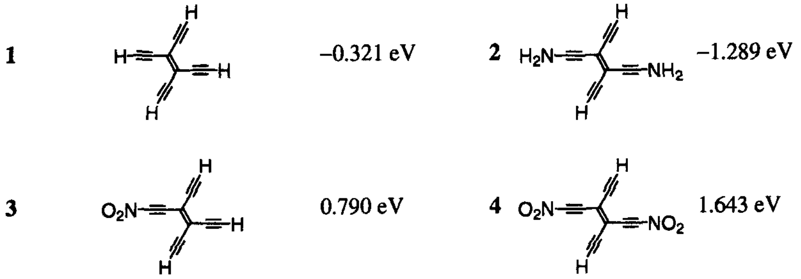

Scheme 5.1. EA comparisons (HF/6-31G** data) between parent TEE **1** and donor- or acceptor-substituted TEEs.

5.3.2 Chain Elongation

As depicted in Scheme 5.2, the nitrosubstituted π-conjugated chain is sequentially lengthened by adding identical segments (double bonds, triple bonds, or phenyl rings) to the carbon chain. For each series (**5**,**7**,**9**,**11**), (**6**,**8**,**10**) and (**12**,**13**), the EA increases with increasing chain length. The largest incremental EA enhancement is found between **5** and **7** (ΔEA = 0.342 eV). Then, the EA difference between consecutive compounds diminishes with additional triple bonds to 0.196 eV between **7** and **9**, and to 0.118 eV between **9** and **11**. Similar considerations apply to the olefinic series with ΔEA = 0.210 eV between

6 and **8** *vs.* 0.176 eV between **8** and **10**. These observations indicate that the EA is likely to eventually reach saturation in these systems.

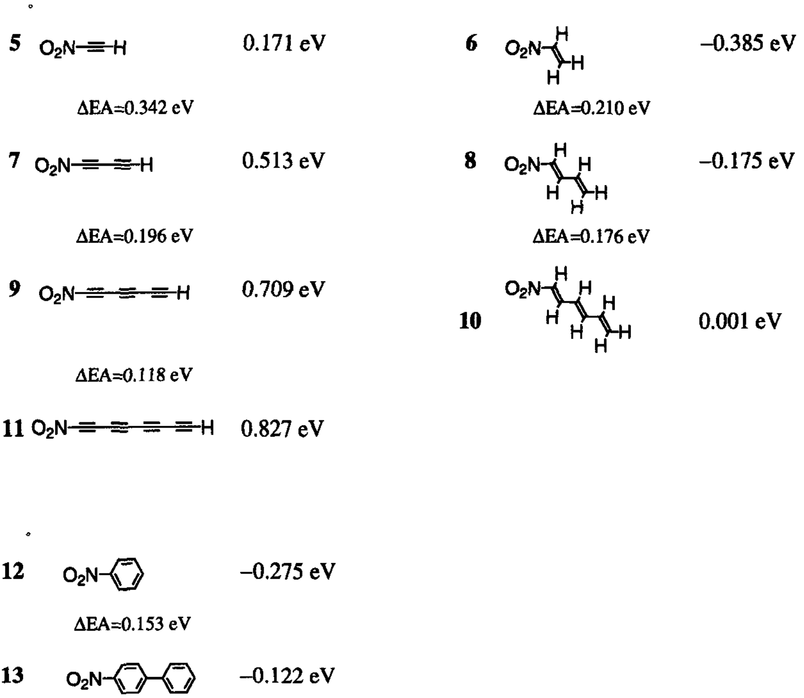
5 O_2N–≡–H 0.171 eV
ΔEA=0.342 eV
7 O_2N–≡–≡–H 0.513 eV
ΔEA=0.196 eV
9 O_2N–≡–≡–≡–H 0.709 eV
ΔEA=0.118 eV
11 O_2N–≡–≡–≡–≡–H 0.827 eV
6 –0.385 eV
ΔEA=0.210 eV
8 –0.175 eV
ΔEA=0.176 eV
10 0.001 eV
12 –0.275 eV
ΔEA=0.153 eV
13 –0.122 eV
O_2N
H

Scheme 5.2. Effects of chain elongation on the EA (HF/6-31G** data) of electron deficient acetylenic, olefinic, and aryl systems.

5.3.3 Nature of the π-Conjugated Backbone

In the following, the effect of different units, forming the conjugated backbone, on the EA is tested (Schemes 5.3 and 5.4). For a systematic comparison, the number of building units (double bonds, triple bonds, aromatic rings) is kept constant. In the present discussion, the numbering of these building units is started at the conjugated segment attached to the nitro group.

Two Building Units

Of the systems composed of two identical building blocks (**8**, **13**, and **7** in Scheme 5.3), the olefinic system **8** displays the lowest EA, followed by the aryl compound **13**, and the acetylenic system **7** yields the highest EA with 0.513 eV. Moreover, the EA of the aryl system **13** is lower than the hybrid systems **15** and **18**, formed of a double and a triple bond. This is particularly interesting, since **13**, composed of two phenyl groups, formally has six π-bonds to contribute to the charge delocalization, and still seems to be less efficient in raising the EA than the two π-systems in **15** and **18**.

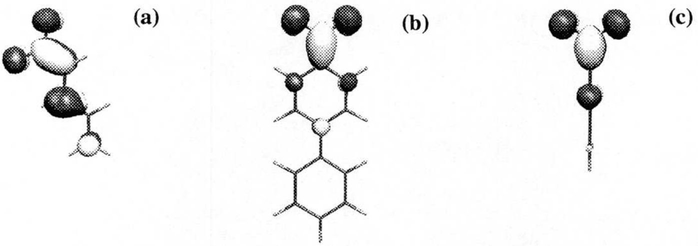

Figure 5.1. Highest occupied molecular orbitals (HOMOs) of (a) radical anion $\mathbf{8}^{\bullet-}$, (b) radical anion $\mathbf{13}^{\bullet-}$, and (c) radical anion $\mathbf{7}^{\bullet-}$.

In order to elucidate the origin of these differences in EA, the electronic characteristics of **8**, **13**, and **7** are examined. The analysis is directed towards how different conjugated moieties influence the charge density distributions in radical anions. The highest occupied molecular orbitals (HOMOs) of the radical anions of $\mathbf{8}^{\bullet-}$, $\mathbf{7}^{\bullet-}$, and $\mathbf{13}^{\bullet-}$ are depicted in Figure 5.1. The HOMO of $\mathbf{8}^{\bullet-}$ shows delocalization of the incurred charge over the nitro group and the two olefinic bonds, whereas in $\mathbf{7}^{\bullet-}$ the charge remains localized on the nitro group and the first adjacent triple bond only. The HOMO of $\mathbf{13}^{\bullet-}$ exhibits that the charge is limited to the nitro group and the first phenyl ring. In accordance with the HOMO picture, the Mulliken charge populations reveal that upon reduction, the charge accumulation on the nitro group is higher for the triple bond containing compound **7** (–0.67 | e |) than for **13** (–0.59 | e |) and **8** (–0.51 | e |). Thus, it can be concluded that triple bonds are less efficient at delocalizing π-charge than double bonds.

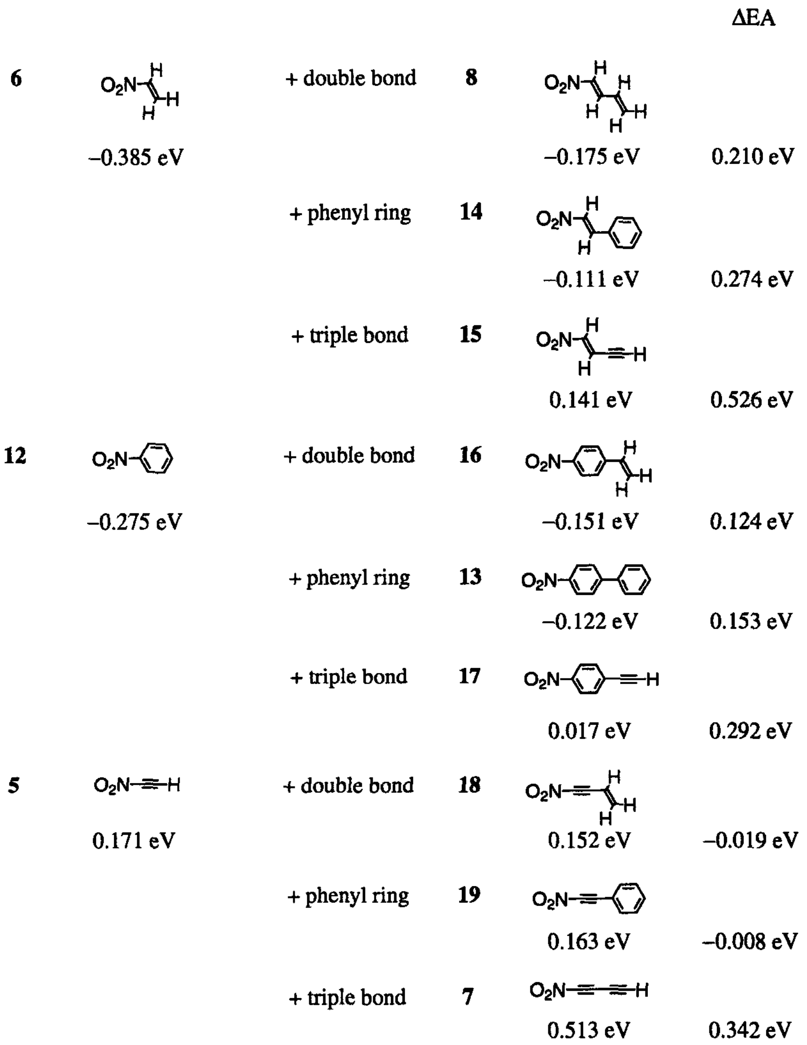
ΔEA
6
O2N
H
H
H
−0.385 eV
+ double bond
8
−0.175 eV
0.210 eV
+ phenyl ring
14
−0.111 eV
0.274 eV
+ triple bond
15
0.141 eV
0.526 eV
12
O2N
−0.275 eV
+ double bond
16
−0.151 eV
0.124 eV
+ phenyl ring
13
−0.122 eV
0.153 eV
+ triple bond
17
0.017 eV
0.292 eV
5
O2N−≡−H
0.171 eV
+ double bond
18
0.152 eV
−0.019 eV
+ phenyl ring
19
0.163 eV
−0.008 eV
+ triple bond
7
O2N−≡−≡−H
0.513 eV
0.342 eV

Scheme 5.3. Effects of the extension of π-conjugation (from one to two conjugated segments) on the EA (HF/6-31G** data).

In the hybrid systems, the EA increases with the nature of the second conjugated segment in the order double bond < phenyl ring < triple bond, independent of the nature of the first conjugated unit:

first unit:	second unit: double bond < phenyl ring < triple bond
double bond →	EA(**8**) < EA(**14**) < EA(**15**),
phenyl ring →	EA(**16**) < EA(**13**) < EA(**17**),
triple bond →	EA(**18**) < EA(**19**) < EA(**7**).

Furthermore, the effect of adding one conjugated segment to nitroethene, nitrobenzene, and nitroacetylene, is considered (Scheme 5.3). Except for the case, where a double bond or a phenyl ring is added to the triple bond (**18** and **19**), an EA increase is predicted upon extension of the system. ΔEA is considerably larger upon adding a triple bond than at the addition of a double bond or a phenyl ring (Scheme 5.3). It appears that this increase in EA originates from the strong σ-accepting character of the electron deficient triple bonds, and not from π-effects, since, as mentioned before, triple bonds do participate less in the π-electron delocalization.

Effect of Phenyl Ring Insertion

Although a lowering of the LUMO and thus, an EA increase would be expected upon extension of the conjugated systems, comparison between molecules composed of two (Scheme 5.3) and three building units (Scheme 5.4), reveals that the EA decreases upon insertion of a phenyl ring between the nitro group and the unsaturated carbon chain, if the chain is composed of at least one triple bond (Scheme 5.5: EA(**7**) = 0.513 eV and EA(**23**) = 0.184 eV). Furthermore, comparing the chain elongation effects, the EA increase is with ΔEA=0.342 eV larger for the all acetylenic pair (**5**,**7**) than for the phenyl containing pair (**17**,**23**) (ΔEA=0.167 eV). These surprising observations indicate that the phenyl ring acts as a buffer between the carbon chain and the nitro group. The electron withdrawing inductive effect of the electron deficient triple bonds is weakened by the intercalation of the phenyl ring. On the other hand, if the carbon chain displays an all olefinic character, the hindering effect of the aryl moiety does not seem to apply. As expected, an increase of the EA is observed upon extension of the π-conjugated system (Scheme 5.5: EA(**6**) = −0.385 eV and EA(**15**) = −0.151 eV, and EA(**8**) = −0.175 eV and EA(**20**) = −0.089 eV).

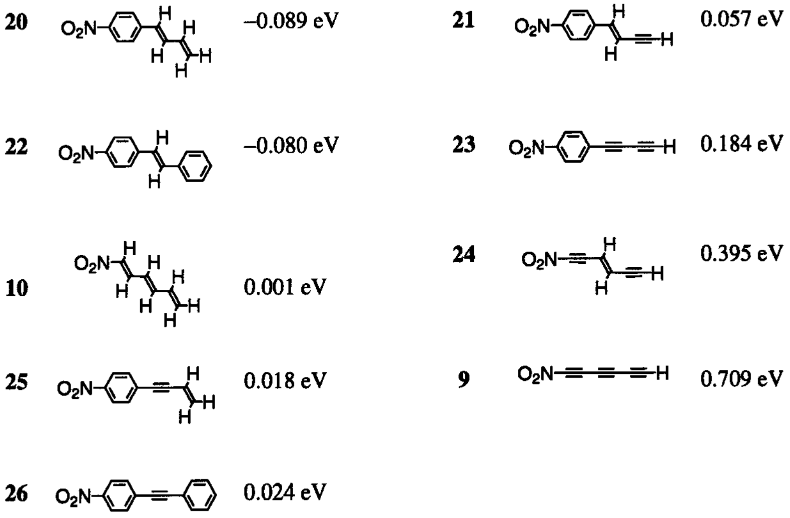
20
H
O2N
H
H
H
H
−0.089 eV
21
H
O2N
H
H
0.057 eV
22
H
O2N
H
−0.080 eV
23
O2N
H
0.184 eV
10
H
O2N
H
H
H
H
H
0.001 eV
24
H
O2N
H
H
0.395 eV
25
H
O2N
H
H
0.018 eV
9
O2N
H
0.709 eV
26
O2N
0.024 eV

Scheme 5.4. EA comparisons between mononitrosubstituted molecules composed of three conjugated segments (HF/6-31G** data).

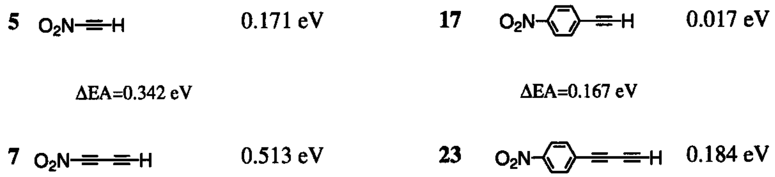
5
O2N
H
0.171 eV
17
O2N
H
0.017 eV
ΔEA=0.342 eV
ΔEA=0.167 eV
7
O2N
H
0.513 eV
23
O2N
H
0.184 eV

Scheme 5.5. Effect of the introduction of a phenyl segment in the acetylenic chain on the EA (HF/6-31G** data).

6	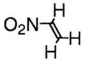	−0.385 eV	**15**	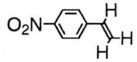	−0.151 eV
8	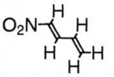	−0.175 eV	**20**	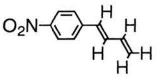	−0.089 eV

Scheme 5.5. Effect of the introduction of a phenyl segment in the acetylenic chain on the EA (HF/6-31G** data).

In order to further examine this behavior the electron distribution in $\mathbf{23}^{\bullet-}$ and $\mathbf{20}^{\bullet-}$ is inspected. The HOMOs of the radical anions $\mathbf{23}^{\bullet-}$ and $\mathbf{20}^{\bullet-}$, sketched in Figure 5.2, show similar shape. This indicates that, indeed, the π-charge is not transmitted by the phenyl ring to the olefinic or acetylenic carbon chain and that the EA difference can be explained on the basis of the σ-charge withdrawing ability of the carbon chain. The σ-charge withdrawing character of triple bonds being superior to that of double bonds, the blocking effect of the incorporated phenyl segment decreases only the EA of **23**.

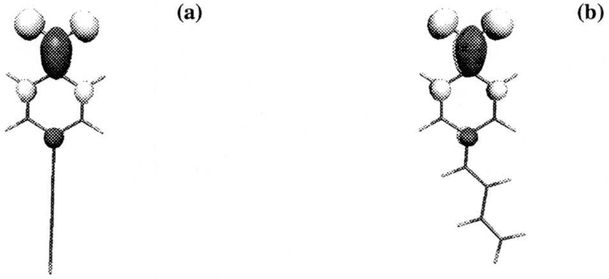

Figure 5.2. Highest occupied molecular orbitals (HOMOs) of (a) radical anion $\mathbf{23}^{\bullet-}$ and (b) radical anion $\mathbf{20}^{\bullet-}$.

Three Building Units

Keeping two segments constant, the same pattern emerges as for the nitro compounds formed of two conjugated units: the EA increases with the third conjugated segment following the order double bond < phenyl ring < triple bond.

first unit:	second unit:	third unit: double bond < phenyl ring < triple bond
phenyl ring	double bond →	EA(**20**) < EA(**22**) < EA(**21**),
phenyl ring	triple bond →	EA(**25**) < EA(**26**) < EA(**23**).

Phenyl vs. Heteroaromatic Ring

In order to test the influence of the cyclic unit on the EA, the phenyl ring has been replaced by the electron-excessive five-membered heterocyclic thiophene and by the electron-deficient six-membered pyridine in a series of systems of **27-38** (Scheme 5.6). Within a series, species containing thiophene gave the highest EA, followed by the pyridine based system, and finally by the corresponding compound with a phenyl ring.

This observation has been explained by examining the aromatic character of the rings with the indicator δr. δr is the average value of the bond length differences between two consecutive C–C bonds within the ring and is reported for the series (**27**, **29**, **31**) in Table 5.1. In the neutral species **27** and **29**, a value of δr = 0.01 is found for the phenyl and pyridine ring, confirming the benzoid character of the rings. Analyses of the monoanions give a δr of 0.04 for the phenyl based **27**$^{\bullet-}$ and a δr of 0.02 for the pyridine based **29**$^{\bullet-}$, showing that the quinoid contribution to the arylated anionic structure **27**$^{\bullet-}$ is stronger. The higher energy cost required to form **27**$^{\bullet-}$ explains the smaller EA of **27** with respect to **29**.

The thiophene ring in the neutral **31**, on the other hand, shows a value of δr = 0.07, indicating the weaker aromatic character of the thiophene unit. For **31**$^{\bullet-}$ δr equals 0.02, which indicates that the monoanion adopts benzoid character. Thus, the energy gain upon structural rearrangement to the benzoid form increases the EA compared to the EA of **27** and **29**.

In conclusion, the quinoid ring structures yield a larger electron affinity than the aromatic structures. These developed considerations apply also to the other series of molecules considered (**33**-**38**).

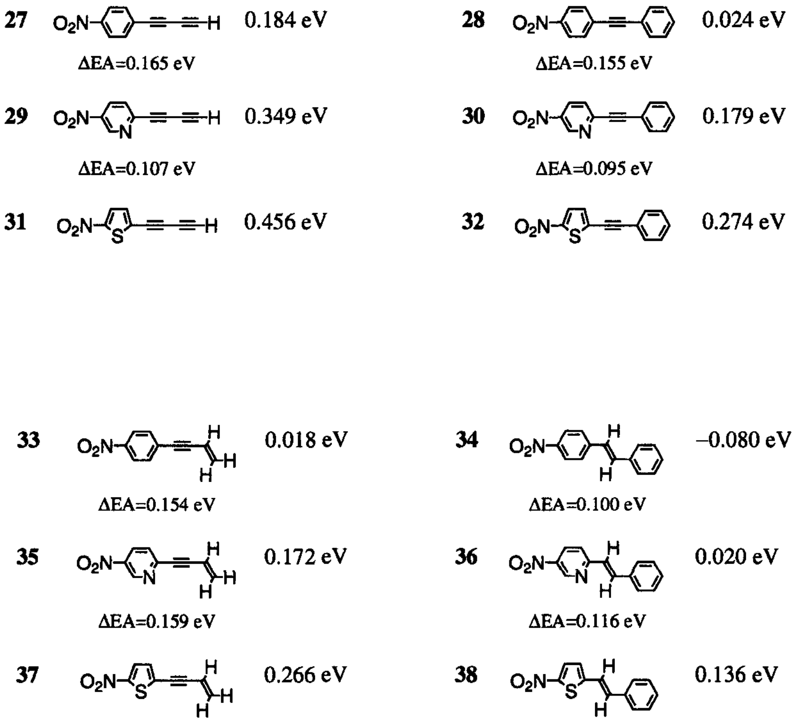
27
O2N
H
0.184 eV
ΔEA=0.165 eV
28
O2N
0.024 eV
ΔEA=0.155 eV
29
O2N
N
H
0.349 eV
ΔEA=0.107 eV
30
O2N
N
0.179 eV
ΔEA=0.095 eV
31
O2N
S
H
0.456 eV
32
O2N
S
0.274 eV
33
O2N
H
H
H
0.018 eV
ΔEA=0.154 eV
34
O2N
H
H
−0.080 eV
ΔEA=0.100 eV
35
O2N
N
H
H
H
0.172 eV
ΔEA=0.159 eV
36
O2N
N
H
H
0.020 eV
ΔEA=0.116 eV
37
O2N
S
H
H
H
0.266 eV
38
O2N
S
H
H
0.136 eV

Scheme 5.6. EA comparisons (HF/6-31G** data) of a number mononitrosubstituted systems differing in their aromatic unit.

Table 5.1. Values of the indicator δr^a for the extent of aromatic character in the rings of **27**, **29**, and **31** (HF/6-31G** data).

compound	$\delta r(ne)^b$	$\delta r(ma)^c$
27	0.01	0.04
29	0.01	0.02
31	0.07	0.02

[a] δr is the average value of the bond length differences between two consecutive C–C in the ring. $\delta r = 0$ in benzene, values between 0.08–0.14 are found in a fully quinoid ring. For the definition of δr see eq. 1 in Chapter 2. [b] ne Designates the neutral species. [c] ma Designates the monoanion.

5.3.4 One- *vs.* Two-Dimensional Architectures

The question of whether the acetylenic side chains offer advantages with respect to the EA has been examined by comparing a series of DEE and TEE based systems **39-46**, as well as the pairs (**47**,**49**) and (**48**,**50**) with olefinic backbones (Scheme 5.7). As expected, the EA increases considerably in some cases upon incorporation of acetylenic side chains to the central bond, since those side chains extend the π-conjugated system and thus, allow a better overall delocalization of the incurred charge. For the parent DEE **39** and TEE **41**, the change in EA is 1.121 eV. Analogously, the EA of bisnitrosubstituted DEE **40** is 0.305 eV lower than the EA of the corresponding TEE **42**. The cases where only a minor increase of the EA is observed are the phenyl containing systems (**44**,**46**) and (**48**,**50**).

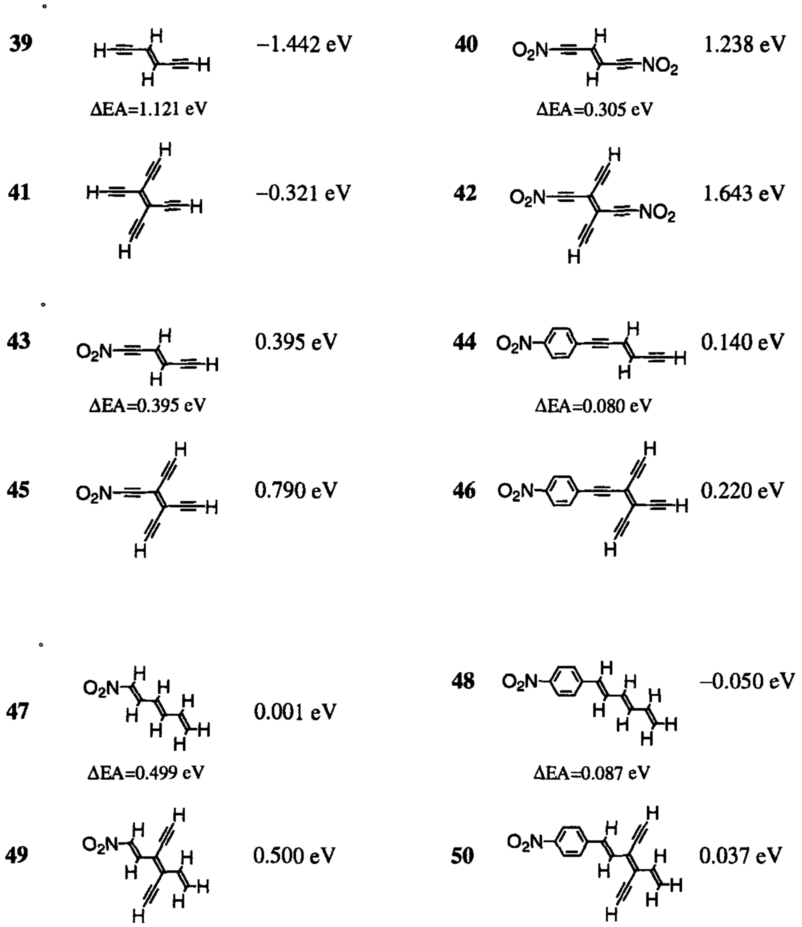
39
H
H
H
H
−1.442 eV
ΔEA=1.121 eV
40
O2N
H
H
NO2
1.238 eV
ΔEA=0.305 eV
41
H
H
H
H
−0.321 eV
42
O2N
H
H
NO2
1.643 eV
43
O2N
H
H
H
0.395 eV
ΔEA=0.395 eV
44
O2N
H
H
H
0.140 eV
ΔEA=0.080 eV
45
O2N
H
H
H
0.790 eV
46
O2N
H
H
H
0.220 eV
47
O2N
H
H
H
H
H
H
0.001 eV
ΔEA=0.499 eV
48
O2N
H
H
H
H
H
H
−0.050 eV
ΔEA=0.087 eV
49
O2N
H
H
H
H
H
H
0.500 eV
50
O2N
H
H
H
H
H
H
0.037 eV

Scheme 5.7. EA comparisons (HF/6-31G** data) between one- and two-dimensional conjugated carbon frameworks.

In order to analyze this different behavior between TEEs and DEEs, the electronic structures of the reduced states are inspected. Examination of the HOMOs (Figure 5.3) of DEE $\mathbf{43}^{\bullet -}$ and TEE $\mathbf{45}^{\bullet -}$ exhibits strong localization of the incurred charge onto the nitro group in $\mathbf{43}^{\bullet -}$, whereas only weak localization onto the nitro group in found in $\mathbf{45}^{\bullet -}$. The

Mulliken charge population analysis shows that, in the neutral species, the amount of negative charge on the nitro groups remains –0.525 | *e* | upon introduction of acetylenic side chains (**43** *vs.* **45**). In the monoanion, however, the charge accumulation (–0.634 | *e* |) on the nitro group of **43**$^{\bullet -}$ is more pronounced than in **45**$^{\bullet -}$ (–0.229 | *e* |). This clearly indicates that the two-dimensional TEE framework allows a better redistribution of the incurred charge due to the acetylenic side chains. In the phenyl containing compounds (**44**,**46**) and (**48**,**50**), the incurred charge is localized on the nitro group and the phenyl ring as shown for **23**$^{\bullet -}$ and **20**$^{\bullet -}$ in Figure 5.2. Charge delocalization to the core is hindered by the insertion of the ring and thus, the acetylenic side chains are not involved in the charge distribution.

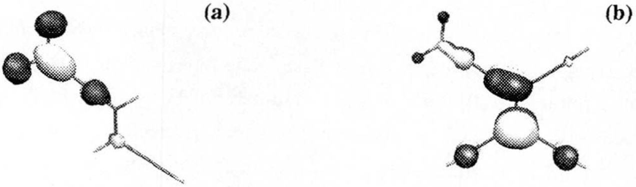

Figure 5.3. Highest occupied molecular orbitals (HOMOs) of (a) radical anion **43**$^{\bullet -}$ and (b) radical anion **45**$^{\bullet -}$.

5.4 Concluding Remarks

A variety of π-conjugated nitrosubstituted systems has been modeled and their adiabatic electron affinities calculated in order to determine criteria for the optimization of the electron affinities in carbon-rich materials. As building blocks for the conjugated chain, double bonds, triple bonds, as well as phenyl, thienyl, and pyridyl rings have been considered.

The first observation that crystallizes out of this analysis is that the EA depends on the nature (donor or acceptor) of the substituents and, as expected, increases with the number of acceptor substituents attached to the conjugated carbon framework. The extension of the conjugated chain by identical units leads also to an EA increase, most presumably reaching saturation at a certain chain length. Summarizing the EA results obtained for mononitro substituted molecules composed of two or three conjugated segments, it is predicted that the acceptor substituted *all acetylenic* systems exhibit the highest EA. Generally, the EA increase follows the order double bond < phenyl ring < triple bond. Interestingly, the insertion of a phenyl ring between the nitro group and the unsaturated carbon chain, containing at least one triple bond, decreases the EA. The phenyl ring seems to diminish the σ-electron withdrawing ability of the electron deficient triple bonds. Replacement of the phenyl ring by heterocycles (thiophene and pyridine) yields larger EAs for all considered systems. Another factor that significantly influences the EA is the introduction of acetylenic side chains to the central olefinic bond in the linear carbon chain. The predicted EA shows considerably higher values in the extended cross conjugated molecular framework.

Given the set of construction segments considered in this study, it can be concluded that the strong electron accepting nitro group contributes significantly to the increase of electron affinities. Triple bonds and the two-dimensional conjugated framework play also an effective role for the design of compounds with high electron affinities. The presence of a phenyl ring between the acceptor substituent and the conjugated carbon chain, however, reduces the electron affinities. The replacement of the phenyl ring with heterocycles seems to result again in an increase of the electron affinities. It has to be mentioned that in this study the ease of synthesis of the different modeled compound was not taken into consideration.

5.5 References

[1] J. H. Burroughes, D. D. C. Bradley, A. R. Brown, R. N. Marks, R. H. Friend, P. L. Burn, A. B. Holmes, *Nature* **1990**, *347*, 539-541. Light-Emitting Diodes Based on Conjugated Polymers.

[2] M. Berggren, O. Inganäs, J. Rasmusson, G. Gustafsson, M. R. Andersson, O. Wennerström, T. Hjertberg, *Nature* **1994**, *372*, 444-446. Light-Emitting Diodes with Variable Colours from Polymer Blends.

[3] A. Kraft, A. C. Grimsdale, A. B. Holmes, *Angew. Chem.* **1998**, *110*, 416-443, *Angew. Chem. Int. Ed.* **1998**, *37*, 402-428. Electroluminescent Conjugated Polymers - Seeing Polymers in a New Light.

[4] A. Heeger, J. Long, *Opt. Photonics News* **1996**, *8*, 24-30. Opto-Electronic Devices Fabricated from Semiconducting Polymers.

[5] A. R. Brown, D. D. C. Bradley, J. H. Burroughes, R. H. Friend, N. C. Greenham, P. L. Burn, A. B. Holmes, A. Kraft, *Appl. Phys. Lett.* **1992**, *61*, 2793-2795. Poly(*p*-phenylenevinylene) Light-Emitting Diodes: Enhanced Electroluminescent Efficiency Through Charge Carrier Confinement.

[6] L. S. Swanson, J. Shinar, A. R. Brown, D. D. C. Bradley, R. H. Friend, P. L. Burn, A. Kraft, A. B. Holmes, *Phys. Rev. B* **1992**, *46*, 15072-15077. Electroluminescence-Detected Magnetic-Resonance Study of Polyparaphenylenevinylene (PPV)-based Light-Emitting Diodes.

[7] I. D. Parker, Q. Pei, M. Marrocco, *Appl. Phys. Lett.* **1994**, *65*, 1272-1274. Efficient Blue Electroluminescence from a Fluorinated Polyquinoline.

[8] S. C. Moratti, R. Cervini, A. B. Holmes, D. R. Baigent, R. H. Friend, N. C. Greenham, J. Grüner, P. J. Hamer, *Synth. Met.* **1995**, *71*, 2117-2120. High Electron Affinity Polymers for LEDs.

[9] N. C. Greenham, S. C. Moratti, D. D. C. Bradley, R. H. Friend, A. B. Holmes, *Nature* **1993**, *365*, 628-630. Efficient Light-Emitting Diodes Based on Polymers with High Electron Affinities.

[10] J. Cornil, D. A. dos Santos, D. Beljonne, J.-L. Brédas, *J. Phys. Chem.* **1995**, *99*, 5604-5611. Electronic Structure of Phenylene Vinylene Oligomers: Influence of

Donor/Acceptor Substitutions.

[11] J.-L. Brédas, A. J. Heeger, *Chem. Phys. Lett.* **1994**, *217*, 507-512. Influence of Donor and Acceptor Substituents on the Electronic Characteristics of Poly(paraphenylene vinylene) and Poly(paraphenylene).

[12] J. Cornil, D. Beljonne, D. A. dos Santos, Z. Shuai, J.-L. Brédas, *Synth. Met.* **1996**, *78*, 209-217. Towards a Better Understanding of Polymer-Based Light-Emitting Diodes: A Theoretical Insight Into the Basic Phenomena.

[13] A. Hilger, J.-P. Gisselbrecht, R. R. Tykwinski, C. Boudon, M. Schreiber, R. E. Martin, H. P. Luethi, M. Gross, F. Diederich, *J. Am. Chem. Soc.* **1997**, *119*, 2069-2078. Electronic Characteristics of Arylated Tetraethynylethenes: A Cooperative Computational and Electrochemical Investigation.

[14] W. J. Hehre, L. Radom, P. v. R. Schleyer, J. Pople, *Ab Initio Molecular Orbital Theory*; John Wiley & Sons: New York, 1986.

[15] R. A. Kendall, T. H. Dunning, R. J. Harrison, *J. Chem. Phys.* **1992**, *96*, 6796-6806. Electron Affinities of the First-Row Atoms Revisited. Systematic Basis Sets and Wave Functions.

[16] R. A. King, J. M. Galbraith, H. F. Schaefer III, *J. Phys. Chem.* **1996,** *100*, 6061-6068. Negative Ion Thermochemistry: The Sulfur Fluorides SF_n/SF_n^- (n = 1-7).

[17] S. E. Boesch, A. K. Grafton, R. A. Wheeler, *J. Phys. Chem.* **1996,** *100*, 10083-10087. Electron Affinities of Substituted *p*-Benzoquinones from Hybrid Hartree-Fock/Density-Functional Calculations.

[18] J. Baker, M. Muir, J. Andzelm, *J. Chem. Phys.* **1995**, *102*, 2063-2079. A Study of Some Organic Reactions Using Density Functional Theory.

[19] B. G. Johnson, P. M. W. Gill, J. A. Pople, *J. Chem. Phys.* **1993**, *98*, 5612-5626. The Performance of a Family of Density Functional Methods.

[20] P. M. W. Gill, B. G. Johnson, J. A. Pople, M. J. Frisch, *Chem. Phys. Lett.* **1992**, *197*, 499-505. The Performance of the Becke-Lee-Yang-Parr (B-LYP) Density Functional Theory with Various Basis Sets.

[21] A. D. Becke, *J. Chem. Phys.* **1993**, *98*, 1372-1377. A New Mixing of Hartree-Fock

and Local Density-Functional Theories.

[22] C. Lee, W. Yang, R. G. Parr, *Phys. Rev. B* **1988**, *37*, 785-789. Development of the Colle-Salvetti Correlation-Energy Formula into a Functional of the Electron Density.

[23] Gaussian 94, M. J. Frisch, G. W. Trucks, H. B. Schlegel, P. M. W. Gill, B. G. Johnson, M. A. Robb, J. R. Cheeseman, T. A. Keith, G. A. Petersson, J. A. Montgomery, K. Raghavachari, M. A. Al-Laham, V. G. Zakrzewski, J. V. Ortiz, J. B. Foresman, J. Cioslowski, B. B. Stefanov, A. Nanayakkara, M. Challacombe, C. Y. Peng, P. Y. Ayala, W. Chen, M. W. Wong, J. L. Andres, E. S. Replogle, R. Gomperts, R. L. Martin, D. J. Fox, J. S. Binkley, D. J. Defrees, J. Baker, J. J. P. Stewart, M. Head-Gordon, C. Gonzalez, J.A. Pople, Gaussian, Inc. Pittsburgh, PA, 1995.

[24] MOLEKEL 2.6, Peter F. Flükiger, University of Geneva and CSCS Manno, Switzerland, 1997.

Appendix A

In the following tables, ne designates the neutral species and ma designates the monoanion. For both, the total energies at their equilibrium structure have been listed.

Table 5.2. HF/6-31G** Total energies (in hartrees) and adiabatic energy differences (in eV) of a series of unsubstituted compounds.

compound	E_{tot} (ne)^{a}	E_{tot} (ma)^{b}	ΔE_{tot} (ne–ma)
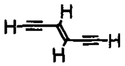	–229.391 646	–229.338 614	–1.442
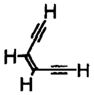	–229.390 294	–229.334 750	–1.511
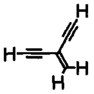	–229.386 131	–229.331 272	–1.492
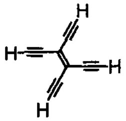	–380.729 714	–380.717 914	–0.321
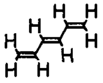	–231.822478	–231.757431	–1.770
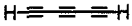	–228.182 520	–228.118174	–1.750
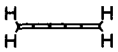	–229.360 931	–229.344 786	–0.439

Table 5.2. HF/6-31G** Total energies (in hartrees) and adiabatic energy differences (in eV) of a series of unsubstituted compounds.

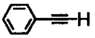	–306.389 246	–306.308 982	–2.183
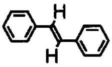	–537.160 252	–537.110 149	–1.363
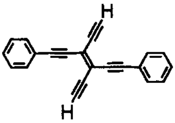	–839.866 982	–839.863 686	–0.090
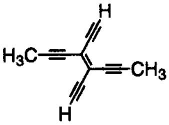	–458.829078	–458.806 529	–0.613
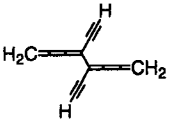	–457.588 238	–457.593 245	0.136

Table 5.3. HF/6-31G** Total energies (in hartrees) and energy differences (in eV) of a series of disubstituted compounds.

compound	E_{tot} (ne)[a]	E_{tot} (ma)[b]	ΔE_{tot} (ne–ma)
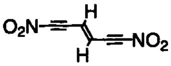	–636.268 033	–636.313 533	1.238
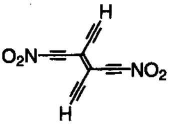	–787.604 099	–787.664 503	1.643

Table 5.3. HF/6-31G** Total energies (in hartrees) and energy differences (in eV) of a series of disubstituted compounds.

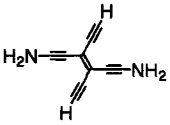	−490.796 567	−490.749 194	−1.289
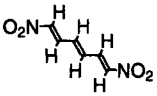	−638.763 256	−638.803 109	1.084
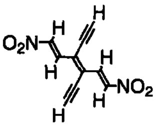	−790.105 228	−790.157 951	1.434
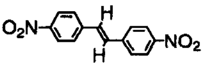	−944.100 292	−944.116 459	0.440
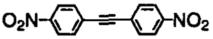	−942.893 345	−942.906 368	0.354

Table 5.4. HF/6-31G* Total energy (in hartrees) and adiabatic energy difference (in eV) of TEE and DEE derivatives, and their radical anions.

compound	E_{tot} (ne)[a]	E_{tot} (ma)[b]	ΔE_{tot} (ne–ma)
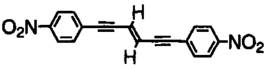	−1095.464 345	−1095.475 186	0.295
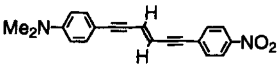	−947.030 794	−947.032 009	0.033
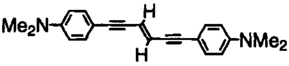	−798.594 642	−798.543 592	−1.388

Table 5.4. HF/6-31G* Total energy (in hartrees) and adiabatic energy difference (in eV) of TEE and DEE derivatives, and their radical anions.

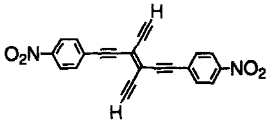	−1246.803 313	−1246.833 336	0.817
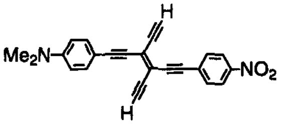	−1098.370 477	−1098.374 247	0.102
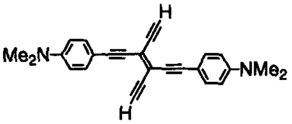	−949.935 138	−949.917 007	−0.493

Table 5.5. HF/6-31G** Total Energies (in hartrees) and Energy Difference (in eV) of mononitro substituted compounds containing double and triple bonds.

compound	E_{tot} (ne)[a]	E_{tot} (ma)[b]	ΔE_{tot} (ne–ma)
O_2N-H	−204.621 095	−204.590 305	−0.838
$O_2N-\equiv-H$	−280.260 020	−280.266 294	0.171
$O_2N-\equiv-\equiv-H$	−355.938 099	−355.956 949	0.513
$O_2N-\equiv-\equiv-\equiv-H$	−431.617 754	−431.643 821	0.709
$O_2N-\equiv-\equiv-\equiv-\equiv-H$	−507.297 780	−507.328 200	0.827
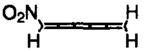	−432.824 845	−432.871 443	1.267

Table 5.5. HF/6-31G** Total Energies (in hartrees) and Energy Difference (in eV) of mononitro substituted compounds containing double and triple bonds.

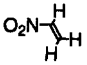	–281.509 569	–281.495 408	–0.385
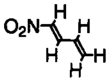	–358.402 755	–358.396 324	–0.175
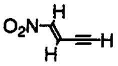	–357.183 068	–357.188 216	0.141
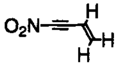	–357.157 203	–357.162 787	0.152
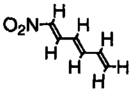	–435.295 899	–435.295 859	0.001
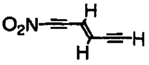	–432.832 231	–432.846 753	0.395
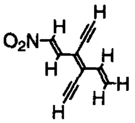	–586.638 826	–586.657 214	0.500
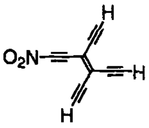	–584.168 915	–584.197 953	0.790

Table 5.6. HF/6-31G** Total energies (in hartrees) and energy differences (in eV) of a series of mononitrosubstituted compounds containing aromatic rings.

compound	E_{tot} (ne)[a]	E_{tot} (ma)[b]	ΔE_{tot} (ne–ma)
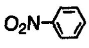	–434.184 268	–434.174 157	–0.275
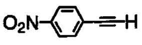	–509.857 834	–509.858 455	0.017
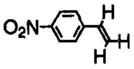	–511.070 415	–511.064 862	–0.151
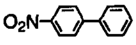	–663.737399	–663.732945	–0.122
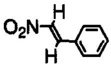	–511.072 789	–511.068 710	–0.111
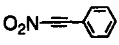	–509.832 032	–509.838 040	0.163
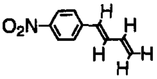	–587.962 629	–587.959 366	–0.089
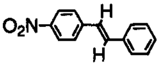	–740.631 440	–740.628 494	–0.080
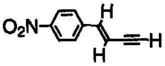	–586.746 472	–586.748 561	0.057
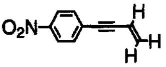	–586.752 035	–586.752 681	0.018
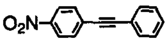	–739.426 003	–739.426 891	0.024

Table 5.6. HF/6-31G** Total energies (in hartrees) and energy differences (in eV) of a series of mononitrosubstituted compounds containing aromatic rings.

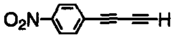	−585.538 124	−585.544 883	0.184
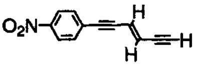	−662.428 188	−662.433 322	0.140
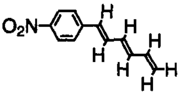	−664.855 125	−664.853 280	−0.050
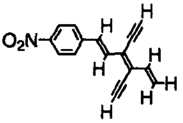	−816.199 630	−816.201 009	0.037
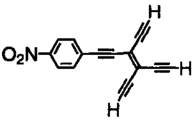	−813.766 675	−813.774 765	0.220

Table 5.7. HF/6-31G** Total energies (in hartrees) and energy differences (in eV) of a series of mononitrosubstituted compounds containing thiophene or pyridine rings.

compound	E_{tot} (ne)[a]	E_{tot} (ma)[b]	ΔE_{tot} (ne−ma)
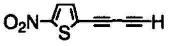	−906.113 275	−906.130 043	0.456
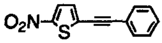	−1060.002 032	−1060.012 094	0.274
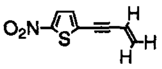	−907.328 074	−907.337 851	0.266

Table 5.7. HF/6-31G** Total energies (in hartrees) and energy differences (in eV) of a series of mononitrosubstituted compounds containing thiophene or pyridine rings.

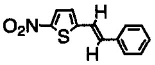	−1061.208 801	−1061.213 817	0.136
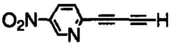	−601.523 018	−601.535 842	0.349
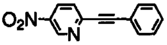	−755.412 123	−755.418 694	0.179
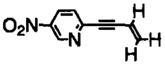	−602.737 948	−602.744 276	0.172
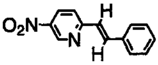	−756.625 593	−756.626 311	0.020

Appendix B

Table 5.8. B3LYP/6-31G** Total energies (in hartrees) and energy differences (in eV) of a series of mononitrosubstituted compounds.

compound	E_{tot} (ne)[a]	E_{tot} (ma)[b]	ΔE_{tot} (ne–ma)
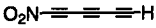	-434.118 541	–434.179 626	1.662
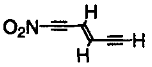	-435.366 207	-435.419 848	1.460
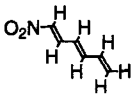	-437.913 680	-437.955 980	1.151
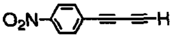	-589.059744	-589.106417	1.270
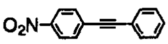	-743.978223	-744.021033	1.165
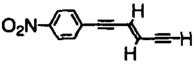	-590.315135	-590.356888	1.136
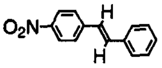	-745.230273	-745.272757	1.156
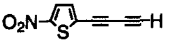	-909.806 737	-909.861 286	1.484
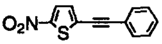	-1064.725 717	-1064.775 637	1.358

Table 5.8. B3LYP/6-31G** Total energies (in hartrees) and energy differences (in eV) of a series of mononitrosubstituted compounds.

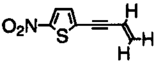	-911.062 661	-911.111 728	1.335
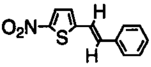	-1065.977 861	-1066.026 647	1.327

Leer - Vide - Empty

6 Electronic Spectra of Nitrophenyl and Nitrothienyl Donor-Acceptor Tetraethynylethenes

6.1 Introduction

The relationship between the molecular structure and electronic absorption provides an important guiding principle for the design of conjugated organic materials. For example, since the color of a light-emitting dye is mainly determined by its conjugated π-electron system,[1-8] a number of theoretical studies[9-14] regarding the connection between π-systems and their electronic absorption spectra have been performed. Furthermore, the effectiveness of a chromophore as a nonlinear optical material is coupled to π-electron delocalization and donor-acceptor charge-transfer type electronic transitions and thus, the analysis of the electronic absorption spectra can often be correlated with the nonlinear optical behavior of a specific compound.[15-17]

Tetraethynylethene (TEE) has proven to be a remarkable conjugated framework for appending electron donating and accepting substituents so that both structural and electronic effects may be studied.[18-20] The possibility to generate a series of structurally related molecules by a controlled exchange of functional groups makes them attractive to analyze the effects of specific elements on the physical properties. Trends have been determined with respect to structural,[21,22] electrochemical,[23] luminescent,[21,22] and nonlinear optical (NLO) properties[24-26] of these materials.

The ultimate goal for designing novel NLO materials has been to combine a highly efficient π-conjugated moiety with the optimal degree of functionalization in order to provide enhanced nonlinear responses. For this purpose, the heteroaromatic thiophene ring system has been chosen to replace phenyl groups as conjugated spacers for assembly of the next generation of TEE chromophores. The weaker aromatic character of the thiophene ring has been predicted to enhance nonlinear optical responses when compared to analogous phenyl substituted systems. This behavior has been demonstrated theoretically[27-31] and experimentally[32-39] for both second and third order NLO applications. It has been recently shown that in combination with specific D-A interactions about the TEE core, thiophene spacers do indeed result in enhanced third order NLO behavior as measured by solution state third harmonic generation.[26]

Both experimental and theoretical studies on the electronic absorption spectra of a series of donor (*p*-*N*,*N*-dimethylaminophenyl)- and acceptor (*p*-nitrophenyl or 2-nitrothienyl)-substituted tetraethynylethenes (TEEs) **1-6** have been performed in order to compare and explain the evolution of the theoretically computed and the experimentally measured absorption spectra. The present investigations aim at providing a theoretical interpretation of the UV/Vis spectra of **1-6** and at determining the extent and magnitude of the donor-acceptor charge transfer as a function of substitution pattern (*trans*, *cis*, or *gem*) and of the conjugated substituent (nitrophenyl group or nitrothienyl group). In Section 6.2, the computational methods as well as the validation of the computational approach used to compute the optical spectra are described. The computed and experimentally measured absorption spectra of **1-6** are presented and compared in Section 6.3. The theoretical results provide a detailed description of the electronic transition bands and, thus, allow the assignment of the molecular orbitals involved in the observed electronic promotion processes. The optical features are analyzed with the aid of molecular orbital considerations, electronic transition analysis, and charge difference distributions. The resulting interpretations on the evolution of the electronic spectra are reported in Section 6.3.

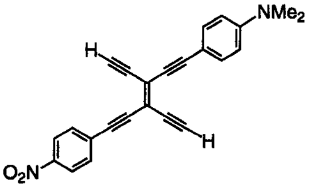

1

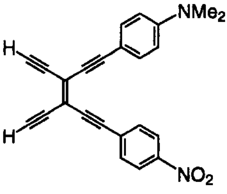

2

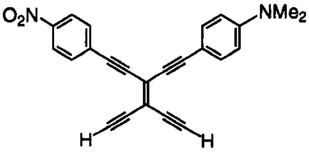

3

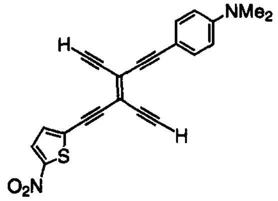

4

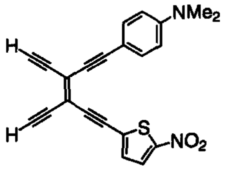

5

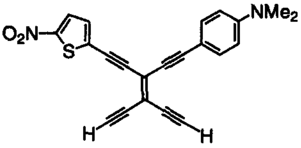

6

6.2 Methodology and Validation of the Computational Procedure

All calculations were carried out using the restricted Hartree-Fock (RHF) scheme. The geometries of the disubstituted TEEs were optimized at the semiempirical AM1 (Austin Modell) level.[40] For comparison, the structures were also optimized using the HF/6-31G** level of theory. As expected, the Hartree-Fock double and triple bonds are shorter and the single bonds are longer than the AM1 distances.[41]

The ground state equilibrium geometries exhibit a stronger carbon-carbon bond alternation in the heteroaromatic ring than in the phenyl ring, indicating the weaker aromatic character of the thiophene unit. Furthermore the presence of thiophene at the electron accepting end of the chromophores affects only the C–C bond connecting the cycle to the nitro group and to the TEE skeleton.

The experimental UV/Vis studies, carried out by Dr. *Rik Tykwinski*, have been performed on the substituted TEEs (**1-6**) endcapped with Si(i-Pr)$_3$ groups in CHCl$_3$. In the calculated species, however, the silylated protecting groups have been replaced by hydrogens and C_s symmetry was retained for all the investigated compounds (**1-6**). Normally, steric interactions between bulky groups can deform the molecular structures and thus, influence the absorption spectra. However, in the case of TEEs, steric hindrance between the silyl groups and the other substituents can be excluded, since the π system remains perfectly planar. Indeed, the nitrophenyl and nitrothienyl bearing donor-acceptor TEEs have been investigated by their single crystal X-ray structures and predominantly show a fully planar conjugated carbon framework, including aryl rings.[21,22,42] This observation justifies the planarity adopted for the computed optical properties.

In order to evaluate the effects of the silyl groups on the optical properties, the UV/Vis spectra of the silylated and deprotected (with tetrabutylammonium fluoride (TBAF)) nitrothienyl substituted derivatives (**4**-**6**) have been measured in tetrahydrofuran (THF). Both sets give similar optical transitions (in absorption wavelength and intensity) for the two lowest energy absorption bands. Small bathochromic shifts of *ca.* 5 nm are observed in the *cis*-**5** and *gem*-**6**. The lowest energy absorption band for the *trans*-**4** does not change, whereas the second band shifts bathochromically by about 10 nm. The only significant difference is detected in the energetically higher lying third band, showing at similar wavelength a considerably more intense band for the silylated derivatives.[42] The fact that the silyl end groups have only a minor influence on the two lowest energy transitions of interest in this study, supports the replacement of the $Si(i\text{-}Pr)_3$ groups by H-atoms in the calculated structures.

The electron transition energies and related oscillator strengths have been calculated by applying the semiempirical quantum chemical Intermediate Neglect of Differential Overlap method parametrized for spectroscopy (INDO/S)[43-45] coupled with a single configuration interaction (SCI) technique.[46] The singly excited configurations have been generated by promoting a single electron from one of the twenty highest occupied molecular orbitals into one of the twenty lowest unoccupied molecular orbitals, yielding a total of 401 configurations. The (20x20) active space is mainly composed of π-orbitals. This approach has yielded optical transition energies for phenylene vinylene oligomers,[10,11] phenylene vinylene derivatives,[12-14] as well as for oligothiophenes[47], that are in good agreement with experimental values. Nevertheless, extensive studies have been undertaken in order to control the suitability of the (20x20) active space for TEE systems. A larger CI size calculation with a (30x30) composition of the active space has been performed to evaluate the CI effect, and the results have yielded the same optical transition spectra as the (20x20) SCI calculation. Thus, the (20x20) active space is appropriate to adopt for this study. Furthermore, these studies reveal that transitions involving σ-orbitals do not participate in the lowest energy excitations. Inclusion of double excitations into the configuration interaction scheme also does not alter the absorption spectra, implying that the low-energy part of the absorption spectra is dominated by one-electron transitions. The electron-electron repulsion terms have been calculated via the Mataga-Nishimoto potential.[48] The theoretical absorption spectra have been simulated with Gaussian functions of 0.2 eV full width at half-maximum.

The shape of the absorption bands are identical, independent of the equilibrium geometries (AM1 or HF/6-31G** optimized) used to calculate the electronic absorption spectra. However, a strong dependence exists between transition energy values and optimized geometry, demonstrating the strong coupling between changes in electronic and molecular structures. The transition energies obtained from the HF optimized structures are lower than those gained with AM1. The AM1 structure derived transition energies agree better with the experimentally obtained values and are therefore chosen for the optical properties analysis.

Surprisingly, the orientation of the thiophene unit is found to affect the absorption spectra. Whether the sulfur atom is directed towards the phenyl ring of the donor end or towards the unsubstituted acetylenic arm of the TEE core plays a considerable role for the determination of the electronic absorption spectra, even though both structures are found to be energetically equal. The calculations demonstrate that the experimental UV/Vis spectra correspond more closely the *trans*- **4** and *gem*-derivative **6** where the sulfur points towards the acetylenic arm, whereas in the *cis*-compound **5** the sulfur is orientated towards the phenyl ring.

The programs used were the Gaussian94[49] and MOPAC packages[50] for the geometry optimization, and the ZINDO package[51] for the calculation of the optical transitions. The molecular structures, molecular orbitals, and charge density differences were represented with the molecular graphics package MOLEKEL.[52]

6.3 Absorption Spectra and Electronic Transitions

The experimental and calculated UV/Vis spectra comparing the absorption bands of nitrophenyl against nitrothienyl group for each isomer **1**-**6** are depicted in Figure 6.1. The following discussions are centered on the electronic characteristics of the first and second absorption bands, since, as mentioned, the third band has been shown to be influenced by the $Si(i\text{-}Pr)_3$ groups,[42] omitted in the calculations. It is important to stress that the study focuses on comparing and explaining the evolutions of the theoretically computed and the experimentally measured absorption spectra, and not on calculating the exact transition energy values. Indeed, the INDO/SCI calculated absorption energies are consistently larger than the experimental values. This may be due to interactions between the solute and solvent upon excitation, that have not been taken into account in the calculated spectra. Indeed, the intensity and energy value of the absorption bands of substituted TEEs have been shown to depend on the surrounding solvent.[21]

6.3.1 Absorption Spectra of Arylated and Heteroaromatic Tetraethynylethenes

The *experimental* absorption spectra of the donor/acceptor substituted TEEs **1-6** are depicted in Figure 6.1. The wavelength (λ_{max}), the corresponding energy absorption maxima (E_{max}), and the molar extinction coefficients ε are summarized in Table 6.1. The spectra for **1-6** exhibit broad *longest wavelength* absorption bands (band I). These bands are characteristic for intramolecular charge-transfer (CT) transitions. Large ε values suggest that the intramolecular donor-acceptor interactions are very efficient. It is noted that the bands of the *trans*-D/A TEE **1** and **4** are more intense than those of *cis*-**2** and **5**, and the *gem*-compounds **3** and **6**. Comparing the position of the CT bands, considered as a measure for the magnitude of the donor-acceptor conjugation, the conjugation is weaker in the geminal system **3** (E = 2.77 eV) than in the *trans*-derivative **1** (E = 2.65 eV) and *cis*-**2** (E = 2.63 eV). Same considerations are applicable to the nitrothienyl functionalized TEEs (E = 2.93 eV for *gem*-**6**, 2.60 eV for *trans*-**4**, and 2.48 eV for *cis*-**5**). Thus, the cross conjugation path is found to be less efficient than the linear conjugation paths.

Surprisingly the *central* absorption band (band II), which shows considerable intensity for *cis*-**2** and *gem*-system **3** (at 3.34 eV for *cis*-**2** and 3.33 eV for *gem*-substituted **3**), is negligibly small in the *trans*-D/A TEE **1** (E = 3.52 eV). Similarly a second large band (band II) is found for *cis*-**5** and *gem*-derivative **6** at 3.09 eV and 3.11 eV, respectively, whereas *trans*-D/A **4** absorbs at 3.46 eV, showing very weak intensity. The origin for this unexpectedly weak absorption in the *trans*-isomers was sought after by calculation of the absorption spectra.

The *calculated* absorption spectra of the diarylated **1-3** and the heteroaromatic **4-6** TEE derivatives are sketched in Figure 6.1 and excellently reproduce the trends observed in the experimental spectra. In order to gain insight into the nature of the excited states, the electron transition energies, oscillator strengths, and a detailed list of the weighted principal configurations involved in the absorption bands are analyzed and reported in Table 6.2.

Table 6.1. Experimental absorption wavelengths λ (nm), corresponding transition energies E (eV), and molar extinction coefficients ε (M^{-1} cm^{-1}) of the first two absorption bands of nitrophenyl TEEs **1**, **2**, and **3**, and of nitrothienyl TEEs **4**, **5**, and **6** in $CHCl_3$.

subst. TEE	band	λ[a]	E[b]	ε
1	I	468	2.65	31200
	II	352	3.52	16300
2	I	471	2.63	17000
	II	371	3.34	30700
3	I	447	2.77	19900
	II	373	3.33	30100
4	I	477	2.60	32900
	II	359	3.46	17900
5	I	500	2.48	14300
	II	402	3.09	33500
6	I	423[c]	2.93	33900
	II	399	3.11	35700

[a] Maximum absorption wavelengths in $CHCl_3$. [b] Corresponding transition energies in eV. [c] Shoulder band.

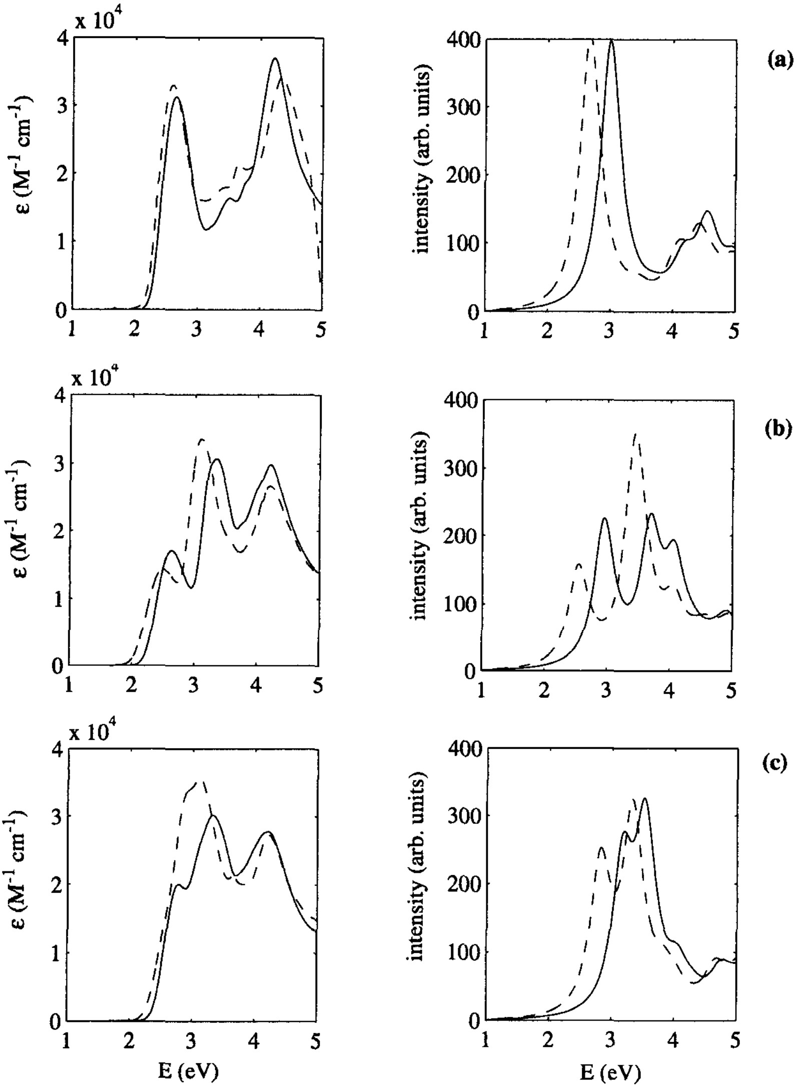

Figure 6.1. Experimental UV/Vis spectra in $CHCl_3$ (left) and ZINDO calculated electronic absorption spectra (right) comparing the effects of nitrothiophene (--) *vs*. nitrophenyl (–) for (a) *trans*-**1** and **4**, (b) *cis*-**2** and **5**, and (c) *gem*-**3** and **6**.

Table 6.2. INDO/SCI Calculated transition energies E_{max} (in eV), oscillator strengths f (in arbitrary units), and principal configurations with CI expansion coefficients of the first two absorption bands of nitrophenyl TEEs **1**, **2**, and **3**, and of nitrothienyl TEEs **4**, **5**, and **6**.

substituted TEE	band	E_{max}	f	principal configurations with CI expansion coefficients
1	I	3.00	1.44	−0.72 [H → L] −0.55 [H → L+1]
	II[a]	3.71	0.03	0.67 [H → L+1] −0.40 [H−1 → L]
2	I	2.94	0.78	−0.76 [H → L] −0.52 [H → L+1]
	II	3.69	0.68	−0.72 [H → L+1] −0.40 [H−1 → L]
3	I	3.17	0.78	−0.68 [H → L] 0.56 [H → L+1]
	II	3.53	0.96	0.59 [H → L+1] −0.50 [H−1 → L]
4	I	2.66	1.47	−0.82 [H → L] −0.39 [H−1 → L]
	II[a]	3.45	0.06	0.76 [H → L+1] −0.40 [H−1 → L]
5	I	2.53	0.53	−0.86 [H → L] −0.32 [H−1 → L]
	II	3.43	1.15	0.71 [H → L+1] 0.49 [H−1 → L]
6	I	2.81	0.79	0.72 [H → L] −0.60 [H−1 → L]
	II	3.33	1.03	−0.69 [H → L+1] −0.43 [H−1 → L]

[a] Band of *trans*-isomers with very weak intensity that could not be detected graphically, but only by numerical inspection of the transition energies data (*cf.* text).

The *lowest energy* absorption bands (band I) are at 3.00 eV and 2.66 eV for *trans*-**1** and **4**, at 2.94 eV and 2.53 eV for *cis*-**2** and **5**, and at 3.17 eV and 2.81 eV for the *gem*-derivatives **3** and **6**, respectively. In accordance with the *experimental* data, the most intense band, *i.e.* the band with the largest oscillator strength, is detected for *trans*-TEEs **1** and **4**. Moreover, whereas the *trans*-**1** and *cis*-**2** isomers show a first transition band at comparable energies (3.00 eV *vs.* 2.94 eV), the geminal D/A-system **3** absorbs at higher energy (3.17 eV). In the nitrothienyl series **4**-**6**, analogous behavior is noted. This demonstrates the lower efficiency of the cross conjugation path in **3** and **6**.

Like the first absorption bands, the calculated *second* bands (bands II) correspond very well to the experimental data. *Cis*-**2** and **5**, and *gem*-derivatives **3** and **6** show intense bands at 3.69 eV and 3.43 eV, and at 3.53 eV and 3.33 eV, respectively. However, the second band for *trans*-**1** and **4** is not detected graphically. Numerical inspection of the computed data, though, has shown very weak transitions with an oscillator strength of 0.03 for **1** at 3.71 eV, and 0.06 for **4** at 3.45 eV. These bands originate from the same one-electron transitions as the *cis*- and *gem*-derivatives (Table 6.2).

6.3.2 Electronic Transition Analysis

In order to explain the observed absorption energies and band intensities, the CI compositions of the electronic transitions (Table 6.2) are examined. Analysis of the nature of the transitions shows that the absorption bands are solely composed of electron promotions between the two HOMOs and the two LUMOs for the both series **1**-**3** and **4**-**6**. Inspection of the different molecular orbitals has shown that their shape does not vary substantially for the different isomers (*trans*, *cis*, and *gem*). Therefore, only the two highest occupied and two lowest unoccupied MOs of the arylated *trans*-TEE **1** and the heteroaromatic *trans*-TEE **4** are depicted in Figure 6.2. All MOs involved in the electronic transitions exhibit π character, thus the two lowest energy absorption bands are formed of $\pi \rightarrow \pi^*$ electronic transitions. Interestingly, the heteroaromatic TEEs show additional charge on the thiophene ring for each MO, due to its electron excessivity compared to the phenyl ring.[53]

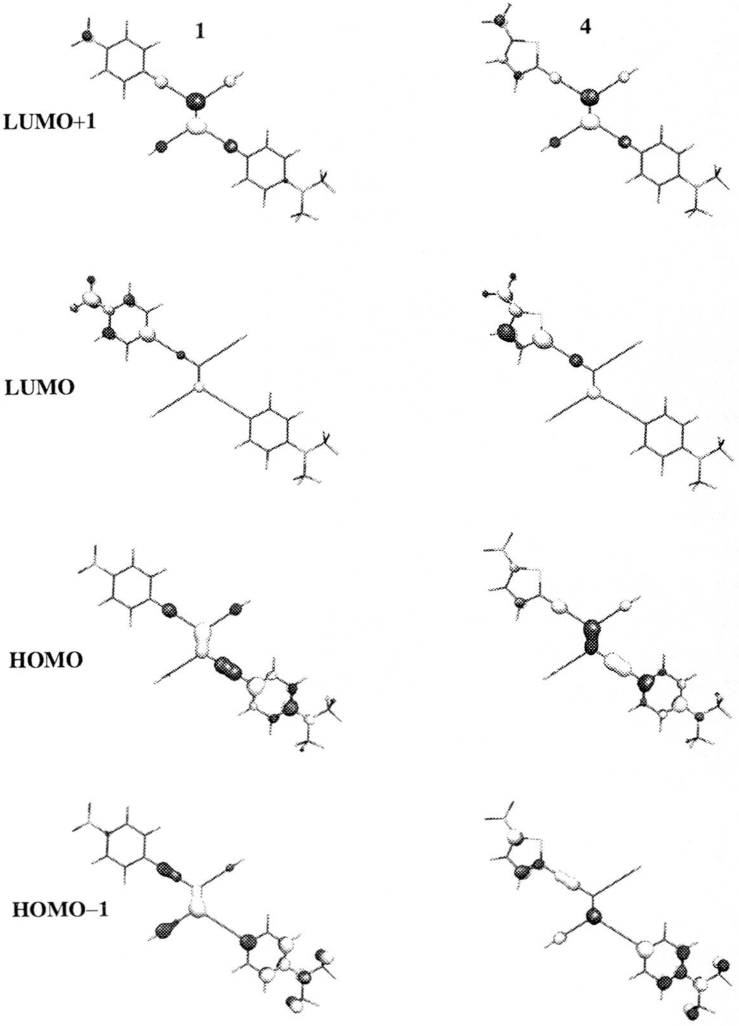
1
4
LUMO+1
LUMO
HOMO
HOMO–1

Figure 6.2. Highest occupied molecular orbitals (HOMO and HOMO–1) and lowest unoccupied molecular orbitals (LUMO and LUMO+1) of arylated **1** (left) and heteroaromatic TEE **4** (right).

The oscillator strength f is related to the transition dipole moment by the expression[54]

$$f = \frac{4\pi m_e}{3e^2 h}\nu M^2 \tag{1}$$

with $M = \|\vec{M}\|$ transition dipole moment

h Planck constant (6.626×10^{-34} J s)

m_e electron mass (9.109×10^{-28} g)

e electron charge ($-1.6022\ 10^{-19}$ C)

ν frequency

For each single excitation between occupied and unoccupied orbitals, a transition dipole moment is calculated and the oscillator strength determined. The square of the transition moment M^2 determines the transition probability and thus, the overall intensity of the transition, whereas the direction of the transition dipole moment vector $\vec{M}$ defines the polarization direction.

The transition dipole moments are examined and their vectors $\vec{M}$ with the corresponding unit vectors $\vec{M}/\|\vec{M}\|$ of the individual configurations are listed in Table 6.4. The molecules have been defined as lying in the xy plane. The x axis is taken as the direction of the olefinic central bond and the z-coordinate, being zero, is omitted in the reported ground state dipole moment vector $\vec{\mu}$ (Table 6.3) and transition dipole moment vector $\vec{M}$ (Table 6.4). Furthermore, for the following discussion, the angle ρ between $\vec{\mu}$ and the different transition dipole moments $\vec{M}$ are reported in Table 6.4. For a better illustration, the directions of $\vec{\mu}$ and of $\vec{M}$ for the principal electronic configurations are sketched in Figure 6.3.

The *lowest energy* absorption band (band I in Table 6.2) is described by the one-electron promotions HOMO → LUMO and HOMO → LUMO+1, for all three nitrophenyl isomers **1**-**3**, and by a HOMO → LUMO and a HOMO–1 → LUMO electronic transition for the three nitrothienyl isomers **4**-**6**. A closer inspection of the transition dipole moment vectors $\vec{M}$ of the individual configurations (Table 6.4), reveals that the HOMO → LUMO and the HOMO → LUMO+1 transition moments in the arylated *trans*-derivative **1** are inclined by $\rho=13°$ to each other. The transition moment vectors of the HOMO → LUMO and the HOMO–1 → LUMO configurations in the heteroaromatic *trans*-**4** form an angle ρ of 7°. Importantly, the coefficients in the linear combination of the two configurations forming the first absorption band (band I) have the same sign, for both *trans*-isomers **1** and **4** (Table 6.2). In these "plus" linear combinations, the almost parallel lying transition moments of the respective principal configurations point therefore in the same direction, as shown in Figure 6.3. This observation explains the predicted high intensity of the first band for the *trans*-derivatives **1** and **4**. For the *cis*-compounds, on the other hand, the angle between the transition moment vectors is larger (67° for **2** and 44° for **5**) and, even though the bands are constructed from a "plus" linear combination, the different orientations of the transition moments decrease the overall oscillator strength. Analogously, in the *gem*-species, the angle ρ between the transition moment vectors is 135° for **3** and 37° for **6**, and the "minus" combination of the singly excited configurations accounts for the lower intensity of band I compared to *trans*-**1** and **4**.

The *second band* (band II in Table 6.2) is composed for all compounds of a HOMO → LUMO+1 and a HOMO−1 → LUMO type transition. It is noticed that, in the *trans*-derivatives **1** and **4**, the transition moments of these two transitions are parallel to each other within 2° and 6° (Table 6.4 and Figure 6.3). According to the "minus" combination of the two singly excited configurations (Table 6.2), these parallel transition moments point into opposite directions and, thus, cancel each other out. The resulting absorption band shows therefore a negligibly small oscillator strength, explaining the calculated and experimentally observed very weak intensity in *trans*-**1** and **4**. The *cis*-**2** and **5** and *gem*-derivatives **3** and **6**, on the other hand, exhibit transition moments with different orientations. Thus, their second absorption bands acquire larger oscillator strength values.

Table 6.3. INDO/SCI Calculated ground state dipole moment $\vec{\mu}$ (in Debye) of substituted TEEs **1**-**6**.

substituted TEE	$\vec{\mu}$	$\lVert\vec{\mu}\rVert$	$\vec{\mu}/\lVert\vec{\mu}\rVert$ [a]
1	(−5.71, 8.25)	10.04	(−0.57, 0.82)
2	(−5.86, 3.13)	6.64	(−0.88, 0.47)
3	(−1.91, 8.09)	8.31	(−0.23, 0.97)
4	(−10.20, 5.61)	11.64	(−0.88, 0.48)
5	(−0.72, 5.20)	5.25	(−0.14, 0.99)
6	(2.35, 10.70)	10.95	(0.21, 0.98)

[a] The unit vector is reported in order to facilitate the numerical comparison between the directions of the dipole moment and the transition moments (Table 6.4).

Table 6.4. INDO/SCI Calculated transition dipole moment $\vec{M}$ of the configurations involved in the absorption bands of substituted TEEs **1-6** and angle ρ between ground state dipole moment vector $\vec{\mu}$ and transition moment vector $\vec{M}$.

substituted TEE	singly excited configuration	$\vec{M}$	$\lVert\vec{M}\rVert$	$\vec{M}/\lVert\vec{M}\rVert$ [a]	ρ
1	[H → L]	(5.26, −5.10)	7.33	(0.72, −0.70)	11
	[H → L+1]	(6.59, −3.89)	7.65	(0.86, −0.51)	24
	[H−1 → L]	(2.90, −1.86)	3.44	(0.84, −0.54)	22
2	[H → L]	(5.24, −1.67)	5.50	(0.95, −0.30)	11
	[H → L+1]	(−6.74, −3.61)	7.65	(−0.88, −0.47)	56
	[H−1 → L]	(−2.89, 4.65)	5.47	(−0.53, 0.85)	30
3	[H → L]	(−4.08, 1.21)	4.26	(−0.96, 0.28)	60
	[H → L+1]	(6.70, 3.59)	7.60	(0.88, 0.47)	75
	[H−1 → L]	(3.73, −4.97)	6.21	(0.60, −0.80)	24
4	[H → L]	(−7.05, 6.26)	9.43	(−0.75, 0.66)	13
	[H → L+1]	(−5.18, 3.60)	6.31	(−0.82, 0.57)	6
	[H−1 → L]	(−4.02, 2.23)	4.60	(−0.87, 0.48)	0
5	[H → L]	(−5.23, 2.89)	5.97	(−0.87, 0.48)	53
	[H → L+1]	(6.41, 4.20)	7.66	(0.84, 0.55)	65
	[H−1 → L]	(−2.21, 6.93)	7.27	(−0.30, 0.95)	9
6	[H → L]	(−4.65, 2.43)	5.25	(−0.89, 0.46)	75
	[H → L+1]	(−6.62, −3.83)	7.65	(−0.86, −0.50)	48
	[H−1 → L]	(3.41, −7.03)	7.81	(0.44, −0.90)	38

[a] The unit vector is reported in order to facilitate the numerical comparison between the transition moments directions of the different configurations.

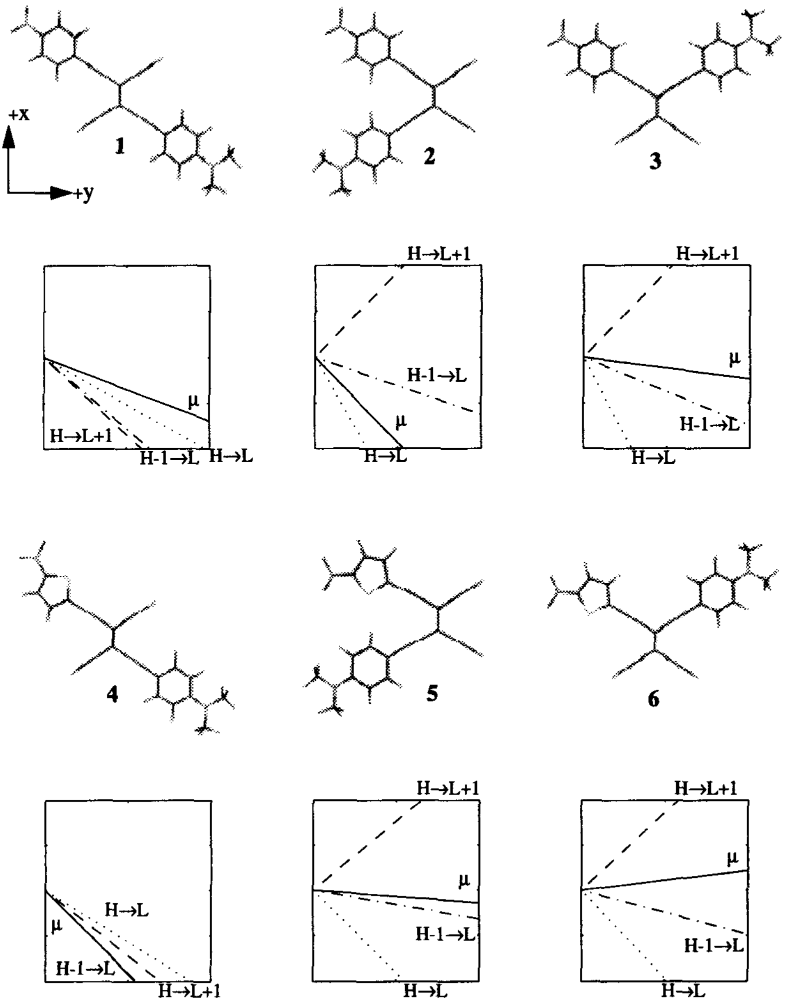
+x
+y
1
2
3
μ
H→L+1
H-1→L
H→L
H→L+1
H-1→L
μ
H→L
H→L+1
μ
H-1→L
H→L
4
5
6
H→L
μ
H-1→L
H→L+1
H→L+1
μ
H-1→L
H→L
H→L+1
μ
H-1→L
H→L

Figure 6.3. Calculated ground state dipole moment direction $\vec{\mu}$ (–) and transition dipole moment $\vec{M}$ directions of the one-electron transitions H→L (...), H→L+1 (--), and H−1→L (-.-.-) of substituted TEEs **1**-**6**.

6.3.3 Charge Difference Density Distribution

The optical behavior of the donor-acceptor TEEs **1-6** is discussed as a function of the magnitude of charge transfer during the transitions. The amount of charge being transferred from and to different subgroups of the substituted TEEs is reported in Table 6.5, and the charge differences are sketched graphically in Figure 6.4. Charge losses (negative differences) are represented in dark, whereas the molecular parts gaining electrons (positive differences) are depicted in white.

Both absorption spectra bands (band I and II) of the donor-acceptor substituted TEEs **1-6** involve charge transfers from the donor to the acceptor ends. The charge transfer in the lowest energy absorption band (band I) occurs from the electron donating aminophenyl substituent and TEE core to the electron accepting nitrophenyl moiety. In the second transition (band II), on the other hand, the charge accumulation concentrates only on the nitro group.

Table 6.5. INDO/SCI calculated Mulliken charge differences in | e | between the ground state and the excited states on different subgroups for nitrophenyl TEEs **1**, **2**, and **3**, and for nitrothienyl TEEs **4**, **5**, and **6**..

	I			II		
subgroup	**1**	**2**	**3**	**1**	**2**	**3**
$-NMe_2$	–0.03	–0.04	–0.03	–0.04	–0.04	–0.06
phenyl-(D)[a]	–0.08	–0.10	–0.07	–0.05	–0.06	–0.05
TEE	–0.10	–0.12	–0.12	–0.23	–0.25	–0.11
phenyl-(A)[b]	0.10	0.13	0.11	–0.04	–0.03	0.01
$-NO_2$	0.11	0.13	0.11	0.36	0.38	0.21
subgroup	**4**	**5**	**6**	**4**	**5**	**6**
$-NMe_2$	–0.02	–0.03	–0.01	–0.05	–0.05	–0.08
phenyl-(D)[a]	–0.06	–0.11	–0.03	–0.07	–0.11	–0.14
TEE	–0.18	–0.19	–0.27	0.02	0.04	0.14
thienyl-(A)[c]	0.07	0.13	0.06	–0.16	–0.16	–0.03
$-NO_2$	0.19	0.20	0.25	0.26	0.28	0.11

[a] Phenyl ring attached to donor (D=amino) group. [b] Phenyl ring attached to acceptor (A=nitro) group. [c] Thienyl ring attached to acceptor (A=nitro) group.

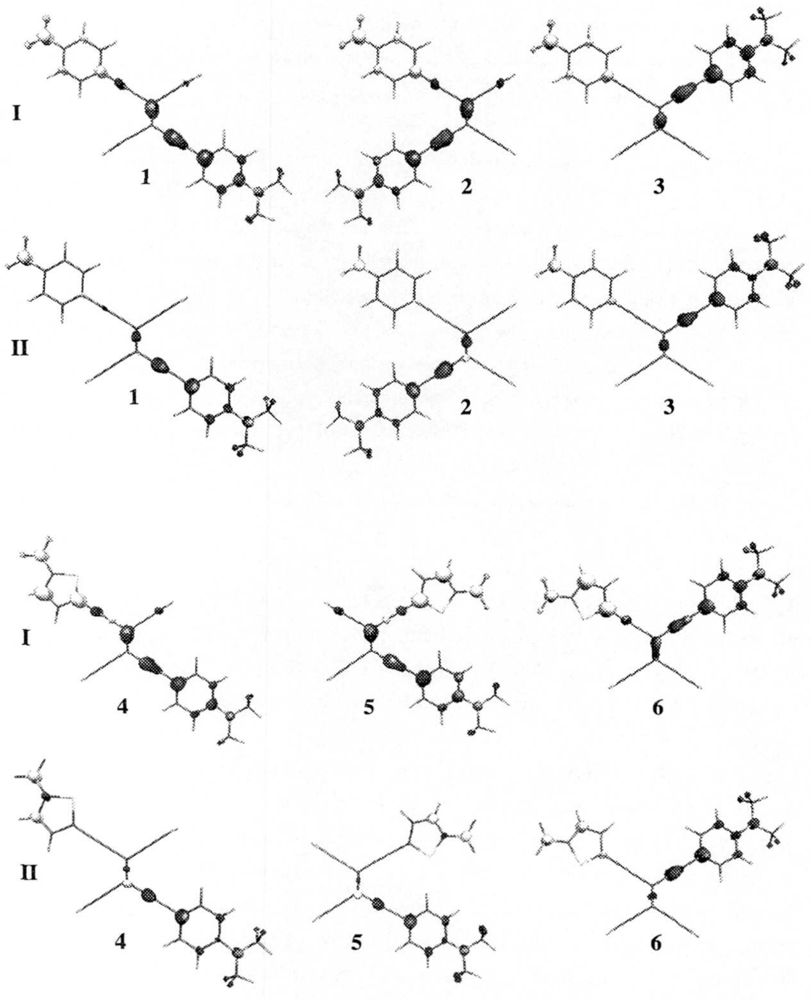
I
1
2
3
II
1
2
3
I
4
5
6
II
4
5
6

Figure 6.4. INDO-SCI Computer charge difference density distributions for band I and II of substituted TEEs **1**-**6**.

6.3.4 Exchange of Aromatic Ring: Comparison Between Arylated and Heteroaromatic Tetraethynylethenes

Apart from slight variances in the oscillator strengths, both sets of molecules **1-3** and **4-6** maintain similar shapes over the UV/Vis analysis region in both calculated and experimental absorption spectra (Figure 6.1).

Generally, the energy absorption maxima of the two investigated bands (band I and II in Tables 6.1 and 6.2) appear at a lower energy for the nitrothienyl functionalized TEEs **4**, **5**, and **6** compared to the nitrophenyl TEE derivatives **1**, **2**, and **3**. The same trend is observed in the experimental spectra for the *trans*- and *cis*-derivatives. The only discrepancy between calculated and experimentally predicted trends occurs for the cross-conjugated *gem*-isomers. Whereas a blue shift of the lowest energy absorption maximum (band I) upon ring exchange to a thiophene moiety is observed experimentally (2.77 eV *vs.* 2.93 eV for **3** and **6**, respectively), a red shift is predicted by the calculations (3.17 eV *vs.* 2.81 eV for **3** and **6**, respectively). Solvent effects can influence the experimental spectra considerably and might explain the observed difference. Very good agreement, however, is found in the 0.2 eV bathochromic shift of the second band (band II) resulting upon thiophene incorporation.

In order to further investigate the bathochromic shift of the lowest energy absorption band (band I), the evolution of the frontier orbitals upon substitution is examined. The INDO calculated energies of the HOMO and the LUMO levels of the unsubstituted TEEs **7-9** and the donor-acceptor substituted TEEs **1-6** are reported in Table 6.6.

The calculated orbital energies show that substitution with donor and acceptor groups (**1-6** compared to **7-9**) leads to very weak changes in the HOMO level, but to a strong stabilization of the LUMO level. These results demonstrate the strong π-electron accepting character of the nitro group. The values of the unsubstituted TEEs **7-9** are larger than those of the functionalized chromophores **1-6**. The bathochromic shift of the nitrothienyl derivatives **4-6** is explained by the decreasing HOMO-LUMO gap compared to the nitrophenyl homologues **1-3** (Table 6.6). The HOMO level remains almost unchanged, but the LUMO level is found to be significantly lowered upon replacement of the phenyl group with a thienyl unit on the acceptor side, since the weaker aromatic character of the thiophene ring decreases the energy cost to break the aromatic stabilization. This orbital energy shift induces a more effective conjugation throughout the whole π-

conjugated system. The bathochromic shift of the lowest energy absorption band (band I) can be explained as a consequence of substituting the nitrophenyl group with a nitrothienyl group.

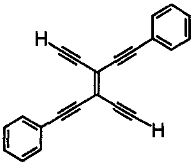

7

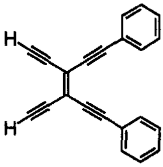

8

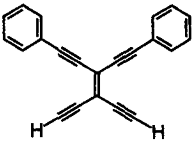

9

Table 6.6. INDO/SCI HOMO, LUMO, HOMO-LUMO energy differences (in eV).

subst. TEE	HOMO	LUMO	Δ (HOMO–LUMO)
7	–7.07	–0.76	6.31
8	–7.08	–0.76	6.32
9	–7.12	–0.73	6.39
1	–7.05	–1.54	5.51
2	–7.07	–1.56	5.51
3	–7.08	–1.55	5.53
4	–7.08	–1.76	5.32
5	–7.03	–1.78	5.25
6	–7.10	–1.77	5.33

6.4 Conclusions

The optical properties of nitrophenyl and nitrothienyl donor-acceptor functionalized chromophores based on the tetraethynylethene (TEE) framework have been investigated as a function of substitution pattern (*trans*, *cis*, and *gem*) and as a function of the nature of the aromatic ring bridging the electron accepting nitro group to the TEE skeleton (phenyl or thienyl). The calculated spectra agree remarkably well with the experimental trends. The obtained UV/Vis absorption spectra provide some very interesting information about the electronic structure of the TEE derivatives.

In accordance with the experimental data, the *lowest energy* absorption band of the geminally substituted compounds **3** and **6** shows a slight blue-shift compared to the analogous *trans*- and *cis*-TEEs, demonstrating that cross conjugation is less effective than linear conjugation.

In addition, the most intense *lowest energy* absorption band is found for the *trans*-derivatives **1** and **4**. This observed enhanced intensity is further elucidated by examining the transition moments of the principal one-electron configurations forming the band. In the “plus” combination of the two one-electron configurations, the almost parallel lying transition moments of the *trans*-compounds **1** and **4** are orientated in the same direction and thus, yield a high oscillator strength for the overall transition.

Furthermore, in both experimental and calculated spectra, the *trans*-derivatives **1** and **4** display very weak intensity of the *second* absorption band. The calculations explain this surprising observation proper to the *trans*-derivatives, by detecting that the transition dipole moments of the two singly excited configurations composing the band, are orientated parallel to each other, but point in opposite directions because of the “minus” combination of the singly excited configurations. Thus, the transition moments cancel each other out and yield a band with a negligibly small oscillator strength.

Finally, the calculated optical transitions exhibit a bathochromic shift of the lowest energy absorption band for the nitrothienyl derivatives **4-6** compared to the corresponding nitrophenyl substituted TEEs **1-3**. Inspection of the frontier orbital energies show that the band gap between the HOMO and the LUMO levels decrease upon incorporation of a thiophene unit. This is due to the weaker aromatic character of the thienyl ring enabling the thiophene group to better participate in charge delocalization. The bathochromic shift of the lowest energy absorption band can thus be explained as a consequence of substituting the nitrophenyl group with a nitrothienyl group.

6.5 References

[1] P. L. Burn, A. Kraft, D. D. C. Bradley, A. R. Brown, R. H. Friend, R. W. Gymer, A. B. Holmes, R. W. Jackson, *J. Am. Chem. Soc.* **1993**, *115*, 10117-10124. Chemical Tuning of the Electronic Properties of Poly(*p*-phenylenevinylene)-Based Copolymers.

[2] D. A. Halliday, P. L. Burn, D. D. C. Bradley, R. H. Friend, O. M. Gelsen, A. B. Holmes, A. Kraft, J. H. F. Martens, K. Pichler, *Adv. Mat.* **1993**, *5*, 40-43. Large Changes in Optical Response Through Chemical Pre-ordering of Poly(*p*-phenylenevinylene).

[3] N. C. Greenham, S. C. Moratti, D. D. C. Bradley, R. H. Friend, A. B. Holmes, *Nature* **1993**, *365*, 628-630. Efficient Light-Emitting Diodes Based on Polymers with High Electron Affinities.

[4] S. Tasch, C. Brandstätter, F. Meghdadi, G. Leising, G. Froyer, L. Athouel, *Adv. Mat.* **1997**, *9*, 33-36. Red-Green-Blue Light Emission from a Thin Film Electroluminescence Device Based on Parahexaphenyl.

[5] T. Christ, A. Greiner, R. Sander, V. Stümflen, J. H. Wendorff, *Adv. Mat.* **1997**, *3*, 219-222. Multicoloured Chromophore for White-Light-Emitting Diodes.

[6] A. Kraft, A. C. Grimsdale, A. B. Holmes, *Angew. Chem.* **1998**, *110*, 416-443, *Angew. Chem. Int. Ed.* **1998**, *37*, 402-428. Electroluminescent Conjugated Polymers - Seeing Polymers in a New Light.

[7] M. Berggren, O. Inganäs, J. Rasmusson, G. Gustafsson, M. R. Andersson, O. WennerstrÖm, T. Hjertberg, *Nature* **1994**, *372*, 444-446. Light-Emitting Diodes with Variable Colours from Polymer Blends.

[8] G. Grem, G. Leditzky, B. Ullrich, G. Leising, *Adv. Mat.* **1992**, *4*, 36-37. Realization of a Blue-Light-Emitting Device Using Poly(*p*-phenylene).

[9] J. Cornil, D. Beljonne, R. H. Friend, J. L. Brédas, *Chem. Phys. Letters* **1994**, *223*, 82-88. Optical Absorptions in Poly(Paraphenylene Vinylene) and Poly(2,5-Dimethoxy-1,4-paraphenylene Vinylene) Oligomers.

[10] J. Cornil, D. Beljonne, Z. Shuai, T. W. Hagler, I. Campbell, D. D. C. Bradley, J. L. Brédas, C. W. Sprangler, K. Müllen, *Chem. Phys. Letters* **1995**, *247*, 425-432. Vibronic Structure in the Optical Absorption Spectra of Phenylene Vinylene Oligo-

mers: A Joint Experimental and Theoretical Study.

[11] J. Cornil, D. Beljonne, J. L. Brédas, *J. Chem. Phys.* **1995**, *103*, 834-841. Nature of Optical Transitions in Conjugated Oligomers. I. Theoretical Characterization of Neutral and Doped Oligo(phenylenevinylene)s.

[12] J. Cornil, D. A. dos Santos, D. Beljonne, J.-L. Brédas, *J. Phys. Chem.* **1995**, *99*, 5604-5611. Electronic Structure of Phenylene Vinylene Oligomers: Influence of Donor/Acceptor Substitutions.

[13] J. Cornil, D. Beljonne, D. A. dos Santos, J.-L. Brédas, *Synth. Met.* **1996**, *76*, 101-104. Poly(*p*-phenylene vinylene) as Active Layer in Light-Emitting Diodes: A Theoretical Investigation of the Effects of Derivatization.

[14] J. Cornil, D. Beljonne, D. A. dos Santos, Z. Shuai, J.-L. Brédas, *Synth. Met.* **1996**, *78*, 209-217. Towards a Better Understanding of Polymer-Based Light-Emitting Diodes: A Theoretical Insight Into the Basic Phenomena.

[15] S. R. Marder, D. N. Beratan, L.-T. Cheng, *Science* **1991**, *252*, 103-106. Approaches for Optimizing the First Electronic Hyperpolarizability of Conjugated Organic Molecules.

[16] C. Bosshard, G. Knöpfle, P. Prêtre, P. Günter, *J. Appl. Phys.* **1992**, *71*, 1594-1605. Second-Order Polarizabilities of Nitropyridine Derivatives Determined with Electric-Field-Induced Second-Harmonic Generation and a Solvatochromic Method: A Comparative Study.

[17] F. Meyers, S. R. Marder, B. M. Pierce, J.-L. Brédas, *J. Am. Chem. Soc.* **1994**, *116*, 10703-10714. Electric Field Modulated Nonlinear Optical Properties of Donor-Acceptor Polyenes: Sum-Over-States Investigation of the Relationship between Molecular Polarizabilities (α, β, and γ) and Bond Length Alternation.

[18] R. R. Tykwinski, F. Diederich, *Liebigs Ann./Recueil* **1997**, 649-661. Tetraethynylethene Molecular Scaffolding.

[19] F. Diederich, in *Modern Acetylene Chemistry*; P. J. Stang, F. Diederich (Eds.), Verlag Chemie: Weinheim, 1995; Chapter 13. Oligoacetylenes.

[20] F. Diederich, L. Gobbi, *Top. Curr. Chem.* **1998**, in press. Cyclic and Linear Acetylenic Molecular Scaffolding.

[21] R. R. Tykwinski, M. Schreiber, R. Pérez Carlón, F. Diederich, V. Gramlich, *Helv.*

Chim. Acta **1996**, *79*, 2249-2281. Donor/Acceptor-Substituted Tetraethynylethenes: Systematic Assembly of Molecules for Use as Advanced Materials.

[22] R. R Tykwinski, M. Schreiber, V. Gramlich, P. Seiler, F. Diederich, *Adv. Mater.* **1996**, *8*, 226-231. Donor-Acceptor Substituted Tetraethynylethenes.

[23] A. Hilger, J.-P. Gisselbrecht, R. R. Tykwinski, C. Boudon, M. Schreiber, R. E. Martin, H. P. Luethi, M. Gross, F. Diederich, *J. Am. Chem. Soc.* **1997**, *119*, 2069-2078. Electronic Characteristics of Arylated Tetraethynylethenes: A Cooperative Computational and Electrochemical Investigation.

[24] C. Bosshard, R. Spreiter, P. Günter, R. R. Tykwinski, M. Schreiber, F. Diederich, *Adv. Mater.* **1996**, *8*, 231-234. Structure-Property Relationships in Nonlinear Optical Tetraethynylethenes.

[25] R. Spreiter, C. Bosshard, G. Knöpfle, P. Günter, R. R. Tykwinski, M. Schreiber, F. Diederich, *J. Phys. Chem. B* **1998**, *102*, 29 -32. One- and Two-Dimensionally Conjugated Tetraethynylethenes: Structure versus Second-Order Optical Polarizabilities.

[26] R. R. Tykwinski, U. Gubler, R. E. Martin, F. Diederich, C. Bosshard, P. Günter, *J. Phys. Chem. B* **1998**, *102*, 4451-4465. Structure-Property Relationships in Third-Order Nonlinear Optical Chromophores.

[27] I. D. L. Albert, T. J. Marks, M. A. Ratner, *J. Am. Chem. Soc.* **1997**, *119*, 6575-6582. Large Molecular Hyperpolarizabilities. Quantitative Analysis of Aromaticity and Auxiliary Donor-Acceptor Effects.

[28] I. D. L. Albert, J. O. Morley, D. Pugh, *J. Phys. Chem.* **1995**, *99*, 8024-8032. Optical Nonlinearities of Azoarenes.

[29] V. Keshari, W. M. K. Wijekoon, P. N. Prasad, S. P. Karne, *J. Phys. Chem.* **1995**, *99*, 9045-9050. Hyperpolarizabilities of Organic Molecules: *Ab Initio* Time-Dependent Coupled Perturbed Hartree-Fock-Roothaan Studies of Basic Heterocyclic Structures.

[30] K. Y. Wong, A. K. Y. Jen, V. P. Rao, K. J. Drost, *J. Phys. Chem.* **1994**, *100*, 6818-6825. Theoretical and Experimental Studies on the Molecular Second Order Nonlinear Optical Responses of Heteroaromatic Compounds.

[31] V. P. Rao, A. K.-Y. Jen, J. Chandrasekhar, I. N. N. Namboothiri, A. Rathna, *J. Am.*

Chem. Soc. **1996**, *118*, 12443-12448. The Important Role of Heteroaromatics in the Design of Efficient Second-Order Nonlinear Optical Molecules: Theoretical Investigation on Push-Pull Heteroaromatic Stilbenes.

[32] L.-T. Cheng, W. Tam, S. R. Marder, A. E. Steigman, G. Rikken, C. W. Spangler, *J. Phys. Chem.* **1991**, *95*, 10643-10652. Experimental Investigations of Organic Molecular Nonlinear Optical Polarizabilities. 2. A Study of Conjugation Dependences.

[33] S.-S. P. Chou, D.-J. Sun, H.-C. Lin, P.-K. Yang, *J. Chem. Soc., Chem. Commun.* **1996**, *1045-1046*. Second-Order Nonlinearities and Crystal Structures of Methylsulfonyl- and Phenylsulfonyl-substituted Thiophene Imino Dyes.

[34] V. P. Rao, K. Y. Wong, A. K.-Y. Jen, K. J. Drost, *Chem. Mater.* **1994**, *6*, 2210-2212. Functionalized Fused Thiophenes: A New Class of Thermally Stable and Efficient Second-Order Nonlinear Optical Chromophores.

[35] V. P. Rao, A. K-Y. Jen, K. Y. Wong, K. J. Drost, *Tetrahedron Lett.* **1993**, *34*, 1747-1750. Novel Push-Pull Thiophenes for Second Order Nonlinear Optical Applications.

[36] V. P. Rao, A. K-Y. Jen, K. Y. Wong, K. J. Drost, *J. Chem. Soc., Chem. Commun.* **1993**, 1118-1120. Dramatically Enhanced Second-Order Nonlinear Optical Susceptibilities in Tricyanovinylthiophene Derivatives.

[37] A. K-Y. Jen, V. P. Rao, K. Y. Wong, K. J. Drost, *J. Chem. Soc., Chem. Commun.* **1993**, 90-92. Functionalized Thiophenes: Second-Order Nonlinear Optical Materials.

[38] K. Y. Wong, A. K-Y. Jen, V. P. Rao, *Phys. Rev. A* **1994**, *49*, 3077-3080. Experimental Studies of the Length Dependence of Second-Order Nonlinear Optical Responses of Conjugated Molecules.

[39] V. P. Rao, Y. Cai, Y.; A. K-Y. Jen, *J. Chem. Soc., Chem. Commun.* **1994**, 1689-1690. Ketene Dithioacetal as a π-Electron Donor in Second-Order Nonlinear Optical Chromophores.

[40] M. J. S. Dewar, E. G. Zoebisch, E. F. Healy, J. J. P. Stewart, *J. Am. Chem. Soc.* **1985**, *107*, 3902-3909. AM1: A New General Purpose Quantum Mechanical

Molecular Model.

[41] W. J. Hehre, L. Radom, P. v. R. Schleyer, J. Pople, *Ab Initio Molecular Orbital Theory*; John Wiley & Sons: New York, 1986.

[42] R. R. Tykwinski, unpublished results.

[43] J. Ridley, M. C. Zerner, *Theor. Chim. Acta* **1973**, *32*, 111-134. An Intermediate Neglect of Differential Overlap Technique for Spectroscopy: Pyrrole and the Azines.

[44] J. Ridley, M. C. Zerner, *Theor. Chim. Acta* **1976**, *42*, 223-236. Triplet States via Intermediate Neglect of Differential Overlap: Benzene, Pyridine, and the Diazines.

[45] J. A. Pople, D. L. Beveridge, P. A. Dobosh, *J. Chem. Phys.* **1967**, *47*, 2026-2033. Approximate Self-Consistent Molecular-Orbital Theory. Intermediate Neglect of Differential Overlap.

[46] M. C. Zerner, G. H. Loew, R. F. Kichner, U. T. Mueller-Westerhoff, *J. Am. Chem. Soc.* **1980**, *102*, 589-599. An Intermediate Neglect of Differential Overlap Technique for Spectroscopy of Transition-Metal Complexes. Ferrocene.

[47] J. Cornil, D. Beljonne, J. L. Brédas, *J. Chem. Phys.* **1995**, *103*, 842-849. Nature of Optical Transitions in Conjugated Oligomers. II. Theoretical Characterization of Neutral and Doped Oligothiophenes.

[48] N. Mataga, K. Z. Nishimoto, *Phys. Chem.* **1957**, *13*, 140-157. Electronic Structure and Spectra of Nitrogen Heterocycles.

[49] Gaussian 94, M. J. Frisch, G. W. Trucks, H. B. Schlegel, P. M. W. Gill, B. G. Johnson, M. A. Robb, J. R. Cheeseman, T. A. Keith, G. A. Petersson, J. A. Montgomery, K. Raghavachari, M. A. Al-Laham, V. G. Zakrzewski, J. V. Ortiz, J. B. Foresman, J. Cioslowski, B. B. Stefanov, A. Nanayakkara, M. Challacombe, C. Y. Peng, P. Y. Ayala, W. Chen, M. W. Wong, J. L. Andres, E. S. Replogle, R. Gomperts, R. L. Martin, D. J. Fox, J. S. Binkley, D. J. Defrees, J. Baker, J. J. P. Stewart, M. Head-Gordon, C. Gonzalez, J.A. Pople, Gaussian, Inc. Pittsburgh, PA, 1995.

[50] J. J. P. Stewart, MOPAC: A General Molecular Orbital Package, version 6.0, Quantum Chemistry Program Exchange (QCPE), 1990.

[51] M. C. Zerner, *Zindo Quantum Chemical Package*; University of Florida, Gains-

ville, FL 32611.

[52] MOLEKEL 2.6, Peter F. Flükiger, University of Geneva and CSCS Manno, Switzerland, 1997.

[53] I. D. L. Albert, T. J. Marks, M. A. Ratner, *J. Am. Chem. Soc.* **1997**, *119*, 6575-6582. Large Molecular Hyperpolarizabilities. Quantitative Analysis of Aromaticity and Auxiliary Donor-Acceptor Effects.

[54] M. Klessinger, J. Michl, *Excited States and Photochemistry of Organic Molecules*; Verlag Chemie: Weinheim, 1995; Chapter 1. Spectroscopy in the Visible and UV Regions.

Curriculum Vitae

Born 28th November 1970 in Luxembourg

Nationality: luxembourgish

Educational Background

1982 – 1989	"Etudes secondaires" at the Athénée de Luxembourg
1989	"Diplôme de fin d'études secondaires", section B (Mathematics, Latin)
1989 – 1993	Studies in Chemical Engineering at the Department of Chemistry of the Swiss Federal Institute of Technology Zürich (ETHZ)
November 1993	Diploma thesis at the Institute for Systems Engineering of the Swiss Federal Institute of Technology Zürich (ETHZ)
February 1994	Diploma as Chemical Engineer ETHZ
1995 – 1998	Ph.D. thesis at the Institute of Organic Chemistry of the Swiss Federal Institute of Technology Zürich (ETHZ) under the supervision of Prof. Dr. François Diederich and PD Prof. Dr. Hans Peter Lüthi

Practical Experience

August 1989	Internship at *DuPont de Nemours* (Luxembourg)
October 1990	Internship at *DuPont de Nemours* (Luxembourg)
March 1992	Internship at *Ciments Luxembourgeois* (Luxembourg)
August – September 1992	Internship at *F. L. Smidth & Co.* (Denmark)
April – October 1994	Teaching assistant at the Institute for Systems Engineering, ETHZ (Switzerland)
1995 – 1998	UNIX System Administrator at the Institute of Organic Chemistry, ETHZ (Switzerland)
1996 – 1998	Research assistant at the Swiss Center for Scientific Computing (SCSC), ETHZ (Switzerland)

Zürich, October 1998 Anouk Hilger